Western Graduate&PostdoctoralStudies

Western University
Scholarship@Western

Electronic Thesis and Dissertation Repository

7-7-2014 12:00 AM

A sensor view model to investigate the influence of tree crowns on effective urban thermal anisotropy

Daniel R. Dyce, *The University of Western Ontario*

Supervisor: James Voogt, *The University of Western Ontario*

A thesis submitted in partial fulfillment of the requirements for the Master of Science degree in Geography

© Daniel R. Dyce 2014

Follow this and additional works at: https://ir.lib.uwo.ca/etd

 Part of the Physical and Environmental Geography Commons

Recommended Citation

Dyce, Daniel R., "A sensor view model to investigate the influence of tree crowns on effective urban thermal anisotropy" (2014). *Electronic Thesis and Dissertation Repository*. 2150.
https://ir.lib.uwo.ca/etd/2150

This Dissertation/Thesis is brought to you for free and open access by Scholarship@Western. It has been accepted for inclusion in Electronic Thesis and Dissertation Repository by an authorized administrator of Scholarship@Western. For more information, please contact wlswadmin@uwo.ca.

A SENSOR VIEW MODEL TO INVESTIGATE THE INFLUENCE OF TREE CROWNS ON EFFECTIVE URBAN THERMAL ANISOTROPY

(Thesis format: Monograph)

by

Daniel R. Dyce

Graduate Program in Geography

A Thesis submitted in partial fulfillment
of the requirements for the degree of
Master of Science

The School of Graduate and Postdoctoral Studies
The University of Western Ontario
London, Ontario, Canada

© Daniel R. Dyce 2014

ABSTRACT

A sensor view model is modified to include trees using a gap probability approach to estimate foliage view factors and an energy budget model for leaf surface temperatures (SUM_{VEG}). The model is found to compare well with airborne thermal infrared (TIR) surface temperature measurements. SUM_{VEG} is used to investigate the influence of trees on thermal anisotropy for narrow field-of-view TIR remote sensors over treed residential urban surfaces. Tests on regularly-spaced arrays of cubes on March 28 and June 21 at latitudes of 47.6°N and 25.8°N show that trees both decrease and increase anisotropy as a function of tree crown plan fraction (λ_V) and building plan fraction (λ_P). In compact geometries (~$\lambda_P > 0.25$), anisotropy tends to decrease with λ_V, with the opposite in open geometries, though trees taller than building height cause anisotropy to increase with λ_V at all λ_P. These results help better understand and potentially correct urban thermal anisotropy.

Keywords: Urban climate, Urban surface temperature, Thermal anisotropy, Urban vegetation, Thermal remote sensing, Sensor view model

DEDICATION

For my mom.

Death leaves a heartache no one can heal, love leaves a memory no one can steal.

ACKNOWLEDGEMENTS

Firstly, I would like to thank my supervisor, Dr. James Voogt. His unwavering support, easygoing nature, and helpful suggestions have greatly improved this thesis and made this endeavour so worthwhile. He has also provided a number of opportunities to travel and present at conferences throughout this project, for which I am forever grateful.

Thank you to my parents and siblings for always being there with love and support. I would not have made it through this past year were it not for all of you and the little ones. Mary, you have been a constant inspiration throughout this entire process and your unwavering support has made this possible.

The connections I have made with faculty, staff, and my fellow graduate students in Geography have made this a truly great experience. The staff within the Geography Department, and in particular Lori and Caroline, have been incredibly helpful and kind. From Wartnz lounge discussions to pub crawl debates, my fellow graduate students have always been there for a laugh or intellectual debate. Thanks are also due to friends back home—thanks for always reminding me that there is more to the world than thermal anisotropy.

S. Leblanc provided the 5-Scale model code as well as helpful suggestions regarding its use. E. Wrona helped collect thermal infrared images for model evaluation purposes. E.S. Krayenhoff provided valuable insight into TUF-3d as well as a number of other research topics—thanks for not getting too exasperated by my many inquiries and countless e-mails.

Financial support was provided by the Natural Sciences and Engineering Research Council in the form of grants to Dr. Voogt and myself as well as a Queen Elizabeth II Graduate Scholarship in Science and Technology. Additional support has been provided by Western University and the Geography Department in the form of research and teaching assistantships.

TABLE OF CONTENTS

Abstract ii
Dedication iii
Acknowledgements iv
List of Tables viii
List of Figures x
List of Symbols xv
INTRODUCTION AND LITERATURE REVIEW 1
1.1 Thermal Remote Sensing and Effective Thermal Anisotropy 1
1.2 Effective Thermal Anisotropy over Urban Surfaces 2
1.3 Sensor View Modelling over Urban Surfaces 4
1.4 TIR Emission from Plant Canopies 5
1.5 Radiative Transfer in Plant Canopies 6
1.5.1 Gap Probability for Direct Beam Radiation 7
1.5.2 Models of Radiative Transfer in Heterogeneous Canopies 11
1.6 Research Questions and Objectives 15
MODEL DESIGN METHODOLOGY 18
2.1 General Model Design and Conceptualization 18
2.2 Adding Vegetation to the Modelled Surface 19
2.2.1 Lawn Surfaces 19
2.2.2 Individual Tree Crowns 21
2.3 Ray Tracing through Tree Crowns 24
2.3.1 Tracing from Sun to Surface Patches 24
2.3.2 Tracing from Sensor to Surface Patches 25
2.4 Interaction of Light with Heterogeneous Tree Crowns 25
2.4.1 Light Extinction along the Solar Ray Path 25
2.4.2 Probability of Gap in Individual Tree Crowns 26
2.5 Leaf View Factor 28
2.5.1 Equating the Probability of Gap to a Leaf View Factor 28
2.5.2 Accounting for the Hot-Spot Effect in Calculation of the Proportions of Seen Foliage 31
2.6 Assigning Radiances to Surface and Tree Crown Patches 33
2.6.1 General Radiance Assignment 33

2.6.2 Tree Crown Foliage Radiance Assignment 33
2.6.3 Partially Shaded Surface Patches 34
2.6.4 Summary of SUM_{VEG} Remotely-Detected Radiance Calculation 39
2.7 Summary of Model Methodology 40
TESTING THE LEAF SURFACE TEMPERATURE AND PROPORTION SUB-MODELS 41
3.1 Leaf Surface Temperature Model Tests 42
3.1.1 Leaf Temperature Model Evaluation with TIR images of Boston ivy and dawn redwood 42
3.1.2 Leaf Temperature Model Evaluation with Airborne TIR Images of the Sunset Residential Neighbourhood 50
3.2 Leaf Proportion Model Tests 55
3.2.1 Investigating the Influence of Foliage Clumping and Density on Sunlit and Shaded Foliage Proportions 55
3.3 Summary of SUM_{VEG} Leaf Temperature and Proportion Routines 59
SUM_{VEG} EVALUATION AND SUNSET CASE STUDY RESULTS 61
4.1 Vancouver Sunset Residential Area: *August 17th, 1992* 61
4.1.1 Site Description 61
4.1.2 Evaluation Data 62
4.1.3 Representation of the Sunset Urban Surface 64
4.1.4 Full Model Validation using Surface Temperature Observations 67
4.2 Influence of Tree Crowns on Thermal Anisotropy over the Sunset Neighbourhood 72
4.2.1 Component Surface Temperatures and Sensor Geometry 72
4.2.2 Thermal Anisotropy over the Sunset Urban Surface 75
4.2.3 Comparison of SUM_{VEG} Calculated Directional Temperature Differences with Observations 82
4.3 Summary of SUM_{VEG} Evaluation and Sunset Residential Case Study 87
SENSITIVITY OF URBAN THERMAL ANISOTROPY TO TREE CROWN VEGETATION 90
5.1 Description of Simulated Urban Surface 91
5.1.1 Forcing Conditions and Urban Geometry 91
5.1.2 Tree Crown Coverage and Biophysical Parameters 94
5.1.3 Estimation of Component Surface Temperatures using TUF-3d 95
5.2 Thermal Anisotropy as a Function of Building and Tree Crown Plan Fractions 97
5.2.1 Simulation Methods 97
5.2.2 Sensitivity of Thermal Anisotropy to Tree crown Plan Fraction 99

5.3 Investigating the Diurnal Trend of Thermal Anisotropy 108
5.3.1 Simulation Methods 108
5.3.2 Diurnal Thermal Anisotropy for the High Density Detached Residential Case Study 110
5.4 Thermal Anisotropy as a Function of Tree Crown Biophysical Parameters 114
5.4.1 General Methods 114
5.4.2 Sensitivity of Thermal Anisotropy to Foliage Area Density 115
5.4.3 Sensitivity of Thermal Anisotropy to Intra-Crown Foliage Clumping and Leaf Width 118
5.5 Summary 121
CONCLUSIONS AND FURTHER WORK 123
6.1 Summary and Conclusions 123
6.1.1 Extension of Thermal Anisotropy Results to Local Climate Zones 126
6.2 Model Limitations and Further Model Development 128
6.3 Future Model Testing 130
6.4 Potential Model Applications 130
APPENDIX A 132
APPENDIX B 137
B.1 Sunlit and Shaded Leaf Temperature 138
B.2 Radiation Absorbed by Leaf Elements 139
B.3 Temperatures for Surfaces Shaded by Tree Foliage 142
REFERENCES 145
Curriculum Vitae 155

LIST OF TABLES

Table 1.1	G-factor and extinction coefficient approximations for several ideal leaf angle distributions (*as in* Baldocchi, 2012 *after* Anderson, 1966; Campbell and Norman, 1998; Monteith and Unsworth, 1990).	8
Table 3.1	Inputs used in the leaf temperature model to estimate T_{ls} and T_{lh}. Values in a range indicate slight variation during the time of imaging.	46
Table 3.2	Time and date information for TIR images acquired on the roof of Talbot college and statistics for modelled leaf temperatures. Plant species A and B represent dawn redwood and Boston ivy, respectively.	49
Table 3.3	Statistics of the comparison between modelled and measured T_{lh}.	52
Table 3.4	Statistics of the comparison between modelled and measured T_{ls}.	52
Table 4.1	Frequency (n), tree height (H_T), trunk height (H_{tk}), and crown radius (r_C) for the general tree types present in the Sunset northwest sub-domain (*adapted from* Voogt and Oke (1997)).	66
Table 4.2	Validation statistics for the SUM_{VEG} evaluation with Sunset airborne T_S and ΔT_S.	70
Table 4.3	Tree crown biophysical parameters and sensor geometrical specifications for the Sunset residential case study.	76
Table 4.4	Sensor and surface geometry and component sunlit (S) and shaded (SH) surface temperatures for the southwest sub-domain and full Sunset domain simulations. Surface temperatures are the same as those used to populate facets in the northwest sub-domain.	82
Table 5.1	Thermal parameters for surface components used to estimate temperatures with TUF-3d for the sensitivity simulations (Krayenhoff and Voogt, 2007b *through personal communication with* Rene Dupuis, 2003).	98
Table 5.2	Sensitivity simulation geometric and tree crown biophysical parameters.	98

Table 5.3	Thermal parameters used in TUF-3d to estimate facet surface temperatures for the investigation of the influence of tree crowns on diurnal thermal anisotropy (Krayenhoff and Voogt, 2007b).	108
Table 5.4	Geometric and tree crown biophysical parameters used for the high density detached residential case study simulations.	109
Table 6.1	Λ_{MAX} for three Local Climate Zones with ($\lambda_V = 0.32$) and without ($\lambda_V = 0.0$) tree crowns on June 21st at 1200 LMST for simulations at ϕ = 47.6°N. λ_P indicates the range provided by Stewart and Oke (2012) with the actual simulation λ_P in brackets (LCZ diagrams from Stewart and Oke, 2012).	128
Table B.1	Input parameters to the modified leaf temperature model incorporated into SUM_{VEG}.	139

LIST OF FIGURES

Figure 2.1	Plan area view of two urban surface configurations consisting of a repeating array of block buildings and differentiated by lawn width on the alley side. Buildings are oriented in a block structure with 4 buildings per block.	20
Figure 2.2	Example tree crown shapes possible in SUM_{VEG}. Tree crown shape controlled by r_C and H_C.	22
Figure 2.3	SUM_{VEG} modelled urban surface configuration ($\lambda_P = 0.16$) for two tree crown plan fractions. Values indicate SUM_{VEG} surface codes.	23
Figure 2.4	Sample of tree crown shapes and the relative influence on gap probability as a function of θ_S. (a), (d), and (e) represent the influence of tree crown shape. (b) and (c) represent the influence of foliage area density (Darker shades indicate increasing u_L).	27
Figure 2.5	Representation of SUM_{VEG} direct and diffuse solar radiation gap probability calculation method. The upper hemisphere is divided into sky sectors based on azimuthal and off-nadir angular intervals. For direct radiation, a single ray is traced from the solar position (*S)* to partially shaded patch *j*. For diffuse radiation, a ray is traced from every sky sector to *j*. Both transmittance calculations require tracking path length through tree crowns (Cube in centre of hemisphere). 'N' indicates North. See text for other variable descriptions.	37
Figure 3.1	Example TIR images of (a) Boston ivy (June 3, 2013) and (b) dawn redwood (May 30, 2013) from which sunlit or shaded leaf surface temperatures are extracted. Points indicated by Sp(#) indicate pixels chosen to represent sunlit leaf elements.	43
Figure 3.2	Comparison of T_{ls} and T_{lh} derived from TIR images of Boston ivy and dawn redwood acquired on May 30, 2013 and June 3, 2013 and the those estimated using the SUM_{VEG} leaf temperature model. Images are numbered chronologically.	48

Figure 3.3	Linear regression of T_{ls} and T_{lh} derived from TIR images of Boston ivy and dawn redwood acquired on May 30, 2013 and June 3, 2013 and estimated by the SUM_{VEG} leaf temperature model. Symbols representing dawn redwood temperatures are circled. The dashed line indicates the 1:1 line.	48
Figure 3.4	Comparison of modelled estimates of (a) T_{ls} and (b) T_{lh} with measurements extracted from TIR images acquired on August 17, 1992 of the Sunset residential neighbourhood of Vancouver, B.C. 'V', 'N', 'S', 'W', and 'E' represent nadir, north, south, west, and east viewing directions, respectively.	54
Figure 3.5	Illustration of the test used to investigate the trend in P_T and Z_T—for a single tree crown—over a range of Ω_C and μ_L.	56
Figure 3.6	Proportion of (a) sunlit and (b) shaded foliage as a function of Ω_C over a range of θ_V with the sun at $\theta_S = 45°$.	58
Figure 3.7	Proportion of (a) sunlit and (b) shaded foliage as a function of μ_L over a range of θ_V with the sun at $\theta_S = 45°$.	59
Figure 4.1	VanMap orthophoto (2002) of a section of the Sunset neighbourhood with the two dominant block orientations (N–S and E–W). Buildings within a block are spaced close together and tree crowns generally line streets with sporadic distribution around residential lots.	62
Figure 4.2	Plan view of the digitized Sunset residential domain used for the SUM_{VEG} full model evaluation and case study. For buildings, values indicate the height in metres while ground level surface values match their declaration type in SUM_{VEG}.	65
Figure 4.3	Plan view 'slice' of the Sunset northwest sub-domain at a height of 4m with ground level surfaces excluded in order to compare tree crown size and location relative to buildings. Values indicate SUM_{VEG} surface codes.	66

Figure 4.4	Visualization of the SUM_{VEG} model evaluation procedure using TIR images from Voogt and Oke (1997; 1998). (a) TIR frame with sensor at nadir and (b) the digitized surface (at 4m) with matching sensor geometry. The dashed circle on the TIR frame is an example of the mask applied to produce a circular IFOV and the dashed circle on the digitized surface indicates the modelled IFOV. Values on the TIR frame indicate surface temperature, in Kelvins, corrected for atmospheric effects. Values on the digitized surface indicate the surface codes within SUM_{VEG}.	67
Figure 4.5	Comparison of T_S with (SUM_{VEG}) and without (SUM) tree crowns to the remotely-sensed temperature for all TIR frames used in the SUM_{VEG} evaluation. V-Nadir, E-East, W-West, N-North, S-South indicates direction sensor is facing relative to North = 0°.	71
Figure 4.6	Linear regression of T_S with (SUM_{VEG}) and without (SUM) tree crowns to TIR-derived surface temperature for all sensor view angles. Dashed line indicates the 1:1 line.	72
Figure 4.7	Polar co-ordinate plots of T_S at 1200 LMST for the Sunset northwest sub-domain (b) with and (a) without tree crowns.	77
Figure 4.8	Polar co-ordinate plots at 1200 LMST for the Sunset northwest sub-domain. (a) ΔT_S between the treed and treeless scenario at each sensor angular position. (b–d) View factors (Ψ) for foliage at each sensor angular position with $\lambda_V = 0.062$.	78
Figure 4.9	Polar co-ordinate plots of T_S at 0900 LMST for the Sunset northwest sub-domain (b) with and (a) without tree crowns.	79
Figure 4.10	Polar co-ordinate plot of ΔT_S between the treed and treeless scenario at each sensor view angle for the Sunset northwest sub-domain at 0900 LMST.	80
Figure 4.11	Polar co-ordinate plots of T_S at 1200 LMST for (a) the full Sunset domain and (b) for the 12 block southwest sub-domain with (RIGHT) and without trees (LEFT).	81

Figure 4.12	(a) Bar plot of thermal anisotropy (ΔT_S) over the Sunset residential surface measured as the difference in T_S between view directions (x-axis) using: (1) all TIR images obtained during the three flights (Voogt and Oke (1998)), (2) using the same subset of TIR images used for the SUM_{VEG} model evaluation, and (3) using SUM_{VEG} for the subset of TIR images. (b) Mean T_S from the same sources used for (a) separated based on view direction. 'V', 'N', 'E', 'S', and 'W' indicate nadir, north, east, south, and west view directions, respectively.	85
Figure 5.1	Illustration of the regularly-spaced, aligned array of block structure buildings used to investigate the sensitivity of thermal anisotropy to treed residential urban forms. Micro-scale structures illustrated on one building (e.g. sloped roof, ancillary structure) are not currently represented in SUM_{VEG} but are included in this graphic to emphasize the potential influence of such structures on thermal anisotropy.	93
Figure 5.2	Surface plot of SUM_{VEG} modelled Λ_{MAX}, as a function of λ_P and λ_V, for ϕ = 47.6°N on June 21st at 1200 LMST with $H_T/BH = 1$. Dashed lines indicate lines of equal *BH/SW*. Each polar co-ordinate plot corresponds to a single λ_P and λ_V combination. 'S' indicates the θ_S and φ_S.	99
Figure 5.3	Surface plots of Λ_{MAX} on June 21st at 1200 LMST using forcing conditions and solar geometry from the Miami International Airport and Basel-Sperrstrasse canyon. Colour scales are equalized to facilitate comparison. Dashed lines indicate lines of equal *BH/SW*.	100
Figure 5.4	Surface plots of Λ_{MAX} for March 28th and June 21st at 1200 LMST using forcing conditions and solar geometry from Basel-Sperrstrasse for several H_T/BH ratios. Dashed lines indicate lines of equal *BH/SW*.	101
Figure 5.5	Surface plots of Λ_{MAX} for three times on June 21st at 1200 LMST with $H_T/BH = 1.0$ using forcing conditions and solar geometry from Basel-Sperrstrasse. Dashed lines indicate lines of equal *BH/SW*.	102
Figure 5.6	Polar co-ordinate plot of ΔT_S between simulations with $\lambda_V = 0.0$ and 0.32, for a surface with $\lambda_P = 0.14$ on June 21st at 1200 LMST for ϕ = 47.6°N.	104

Figure 5.7	Polar co-ordinate plot of ΔT_S between simulations with $\lambda_V = 0.0$ and 0.32, for a surface with $\lambda_P = 0.41$ on June 21st at 1200 LMST for ϕ = 47.6°N.	105
Figure 5.8	Polar co-ordinate plot of $\mathbf{\Delta}\Psi_{\mathrm{di,jVh}}$—with $\lambda_V = 0.32$—between simulations with $\lambda_P = 0.14$ and 0.41 on June 21st at 1200 LMST for ϕ = 47.6°N.	106
Figure 5.9	Hourly Λ_{MAX} for a high density detached residential land use class ($\lambda_P = 0.17$) at ϕ = 47.6°N on (a) March 28th and (b) June 21st for a number of tree crown configurations. NV indicates the treeless simulation.	113
Figure 5.10	Modelled Λ_{MAX} as a function of (a) Ω_{C}, (b) μ_L, and (c) f_{width} on June 21st at 1200 LMST for ϕ = 47.6°N and $\lambda_V = 0.13$.	116
Figure 5.11	Modelled normalized view factors occupied by surface facets as a function of μ_L for a south-facing sensor at $\theta_V = 45°$ viewing a surface with $\lambda_P = 0.28$.	117
Figure 5.12	Modelled normalized view factors occupied by surface facets as a function of Ω_C for a south-facing sensor at $\theta_V = 45°$ viewing a surface with $\lambda_P = 0.28$.	119
Figure 5.13	Temperatures for surface facets as a function of f_{width} with $\lambda_P = 0.28$.	120
Figure B.1	Linear regression of modelled ($T_{j_{MOD}}$) and observed ($T_{j_{OBS}}$) temperature for lawn surfaces shaded from direct solar radiation by tree crown foliage. Dashed line indicates the 1:1 line.	144

LIST OF SYMBOLS

ROMAN		
ALW	patch units[1]	Alley width
b_{frac}	—	Fraction of direct to total incoming radiation
BH	patch units	Building height
BL	patch units	Building length
C	$MJm^{-3}K^{-1}$	Volumetric heat capacity
C_P	$MJkg^{-1}°C^{-1}$	Heat capacity of air
d	m	Characteristic leaf dimension
d_{bld}	patch units	Distance from nearest tree crown edge to building wall
d_{frac}	—	Fraction of diffuse to total incoming radiation
e_a	kPa	Water vapour pressure
f_{width}	m	Maximum leaf width
$F(\xi)$	—	Hot spot function
$G(\theta, \varphi)$	m^{-2}	Mean projection of unit foliage area in a particular direction
G_S, G_V	m^{-2}	Mean projection of unit foliage area along a line from the sun, sensor
g_{HA}	$molm^{-2}s^{-1}$	Boundary-layer conductance for heat
g_{HR}	$molm^{-2}s^{-1}$	Heat and radiative conductance
g_R	$molm^{-2}s^{-1}$	Radiative conductance
g_v	$molm^{-2}s^{-1}$	Vapour conductance
g_{va}	$molm^{-2}s^{-1}$	Vapour conductance in air
g_{vs}	$molm^{-2}s^{-1}$	Stomatal conductance of water vapour
H_{tk}	patch units	Trunk height
H_C	patch units	Tree crown height
H_T	patch units	Total tree height
I_d	—	Proportion of diffuse radiation received at Earth's surface
I_{P0}	—	Extraterrestrial flux density index
k	$Wm^{-1}K^{-1}$	Thermal conductivity
K_b , K_{be}	—	Extinction coefficient for beam radiation, for an elliptical *LAD*
K_{dir}	Wm^{-2}	Downwelling direct shortwave radiant flux
K_{diff}	Wm^{-2}	Downwelling diffuse shortwave radiant flux
K_{dn}	Wm^{-2}	Total downwelling shortwave radiant flux
K_S	Wm^{-2}	Shortwave radiation receipt for sunlit leaf elements
K_{SH}	Wm^{-2}	Shortwave radiation receipt for shaded leaf elements

[1] Patch units are dimensionless though can be matched to actual scales of urban geometries.

L	—	Leaf area index
L_{90}	—	Leaf area index accumulated horizontally through tree crown
LAD	—	Leaf angle distribution
L_{dn}	Wm^{-2}	Downwelling longwave radiant flux
L_j	$Wsr^{-1}m^{-2}$	Radiance value for patch *j*
L_{S_j}	$Wsr^{-1}m^{-2}$	Sensor-detected radiance for patch *j*
L_S	$Wsr^{-1}m^{-2}$	Sensor-detected radiance for surface with sensor IFOV
L_{MAX_j}	$Wsr^{-1}m^{-2}$	Sensor-detected radiance for sunlit patch *j*
L_{MIN_j}	$Wsr^{-1}m^{-2}$	Sensor-detected radiance for shaded patch *j*
LW_A	patch units	Lawn width on street side
LW_B	patch units	Lawn width on alley side
m	—	Optical air mass number
$N_S(\xi)$	—	Gap number density function
N_{H_T}	patch units	Number of tree crown patches at maximum crown height
N_{hz}	patch units	Number of horizontal ground patches
N_{rf}	patch units	Number of roof patches
N_X	patch units	Number of domain patches in x-direction
N_Y	patch units	Number of domain patches in y-direction
P_a	kPa	Air pressure
P_b	—	Gap probability for direct beam radiation
P_d	—	Gap probability for diffuse radiation
P_V	—	Gap probability along line from the sensor
P_T	—	Sunlit foliage proportion
P_{Tf}	—	Probability of viewing sunlit foliage far from the hot spot
P_{ti}	—	Relative proportion of sunlit tree crown visible to sensor
Q_1	—	Proportion of sunlit foliage visible on sunlit crown side
Q_2	—	Proportion of sunlit foliage visible on shaded crown side
R_{abs}	Wm^{-2}	Radiation absorbed by leaf surface
$R_{S_{abs}}$	Wm^{-2}	Radiation absorbed by sunlit leaf surface
$R_{SH_{abs}}$	Wm^{-2}	Radiation absorbed by shaded leaf surface
r_C	patch units	Tree crown radius
ΔS	$kPa°C^{-1}$	Slope of the saturation vapour pressure curve
$LMST$	hr	Local mean solar time
S_{g0}	m^2	Tree crown projection area along line from sun
$S(\theta, \varphi)$	patch units	Generic path length
S_S	patch units	Pathlength through crown along line to sun
S_V	patch units	Pathlength through crown along line to sensor

SW	patch units	Street width
T_a	°C	Air temperature
T_{ab}	m^2	Total crown surface visible to sensor
T_{ib}	m^2	Sunlit crown surface visible to the sensor
T_d	°C	Dewpoint temperature
T_j	°C	Brightness surface temperature for patch j
T_{ls}	°C	Sunlit leaf temperature
T_{lh}	°C	Shaded leaf temperature
T_S	°C	Sensor-detected brightness surface temperature
T_{spc}	patch units	Spacing between tree crown edges
U, U_{avg}	ms^{-1}	Wind speed, average wind speed
V_C	m^3	Tree crown volume
V_{g0}	m^2	Tree crown projection area along line from the sensor
VPD	kPa	Vapour pressure deficit
Δx	m	Building wall layer thickness
YD	—	Day of year
Z_T	—	Shaded foliage proportion
Z_S	m	Sensor height
GREEK		
α	—	Leaf absorptivity (wavelength dependent)
α_L	—	Leaf albedo
γ, γ^*	$kPa°C^{-1}$	Psychometric constant, apparent psychometric constant
$\Gamma(\xi)$	—	Phase function for leaf scattering
ε_L	—	Leaf emissivity
η	°	Street orientation (relative to north = 0°)
θ_L	°	Inclination angle of foliage normal
θ_S	°	Solar zenith angle
θ_V	°	Sensor off-nadir angle
φ_L	°	Azimuth angle of foliage normal
φ_S	°	Solar azimuth angle
φ_V	°	Sensor azimuth angle
$\Delta\varphi_{S,V}$	°	Angular separation between solar and sensor azimuth angle
λ	—	Tree crown gap size
λ_V	—	Tree crown plan fraction
λ_P	—	Building plan fraction
μ_L	m^{-1}	Foliage area density
ξ	°	Scattering angle

σ	$Wm^{-2}K^{-4}$	Stefan-Boltzmann constant
τ_{atm}	—	Atmospheric transmittance
τ_b	—	Transmittance for direct beam radiation through tree crown
ϕ	decimal degrees	Latitude
χ	—	Ratio of average projected areas of tree crown on horizontal and vertical surfaces
$\psi_{di,j}$	—	Total patch view factor
$\psi_{di,jS}$	—	View factor occupied by surface partially occluded by foliage
$\psi_{di,jV}$	—	View factor occupied by foliage
$\psi_{di,jVs}$	—	View factor occupied by sunlit foliage
$\psi_{di,jVh}$	—	View factor occupied by shaded foliage
Ω_C	—	Individual crown foliage clumping index

Chapter 1

INTRODUCTION AND LITERATURE REVIEW

1.1 THERMAL REMOTE SENSING AND EFFECTIVE THERMAL ANISOTROPY

The research in this thesis pertains to enhancing our understanding of urban surface temperature measured using remote sensing techniques. Accurate surface temperatures are important for applications such as modelling the urban energy balance, determining the internal climates of buildings, and studying urban dweller thermal comfort (Voogt and Oke, 2003). Remote sensors operating in the thermal infrared (TIR) portion of the electromagnetic spectrum calculate surface temperature as a function of the radiance measured by the sensor. Airborne or satellite TIR remote sensors can provide efficient and spatially representative estimates of surface temperature over large urban areas (Voogt and Oke, 1997). However, the use of TIR remote sensors over urban surfaces presents a number of complications that limit the application of temperature measurements, including: 1) surface emissivity effects, 2) atmospheric influences on the radiant surface emission, and 3) angular variation of upwelling radiance (Voogt and Oke, 1997). Here, the influence of tree crown vegetation on the latter complication is investigated.

At the land-use scale, urban and many natural surfaces consist of a three-dimensional (3d) assemblage of surface elements. This 3d surface geometry, combined with differential patterns of solar insolation which generate micro-scale variations in surface temperature, create an angular variation in remotely-detected radiance. Voogt and Oke (1998) termed this the ‘effective thermal anisotropy’ of a surface in order to distinguish it from directional variation in radiance arising from the non-lambertian nature of individual surface components.

1.2 Effective Thermal Anisotropy over Urban Surfaces

Roth *et al*. (1989) were the first to recognize the potential for directional variation in remotely-detected urban surface temperatures when they used NOAA AVHRR[2] TIR images to characterize the surface temperature urban heat island of several North American cities. They noted that satellite imagery neglects vertically oriented surface facets in favour of horizontal surfaces. This biases the temperature measurement disproportionally towards horizontal surfaces. The sensor response is a function of the radiative source area which is in turn a function of instrument geometry (i.e. instantaneous field-of-view (IFOV), sensor height above the surface, sensor view angle, etc.). The disproportionate contribution of horizontal surfaces may therefore lead to over- or underestimation of the true temperature for the surface features within the sensor IFOV projected onto the surface. Roth *et al*'s (1989) description of the possible errors arising from the method of observation was purely qualitative and they identified the need for further study of this potentially significant bias.

In order to examine the deviation of remotely-detected surface temperatures from what they termed the 'complete surface temperature', Voogt and Oke (1997) characterized the structural form of three Vancouver, B.C. land-uses. Using a variety of methods to estimate the complete urban surface temperature by accounting for the temperatures of all surface facets and weighting the facets by their areal fraction, they demonstrated that including vertical surface facets significantly lowers the complete surface temperature in relation to the remotely-sensed estimate. Thus Voogt and Oke (1997) confirmed that urban surfaces are characterized by strong directional variations of apparent surface temperatures.

Voogt and Oke (1998) directly observed the "effective thermal anisotropy" of an urban surface using airborne observations. The intersection of a remote sensor IFOV with the urban surface means that only a subset of surfaces are viewed from any one viewing position and, unless all facets are sampled appropriately (i.e. according to the relative areal fraction of each), there will be bias in the form of under- or oversampling of the distinct surface facets.

[2] NOAA AVHRR- National Oceanic and Atmospheric Administration Advanced Very High Resolution Radiometer

Other observational campaigns have reported similar findings of urban thermal anisotropy (e.g. Lagouarde *et al*., 2004; Lagouarde and Irvine, 2008). However, while it is arguably the most accurate method of estimating urban thermal anisotropy, direct observation is often prohibitively expensive and requires specialized techniques. For example, Voogt and Oke (1997; 1998) used ground-based and helicopter-mounted remote sensing instruments with multiple flight paths covering a distribution of sensor view angles to characterize surface temperatures and urban thermal anisotropy over a number of urban land use types in Vancouver, BC, Canada. Similarly, Lagouarde *et al*. (2004) and Lagouarde and Irvine (2008) used an aircraft-mounted TIR camera to directly observe the effective thermal anisotropy over Marseilles (Lagouarde *et al*., 2004) and Toulouse City Centre (Lagouarde and Irvine, 2008). The magnitude of observed urban thermal anisotropy is large relative to natural surfaces (e.g. forest canopies, agricultural row crops, etc.) (Voogt and Oke, 1998). For example, Voogt and Oke (1998) observed thermal anisotropy[3] in excess of 9°C over downtown areas in Vancouver though they found a wide range in measurements in relation to the particular surface-sensor-sun relations examined. Lagouarde *et al*. (2004) noted differences between nadir and off-nadir measured surface brightness temperatures of between -5 and 7K.

Given the significant role of urban geometry and surface shading in the magnitude of urban thermal anisotropy, there is also potential for the use of scale models in estimating urban thermal anisotropy (Roberts *et al*., 2009). However, these models suffer from their inability to fully replicate the complex structure and appropriately scale the exchange processes within urban environments (Roberts *et al*., 2009; Kanda, 2006).

Since effective urban thermal anisotropy is the result of surface-sensor-sun relations that display high spatial and temporal heterogeneity, recent efforts at characterizing urban thermal anisotropy have shifted towards numerical modelling methods. Such models are able to estimate thermal anisotropy with high spatial and temporal applicability (e.g. Soux *et al*., 2004; Voogt, 2008; Gastellu-Etchegorry, 2008; Lagouarde *et al*., 2010; Lagouarde *et al*., 2012). However, Soux *et al*. (2004) emphasized that numerical modelling and direct observation methods are not mutually exclusive; instead they can complement one

[3] Voogt and Oke (1998) estimated thermal anisotropy as the difference in remotely-detected brightness temperature between any two sensor view angles.

another in order to identify and potentially eliminate sources of bias in surface temperature measurements.

1.3 SENSOR VIEW MODELLING OVER URBAN SURFACES

Numerical modelling of urban thermal anisotropy requires two sources of information: 1) the relative contribution of each component surface or surface type, within a sensor IFOV, to the remotely-detected radiance and 2) surface radiance values for individual surface components within the remote sensor IFOV. While the majority of studies that have modelled thermal anisotropy have concentrated on plant canopies (e.g. forest or agricultural crops), the same basic model principles can be used as the foundation for sensor view models of urban surfaces (Soux *et al*., 2004). Soux *et al*. (2004) note that, of all the surface representations used in vegetation canopy models, row crops provide the closest analogy to urban areas due to their similarity to the canyon structure typical of many urban areas.

Soux *et al.* (2004) developed the surface-sensor-sun urban model (SUM) as a sensor view model with a three-dimensional urban surface representation. SUM simulates an urban environment as a grid of cells. Using a combination of ray tracing to determine surface shading patterns and solid angle geometry to estimate surface view factors, SUM can be used to investigate thermal anisotropy as a function of any combination of surface-sensor-sun geometries (Soux *et al*., 2004). Individual facet surface temperatures come from measurements (Voogt, 2008), scale model experiments (Roberts *et al.,* 2009), or are calculated using an energy budget model (Krayenhoff and Voogt, 2007a). The ability of SUM to estimate remotely-detected surface radiance was evaluated using surface temperature and view factor observations over an urban site in Vancouver B.C. and from a scale model and found to perform well (Soux *et al.,* 2004).

While the three-dimensional surface representation in SUM represents a marked improvement over two dimensional canyon models, it still uses a relatively simple urban geometry comprised of regularly-spaced, aligned arrays of block structure buildings. Voogt (2008) modified SUM to use GIS-based urban surfaces with variable building height, footprint, and spacing. An evaluation and sensitivity test of the modified SUM indicated the important role of individual facet surface temperatures and micro-scale

structures (e.g. balconies, windows, chimneys, etc.) on the resultant magnitude of effective thermal anisotropy.

Voogt (2008) also indicated the potential for a coupling of SUM with a sub-facet scale three-dimensional energy budget model (Temperatures of Urban Facets in 3d (TUF-3d) —Krayenhoff and Voogt, 2007a) to investigate effective thermal anisotropy in urban areas. Preliminary work using a coupled SUM + TUF-3d model has investigated the control of urban geometry (e.g. building plan fraction, canyon aspect ratio, street orientation, etc.) on effective urban thermal anisotropy over a range of locations and dates (Voogt and Krayenhoff, 2005; Krayenhoff and Voogt, 2007b). Additionally, the coupled SUM + TUF-3d model has been used to investigate the sensitivity of effective thermal anisotropy to surface thermal properties (i.e. thermal admittance) (Dyce and Voogt, 2012). However the inability of SUM to treat tree crown vegetation limits its application to urban areas with little to no tree crown elements or ground-level vegetation.

Inclusion of tree crown vegetation into sensor view models such as SUM, in order to study thermal anisotropy in vegetated urban domains, requires consideration of foliage surface temperatures (radiance) and the relative contribution of foliage elements to the remotely-detected temperature (radiance). This in turn requires consideration of the TIR radiation field over plant canopies in order to extend this to urban sensor view models.

1.4 TIR EMISSION FROM PLANT CANOPIES

Emission of TIR radiation from natural forest canopies and agricultural crops has been extensively investigated and, similar to urban areas, found to exhibit strong angular dependence (Kimes *et al*., 1980; McGuire *et al*., 1989; Paw U *et al*., 1989). Paw U (1992), in a review of TIR emission studies over natural and agricultural vegetated canopies using narrow IFOV TIR remote sensors, reported radiant surface temperature differences from 1 to 13K as a function of changing sensor azimuth angle and 1.5 to 16K when varying the sensor off-nadir angle. However, Paw U (1992) notes that some of these studies may have combined temperature differences resulting from changing time with differences attributable to varying the sensor view angle.

Directional variation of upwelling radiance measured over natural and agricultural vegetated canopies is caused by spatial variations in energy flow processes resulting from

three-dimensional canopy geometry (Kimes *et al.*, 1981). For example, relatively homogeneous vegetated layers such as grass cover typically exhibit small thermal anisotropy magnitudes while heterogeneous vegetation such as row crops or sparse forest canopies typically exhibit much larger magnitudes as a result of more distinct shading patterns on the geometrically 'rough' surface. Measurements of surface temperature using TIR remote sensors also exhibit hot spot effects whereby alignment of the sensor with the surface directly opposite the sun causes mainly sunlit surfaces to be visible to the sensor (Lagouarde *et al.*, 2000).

The majority of models simulating radiative transfer in plant canopies have been restricted to simulating shortwave radiation fields. Fewer models have been developed to simulate the transfer of longwave (e.g. TIR) transfer within vegetated canopies. However, Kimes (1980; 1981) extended the traditional shortwave radiative transfer concept (i.e. gap probability) to develop a longwave radiative transfer model. Subsequently, the use of tree crown gap probabilities to simulate both shortwave and longwave radiation fields over plant canopies has become commonplace (e.g. McGuire *et al.*, 1989; Verhoef *et al.*, 2007). A complete review of photon transport theory in vegetated canopies and individual tree crowns is beyond the scope of this dissertation. Instead the review of radiative transfer-based numerical models here is limited to those that represent heterogeneous canopies or individual tree crowns that could potentially be incorporated into the framework of the SUM model of Soux *et al.* (2004).

1.5 RADIATIVE TRANSFER IN PLANT CANOPIES

Goel (1988) identified four general categories of models that treat the interaction of the radiation field with vegetation canopies including: turbid medium models for homogeneous canopies, geometric-optical models, hybrid models for heterogeneous canopies, and computer simulation models (e.g. Monte Carlo methods). Here, the review is mainly restricted to radiative transfer-based geometric optical models since such models allow for treatment of the heterogeneous nature of tree crowns in urban areas and are generally less computationally-expensive than their Monte Carlo counterparts. Myneni *et al.* (1989) provide a comprehensive review of the theory behind photon transport in horizontally homogeneous vegetation canopies including discussion of the

plethora of numerical solutions available for the transport equations. Additionally, the edited monograph of Myneni and Ross (1991) provides a detailed discussion of radiative transfer within vegetation canopies and heterogeneous three-dimensional crown distributions including several models particularly relevant to this dissertation. The reader is referred to these sources for a more detailed discussion of the theory behind photon transport in plant canopies.

1.5.1 Gap Probability for Direct Beam Radiation

Radiative transfer through tree crown foliage requires the solution of complex transfer equations governing the interaction of the radiation field with foliage elements (Myneni and Ross, 1991). The primary forms of interaction between photons and foliage elements are scattering, absorption, and emission (Myneni *et al*., 1991). Quantifying the interaction of light with tree crowns therefore requires information on the relative frequency and proportion of each interaction. Solution for each interaction within tree crowns or canopies typically requires probabilistic assumptions related to leaf angle distributions and densities, as well as simplifying assumptions such as assuming a horizontally homogeneous canopy or simple geometric crown volumes.

The overall interaction of electromagnetic radiation with vegetation crowns can be described using an extinction coefficient to describe the attenuation of electromagnetic radiation with depth through foliage. The extinction coefficient does not directly quantify or describe the three forms of interaction. Instead, it provides an overall estimate of the total interaction between light radiation and tree crown elements. In this method, tree surfaces are typically described as either horizontally homogeneous layers or envelopes of a turbid medium that attenuate a portion of incoming radiant energy as it passes through based on a form of the Beer-Lambert-Bouguer law. An exponential variation of this law is described by Nilson (1971) to determine the frequency of gaps for direct beam radiation within horizontally homogeneous plant canopies (P_b) as a function of incident solar zenith (θ_S) and azimuth (φ_S) angle ($r = [\theta_S, \varphi_S]$) and downwards cumulative foliage area index (L) as

$$P_b(r) = \exp(-G(r) \cdot L / \cos\theta_S) \qquad (1.5.1).$$

This formulation assumes randomly dispersed foliage with no azimuthal dependence for leaf inclination angle classes. This azimuthal independence is a common assumption for gap frequency/probability models. $G(r)$ is Nilson's G-factor and is defined as the mean projection of unit foliage area in a particular direction r, calculated as

$$G(L,r) = \frac{1}{2\pi}\int_0^{2\pi} d\varphi_L \int_0^1 g(L,\cos\theta_L,\varphi_L)|\cos r\, r_L| d\cos\theta_L \quad (1.5.2)$$

where

$$\cos r\, r_L = \cos\theta_S \cos\theta_L + (1-\cos^2\theta_S)^{1/2}(1-\cos^2\theta_L)^{1/2}\cos(\varphi_S-\varphi_L) \quad (1.5.3).$$

$g(L,\cos\theta_L,\varphi_L)$ is the leaf angle distribution and θ_L and φ_L are the inclination and azimuth angles of the leaf normal (Nilson, 1971). Several simplifications for $G(r)$ have been developed for different classes of leaf angle distributions assuming azimuthal independence (Table [1.1]).

Table 1.1: G-factor and extinction coefficient approximations for several ideal leaf angle distributions (*as in* Baldocchi, 2012 *after* Anderson, 1966; Campbell and Norman, 1998; Monteith and Unsworth, 1990).

Leaf Angle Distribution	***G***	K_b
Horizontal	$\cos\theta_S$	1
Vertical	$2/\pi \cdot \sin\theta_S$	$2\cdot\tan(\theta_S/\pi)$
Conical	$\cos\theta_S \cdot \cos\theta_L$	$\cos\theta_L$
Spherical	0.5	$1/(2\cdot\cos\theta_S)$
Heliotropic	1	$1/\cos\theta_S$

Building on Nilson's work, Campbell and Norman (1998) used a modified version of the Beer-Lambert-Bouguer law to determine the transmissivity of direct beam light radiation (τ_b), equivalent to the gap probability for direct beam light radiation when black leaf elements are assumed (i.e. no transmittance through leaf elements), through a layer of vegetation as

$$\tau_b(\theta_S) = \exp(-\sqrt{\alpha}\cdot K_b(\theta_S)\cdot L) \quad (1.5.4)$$

where α is the leaf absorptivity which is dependent on the wavelength of interest with α = 0.8 for photosynthetically active radiation (PAR), α = 0.2 for near infrared radiation (NIR), α = 0.5 for total solar radiation, and α = 1.0 for black leaf elements. K_b is the

extinction coefficient for direct beam light radiation defined as the projection of a unit leaf area onto the plane perpendicular to the direction of the light beam (Campbell and Norman, 1998). The extinction coefficient (K_b) and G-factor (G) are thus associated through the following relationship assuming leaf angle azimuthal independence:

$$K_b(\theta_S) = G(\theta_S)/\cos(\theta_S) \quad (1.5.5).$$

The distribution of leaf element inclination angles within a tree crown layer is an important parameter that directly controls the extinction coefficient (Wang *et al*., 2007). There have been several methods developed to describe the relationship between the leaf angle distribution and extinction coefficient. Wang *et al*. (2007) present a detailed description of several methods. Typically, leaf angle distributions are described based on the dominant leaf angle. Common leaf angle distributions include planophile (horizontal leaves dominant), erectophile (vertical leaves dominant), plagiophile (dominant leaves at some oblique angle), and spherical (Table [1.1]). Spherical leaf angle distributions in particular have been found to approximate many actual leaf angle distributions where the frequency of leaf inclination angles is the same as the surface elements of a sphere (Campbell and Norman, 1998).

Campbell (1990) and Campbell and Norman (1998) determined the relationship between a crown extinction coefficient and an elliptical leaf angle distribution (K_{be}) as

$$K_{be}(\theta_S) = \frac{\sqrt{\chi + \tan^2 \theta_S}}{\chi + 1.774 \cdot (\chi + 1.182)^{-0.733}} \quad (1.5.6).$$

In this equation, χ is defined as the ratio of the average projected area of foliage elements on horizontal and vertical surfaces (Campbell and Norman, 1998). The convenience of using an elliptical leaf angle distribution is its inherent ability to represent a range of leaf angle distributions by varying the χ value. For example, a χ value of unity, zero, and infinity approximate a spherical, vertical, and horizontal leaf angle distribution, respectively. Table 15.1 in Campbell and Norman (1998) provides several χ values representative of actual vegetation types.

The previous formulations for the probability of gap through a horizontally homogeneous layer(s) of vegetation can be expanded to represent the gap probability through heterogeneous crowns represented as envelopes of a turbid media. This requires

knowledge of the path length through crown envelopes and the distribution of foliage within the crown envelope. Welles and Norman (1991) calculated the probability ($P_b(\vec{r},\Omega)$) that a beam light ray incident along direction Ω will pass unaltered from outside a crown to a point $\vec{r}$ within a crown for elliptical foliage envelopes as

$$P_b(\vec{r},\Omega) = exp\left[-\int_0^S G(\vec{r},\Omega)\cdot u_L(\vec{r})d\vec{r}\right] \quad (1.5.7)$$

where *S* is the path length through the canopy, $G(\vec{r},\Omega)$ the fraction of foliage area projected towards the radiation source (i.e. Nilson's G-factor), and $u_L(\vec{r})$ is the foliage area per crown volume function. Assuming a constant u_L and $G(\Omega)$ within tree crown envelopes, the integration along the length of the path through tree crowns can be further simplified as

$$P_b(\vec{r},\Omega) = exp\left[-G(\Omega)\cdot u_L \cdot S_j(\vec{r},\Omega)\right] \quad (1.5.8)$$

where $S_j(\vec{r},\Omega)$ is the path length through tree crown *j* along direction Ω to point $\vec{r}$ (Welles and Norman, 1991). Campbell and Norman (1998) provide a similar calculation of the gap probability of beam radiation through heterogeneous crowns utilizing the geometric relationship between the G-factor and extinction coefficient:

$$P_b(\theta_S,\varphi_S) = \exp[-K_{be}(\theta_S)\cdot u_L \cdot S(\theta_S,\varphi_S)\cdot\cos(\theta_S)] \quad (1.5.9).$$

$S(\theta_S,\varphi_S)$ is the path length which is a function of the zenith and azimuth of the angle of incidence.

Foliage is typically not uniformly or randomly distributed within individual tree crowns as [1.5.8] and [1.5.9] inherently assume. Instead foliage clumping occurs over a wide range of scales. Within a forest canopy, individual tree crowns tend to gather around resource rich areas. Several numerical models have used Poisson or Neyman tree crown distributions to simulate this form of clumping (e.g. Chen and Leblanc, 1997). Additionally, leaf elements within individual tree crowns tend to group along branches and whorls. Conifers display a further form of grouping with the tendency of needles to clump along shoots (Campbell and Norman, 1998). Clumping at all scales increases the probability of gap through forest canopies or tree crowns by creating larger openings through which radiation can penetrate to depth. Chen and Leblanc (1997) accounted for clumping at all scales using the clumping index (Ω_C). The clumping index ranges from 0

(highly clumped foliage) to 1 (randomly distributed foliage). Clumping index values greater than unity indicate more uniformly distributed foliage elements within the crown volume. Incorporation of a clumping index into gap probability calculations can account for the influence of foliage clumping on the ability of light radiation to penetrate through individual tree crowns:

$$P_b(\theta_S, \varphi_S) = \exp[-K_{be}(\theta_S) \cdot u_L \cdot S(\theta_S, \varphi_S) \cdot \Omega_C \cdot \cos(\theta_S)] \quad (1.5.10)$$

$$P_b(\vec{r}, \Omega) = exp\left[-G(\Omega) \cdot u_L \cdot S_j(\vec{r}, \Omega) \cdot \Omega_C\right] \quad (1.5.11).$$

1.5.2 Models of Radiative Transfer in Heterogeneous Canopies

Models simulating radiative transfer within tree crowns or vegetation canopies stem from the pioneering work of Ross (1975) which addressed the formulation of equations governing the interaction of optical radiation with homogeneous layers of vegetation. Given the large number of radiative transfer models available, the radiation transfer model intercomparison (RAMI) initiative was developed with the goal of comparing the numerous models available that simulate the radiation fields at the Earth's surface, including homogeneous and heterogeneous vegetation canopies (Pinty *et al.,* 2001; 2004; Widlowski *et al.,* 2007). The basic premise of the majority of models dedicated to simulating radiative transfer in vegetation canopies is the simplification of tree crown foliage as a turbid media (Myneni *et al.,* 1989). This applies whether a canopy is considered a horizontally homogeneous layer or discrete envelopes of foliage elements (Myneni *et al.,* 1989). Within the turbid medium approach, describing the architecture of leaf elements within either a layer or envelope requires three main parameters: leaf area density, leaf angular distribution, and the dispersion of leaf elements within the volume (Myneni *et al.,* 1989).

Many of the models that simulate radiative transfer within tree canopies and crowns use the discrete ordinates method whereby an angular variable is discretized into a smaller number of directions or rays (Myneni *et al.,* 1991). Kimes and Kirchner (1982), Kimes *et al.* (1985), and Kimes (1991) detail the development of a model of radiative transfer through vegetation canopies that simulates a canopy as a three-dimensional grid of cells identified by an X, Y, and Z co-ordinate system. Radiant energy within the

system propagates in a finite number of directions using a spherical co-ordinate system defined by azimuthal and zenithal angular intervals (Kimes, 1991). Radiation propagates through the system until all flux vectors are either absorbed by canopy elements, escape from the canopy, or reach a zero threshold level of flux (Kimes, 1991). Similarly, the Discrete Anisotropic Radiative Transfer Energy Budget (DART EB) model also uses a discrete ordinates method to treat the interaction of solar and TIR radiation with canopy elements (Gastellu-Etchegorry *et al.*, 1996; 1999; 2004; Gastellu-Etchegorry, 2008). One of the difficulties with this treatment of radiative transfer through vegetation canopies is the high computational expense required to process all interactions within a canopy domain. However, this method allows for a more detailed treatment of the total interaction (i.e. absorption, scattering, emission) both within and between crown elements than is possible using the current geometric-optical models.

Geometric-optical models represent forest canopies as assemblages of opaque geometric shapes (cones, spheroids, or ellipsoids). Using parallel-ray geometry, these models use projected areas and shading patterns to determine sunlit and shaded background and foliage proportions based on a sensor and sun position (Strahler and Jupp, 1991). Hybrid geometric-optical radiative transfer models use geometric shapes to represent tree crowns and use radiative transfer concepts to describe the interaction of the radiation field within crowns. Li and Strahler (1985; 1986) describe a three-dimensional geometric-optical model that uses cones to represent conifer tree crowns and estimates the bi-directional reflectance distribution function over a canopy of cone shaped tree crowns. Li and Strahler (1988; 1992) adapted the model of Li and Strahler (1985; 1986) to treat spheroid and elliptical crown shapes. These models rely on two scales of canopy architecture derived as a function of leaf area index and leaf angle distribution, and count density and size of plant canopies. Light interaction within individual tree crowns is modelled using a negative exponential to estimate the probability of gaps along the length of beam path through the crown (Li *et al.*, 1995). Tree crowns can be modelled as any geometric shape assuming proper consideration of the influence on beam path length through crown elements.

Chen and Leblanc (1997) developed a model similar to the two scale model of Li and Strahler (1985; 1986) adapted to use four scales of canopy architecture: tree groups,

tree crowns, branches, and shoots. The resultant 4-Scale model accounts for the complex nature of tree crown surfaces by treating the hotspot and self-shadowing among foliage elements. The result of this complex surface is that sunlit foliage may be viewed on the shaded crown side (side facing away from the sun) and shaded foliage may be viewed on the sunlit crown side (Chen and Leblanc, 1997). Section [2.5.2] and Appendix [A] detail the 4-Scale computations relevant to the current research.

The 4-Scale model uses a series of probabilities to describe the distribution of tree crowns within an area and distribution of foliage within individual tree crown elements rather than the more clearly defined canopy geometry of Li and Strahler's 2-Scale model. Chen and Leblanc (2001) adapted the 4-Scale model to also treat multiple scattering within tree crowns using a series of view factors between sunlit and shaded components and Leblanc *et al.* (1999) adapted the model to treat spheroidal crown shapes. However, since the stated objective of both models is to study the bi-directional reflectance distribution, no attempt is made to account for interaction of crown elements with TIR radiation.

Charles-Edwards and Thornley (1973) and Mann *et al.* (1979) both detail models that simulate the interaction of light radiation with individual tree crowns shaped as ellipsoids or hemi-ellipsoids. Mann *et al.* (1979) considered the additional complexity of intra-crown variable foliage distribution (which Charles-Edwards and Thornley (1973) consider to be uniformly distributed). Similarly, Norman and Welles (1983) developed the General Array Model (GAR) using the same approach as Charles-Edwards and Thornley (1973) to treat radiative transfer in an array of tree crowns but have added the ability for foliage density to be a function of location within a canopy. In this approach, tree crowns are composed of a number of "subcanopies" with the outer envelope defined by an ellipsoid or hemi-ellipsoid (Norman and Welles, 1983). This "weighted random approach" allows for overlapping crowns and random positioning of crowns (Norman and Welles, 1983). Additionally, while foliage within each subcanopy is assumed randomly distributed, each subcanopy can possess a distinct foliage density (Norman and Welles, 1983).

Several numerical models have been developed to specifically simulate the TIR radiation regime within vegetation canopies (e.g. Kimes *et al*., 1981; Smith *et al*, 1997,

Guillevic *et al*., 2003). These models range from relatively simple representations of vegetation canopies as homogeneous layers (e.g. Kimes *et al*., 1981; Smith *et al.,* 1981) to more complex representations as discrete three-dimensional vegetation envelopes or structures (e.g. Kimes and Kirchner, 1982; McGuire *et al*., 1989; Smith *et al.,* 1997; Guillevic *et al.,* 2003). Additionally, individual foliage elements within layers or envelopes have been represented with varying degrees of complexity as statistical assemblages (e.g. Kimes *et al.,* 1981) or discrete objects (e.g. Smith *et al.,* 1997; Otterman *et al.,* 1999). The more advanced models typically account for the non-opaque nature of vegetation, such that a sensor viewing a layer of vegetation will 'see' a mix of canopy foliage and ground, with the most developed models partitioning the two surface types into sunlit and shaded fractions (e.g. Jackson *et al.,* 1979; Verhoef *et al.,* 2007).

Conversely, few numerical models *explicitly* treat tree crown vegetation when modelling radiative transfer in urban environments (i.e. not a tile approach). Krayenhoff *et al.* (2014) describe a multi-layer radiation model that explicitly treats tree crown foliage within and above the urban canyon. However, the representation of tree crowns as layers and restriction to the canyon concept precludes the model from providing built or vegetation temperatures required to populate a three-dimensional sensor view model, such as SUM. DART EB can be used to model the radiative and energetic budget for complex urban scenes with an explicit treatment of tree crowns (Gatellu-Etchegorry *et al.,* 2008). This model can also be used to simulate remotely-sensed images of urban surfaces. However, DART EB's treatment of the TIR radiation field in urban domains with tree crowns remains to be validated (Gastellu-Etchegorry *et al.,* 2008). The computer graphics community is also developing models of radiative transfer in vegetated urban domains (e.g. Overby *et al.,* 2014). Radiative transfer methods such as discrete ordinates or Monte Carlo ray tracing are ideally suited to take advantage of the parallelization offered by conventional CPU processors, such as in view factor computations or treating the radiation field above a surface (Krayenhoff *et al.,* 2014).

Numerical models allow for increased flexibility and manipulation of factors expected to influence the magnitude of effective thermal anisotropy. Additionally there is potential for such models to be inverted in order to obtain surface properties based on surface temperature measurements from several view angles (Kimes, 1981; Paw U,

1992). While a number of sensor view models exist that simulate the thermal anisotropy over vegetation canopies and urban areas, separately, few have attempted to combine the two in order to treat urban surfaces with tree crown elements and none have done so with the specific objective of examining the influence of tree crowns on effective thermal anisotropy magnitude in urban areas.

1.6 Research Questions and Objectives

The overall purpose of this thesis is to examine the influence of tree crowns on brightness surface temperature measured by narrow IFOV TIR remote sensors over urban surfaces. Given the large number of factors that influence effective thermal anisotropy in urban areas, it is not feasible to develop an observational campaign with enough breadth to cover the range of scenarios necessary to isolate and examine the influence of tree crowns.

The paucity of effective urban thermal anisotropy observational campaigns that have included tree crown vegetation makes it difficult to predict how the addition of trees will influence the directional nature of remotely-detected brightness temperature over urban areas. However, it is hypothesized that tree crowns in urban areas will influence effective thermal anisotropy in one of two ways:

1) In urban geometries characterized by low building plan fraction and low canyon aspect ratio, the shadows cast by tree crowns may increase the magnitude of thermal anisotropy due to tree crown shadows generating contrast between opposing sensor view angles. Similarly, tree crown foliage, with surface temperatures generally lower than built facet temperatures and close to air temperature, replaces the view factor previously occupied by built surface facets, which also may increase the magnitude of thermal anisotropy by generating temperature contrasts.
2) Tree crown elements may shade otherwise sunlit built surfaces and consequently reduce the temperature contrast between opposing sensor view angles thereby lowering the magnitude of effective thermal anisotropy.

The present research aims to fill the gap in knowledge regarding the influence of tree crowns on urban thermal anisotropy through the use of a numerical modelling approach.

Specifically, modification of a sensor view model (Soux *et al*., 2004) to include tree crown features addresses the primary research question: *How do tree crowns influence the magnitude of effective thermal anisotropy in urban areas?* This model is hereafter termed the "Vegetated Surface-Sensor-Sun Urban Model" (SUM_{VEG}).

The development of this model will enable a high degree of flexibility when examining the total influence of tree crowns on effective thermal anisotropy in a diverse range of surface geometries and atmospheric forcing conditions. Manipulation of such a tool will also permit investigation of the influence of a number of tree biophysical parameters that would not be feasible in an observational campaign. Effective thermal anisotropy presents a significant bias—on par with atmospheric influences (Voogt and Oke, 1998)—and potential source of error in urban surface temperatures obtained using passive TIR remote sensors. However, information on the angular distribution of upwelling radiance over urban surfaces may provide valuable insight with regards to inferring surface thermal properties and component surface temperatures from remotely-detected temperatures.

Following development of the model, three main research objectives are identified:

1) Validate SUM_{VEG} using directional brightness surface temperature measurements of the Sunset residential neighbourhood of Vancouver, B.C., acquired using a helicopter-mounted TIR camera as part of an observational campaign conducted by Voogt and Oke (1997; 1998).
2) Use the Sunset residential neighbourhood as a case study to investigate the influence of tree crowns on thermal anisotropy for a realistic GIS-based surface geometry with facet temperatures extracted from TIR images.
3) Examine the sensitivity of effective urban thermal anisotropy to tree crown vegetation, as a function of urban form and solar path, for regularly-spaced aligned arrays of block structure buildings representative of typical residential neighbourhood geometries.

The next chapter deals with the model design (Chapter 2), followed by a chapter detailing the testing of the leaf temperature model (Campbell and Norman, 1998) and leaf proportion model (Chen and Leblanc, 1997; 2001) incorporated into SUM_{VEG} (Chapter 3). Chapter 4 presents the results of the SUM_{VEG} full model evaluation as well as a case

study examining the influence of tree crowns on thermal anisotropy magnitude using remotely-detected brightness surface temperature measurements from the Sunset residential area of Vancouver, B.C. Chapter 5 presents the results of the use of SUM_{VEG} to examine the sensitivity of thermal anisotropy to a range of treed residential urban geometries using regularly-spaced, aligned arrays of block structure buildings. Finally, Chapter 6 provides the main study conclusions and discusses further work and potential applications of SUM_{VEG}.

Chapter 2

MODEL DESIGN METHODOLOGY

2.1 General Model Design and Conceptualization

The SUM model of Soux *et al*. (2004) is a numerical model that simulates an urban surface as a three-dimensional assemblage of repeating, identical block buildings separated by equal width streets or alleys. The urban geometry is directly controlled by the user with the individual surface facets comprised of arrays of cubic cells or patches defined by an X, Y, and Z coordinate system and orientation. Surface patches may be classified as wall, roof, street, or alley though any surface type is possible given appropriate temperatures and consideration of influence on view factors. Descriptors that define the surface geometry include the building plan fraction (λ_P), building aspect ratio (*BH/BW*), and canyon aspect ratio (*BH/SW*) where *BH*, *BW*, and *SW* represent the building height, building width, and street width, respectively, all measured in number of patches.

Based on solar geometry (θ_S and φ_S), SUM uses ray tracing techniques to determine the shading patterns within the modelled domain. Using solid angle geometry, SUM calculates the view factor ($\psi_{di,j}$) occupied by each surface patch within a sensor IFOV, projected onto the surface, following a contour integration approach based on Stokes theorem between a finite area (surface patch *j*) and a differential area (sensor *di*). With accurate radiance values to populate the various sunlit and shaded surface patches (L_j), SUM can then estimate a remotely-detected radiance (L_S) for the surface within the sensor IFOV by weighting facets using calculated view factors as

$$L_S = \sum_{j=1}^{n} \psi_{di,j} \cdot L_j \tag{2.1.1}$$

where *n* is the number of component surface patches comprising the surface array. Surface radiance values may be derived from observations, energy budget models, or scale model experiments.

Voogt (2008) added the ability to use GIS-generated surfaces in SUM. While buildings still consist of block structures, GIS-generated surfaces allow for variable building height, building footprint, and street width. However, current versions of SUM are limited due to their inability to treat either ground-level or tree crown vegetation despite their relatively high abundance in urban areas (Oke, 1989) and expected influence on the directional nature of remotely-detected surface temperatures. SUM_{VEG} incorporates the ability to treat tree crowns by simulating individual crown volumes as groupings of cubic cells containing a turbid media. Tree crown dimensions and biophysical parameters (e.g. foliage density and orientation) are directly controlled by the user and the model calculates geometrical relations including the tree height to building height ratio (H_T/BH) and tree crown plan fraction (λ_V). When regular, repeating surface geometries are employed, tree crowns are added along the length of building walls a user specified distance from the wall (d_{bld}) and from adjacent crown edges (T_{spc}). When a GIS-generated surface is used, tree crown locations may be placed anywhere not currently classified as building wall or interior.

This chapter begins by describing the procedure used to add lawn and tree crown vegetation to SUM_{VEG}. Following this the treatment of radiation transfer with tree crown canopies is detailed including the influence on view factors occupied by foliage and surface components within the sensor IFOV. Finally the methodology used to assign temperatures to surface patches is described, including the procedure used to estimate temperatures for surfaces partially shaded from direct solar radiation by tree crown foliage.

2.2 Adding Vegetation to the Modelled Surface

2.2.1 Lawn Surfaces

SUM_{VEG} includes a very simple representation of lawn surfaces as flat, ground level surfaces surrounding modelled buildings on all four sides. For regular repeating arrays of

identical buildings, lawn surfaces extend from the edge of building walls to a user specified distance from building edges with the user able to specify the distance on both the street (LW_A) and alley side (LW_B) (Figure [2.1]). This allows the model to more accurately replicate the general nature of grassed lawns in many urban residential areas, characterized by variable front and back lawn width.

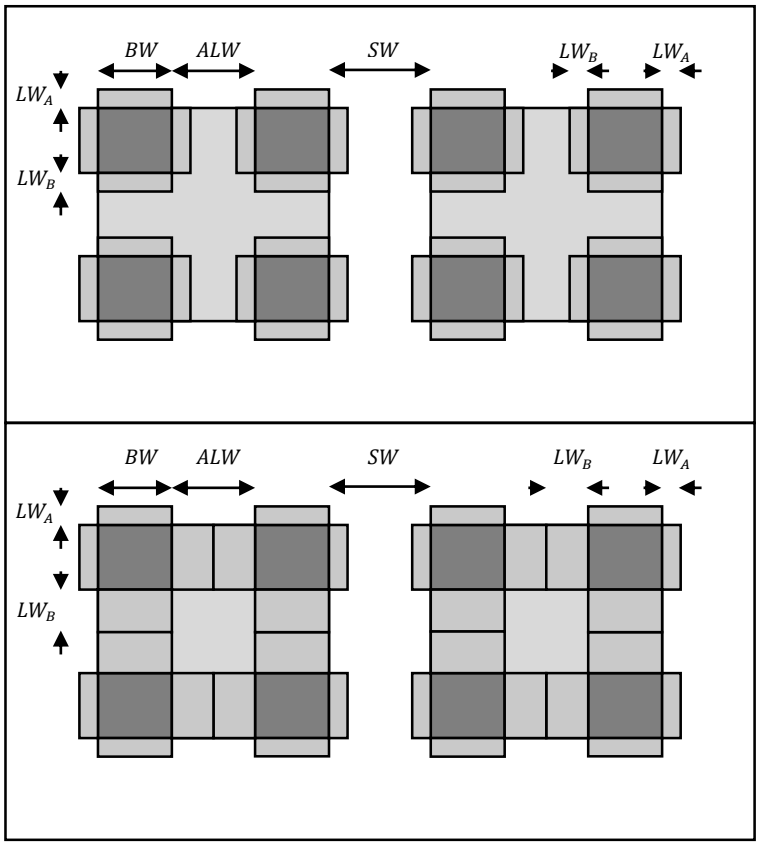


Figure 2.1: Plan area view of two urban surface configurations consisting of a repeating array of block buildings and differentiated by lawn width on the alley side. Buildings are oriented in a block structure with 4 buildings per block.

Lawn surface patches are treated the same as built component patches when calculating view factors. That is, when calculating the view factor occupied by lawn patches within the remote sensor IFOV, lawn surface patches have no effective depth and are either fully sunlit or shaded. In actuality, lawn surface patches with some vertical extent may contain both sunlit and shaded portions depending on the solar and sensor positions. Indeed, short grass surfaces have been found to exhibit effective anisotropy and a hot spot effect (Monteith and Szeicz, 1962; Zhan *et al.*, 2012). Zhan *et al.* (2012) reported thermal anisotropy magnitudes over urban grasses of between 1 and 4K and noted that, while these magnitudes are generally less than those for urban building

components, they also tend to fluctuate more than flat ground (i.e. concrete). They concluded that this is due to the high variability of grass leaf surface temperatures and the micro-scale 3d structure that is not present over flat concrete surfaces. However, the addition of even simple lawn surfaces is expected to increase the applicability of SUM_{VEG}, specifically in urban residential neighbourhoods which often exhibit an abundance of grassed lawn surfaces.

In GIS mode, SUM_{VEG} allows for specification of lawn surfaces on an individual patch by patch basis and can therefore allow a simulated surface to correspond more closely to an actual urban surface. In model evaluation tests utilizing surface temperature data from the Sunset area of Vancouver, B.C., Canada, lawn surfaces are defined as the residual patches at ground level after all building, street, and alley surfaces had been digitized from VanMap[4] images.

2.2.2 Individual Tree Crowns

Tree crowns in SUM_{VEG} do not have trunks or branches and instead consist of groupings of cells that form cuboid shapes based on user specified geometrical parameters (e.g. Figure [2.2]). Tree shape is determined based on inputs of canopy radius (r_C), trunk height (H_{tk}), and tree height (H_T). Different values for trunk and tree height allow the user to control the actual crown height (H_C) (i.e. height of the tree minus the trunk height).

In order to reduce run time, all tree crowns are identical in this implementation of SUM_{VEG}. Calculating the proportion of sunlit and shaded foliage as 'seen' by the simulated remote sensor— necessary for tree crown view factor computation—requires information on tree crown dimensions and the required calculations, and hence computation time, are significantly reduced if all crowns are identical. However, the identical nature of SUM_{VEG} tree crowns means it is important to use a set of crown dimensions representative of the urban surface being simulated.

[4] VanMap images are provided free of charge by the City of Vancouver (http://vancouver.ca/your-government/vanmap.aspx).

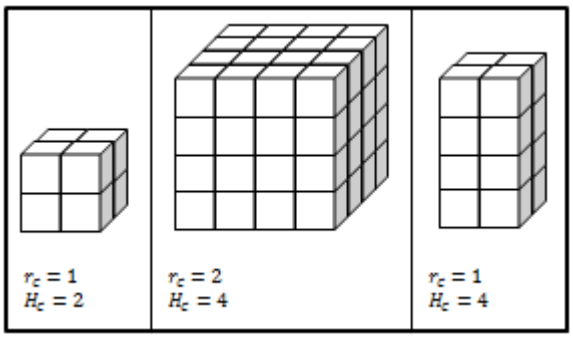


Figure 2.2: Example tree crown shapes possible in SUM_{VEG}. Tree crown shape controlled by r_C and H_C.

Tree crown elements are placed on the edge of streets and along the length of building walls. This is intended to match the most common configuration of urban tree crowns, namely the exclusion of trees from roadways and intersections and presence of trees along the sides of streets (Figure [2.3]). The number of trees within the simulated domain is therefore controlled by the shape of trees, the urban geometry (building width), and the distance between tree canopies as specified by the user. Tree crown plan fraction (λ_V) within simulated urban geometries is calculated as the ratio of number of tree crown patches at the maximum crown height (N_{H_T}) and the total number of patches in a horizontal slice of the entire simulated domain ($N_X \cdot N_Y$):

$$\lambda_V = \frac{N_{H_T}}{N_X \cdot N_Y} \quad (2.2.1).$$

For example, in Figure [2.3], λ_V increases from 0.10 (10%) to 0.23 (23%) by increasing crown radius and decreasing spacing between adjacent crown elements.

When a GIS-generated surface is used, this method of λ_V computation is no longer sufficient since horizontal surface variability will result in a range of tree crown plan fractions depending on the sensor viewing position. Therefore, it is necessary to estimate a λ_V and building plan fraction (λ_P) for the simulated surface within the sensor IFOV. SUM_{VEG} counts the number of tree crown patches at the maximum crown height and roof patches (N_{rf}) within the IFOV as seen by sensor *di*. Subsequently the tree crown and building plan fractions are estimated as the ratio of each count and the total number of horizontal surface cells within the sensor IFOV (N_{hz}) as

$$\lambda_V = \frac{N_{H_T}}{N_{hz}} \quad (2.2.2)$$

and

$$\lambda_P = \frac{N_{rf}}{N_{hz}} \quad (2.2.3).$$

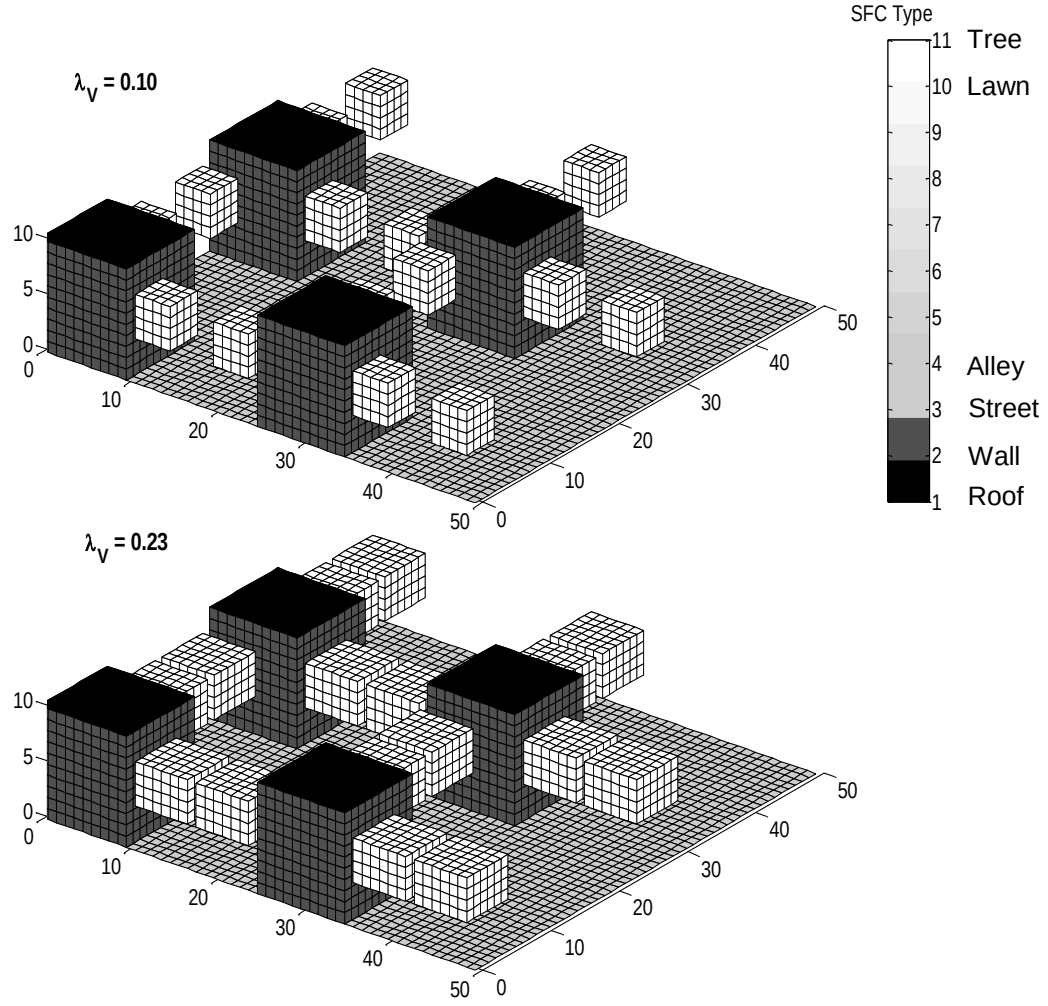


Figure 2.3: SUM_{VEG} modelled urban surface configuration ($\lambda_P = 0.16$) for two tree crown plan fractions. Values indicate SUM_{VEG} surface codes.

Several tree crown biophysical parameters related to the foliage elements are required inputs to the model. These inputs include the foliage area density (μ_L ; m^2 leaf area/m^3 crown volume), the clumping index (Ω_C ; non-dimensional), the maximum leaf element width (f_{width} ; m), and the leaf angle distribution (LAD). These variables

directly control the proportion of foliage within individual crown volumes, and subsequently within the sensor IFOV, as well as the interaction of direct and diffuse solar radiation with tree crown foliage.

In GIS mode, tree crown locations can be individually specified using GIS co-ordinates. In this procedure, tree crowns remain geometrically identical in order to lower computation time. However, the ability to directly specify crown location can allow SUM_{VEG} simulations to more closely approximate actual urban areas. For example, in the Sunset area validation tests, tree crown locations are digitized from VanMap images and subsequently used to create a GIS layer of tree crowns within the Sunset residential area.

2.3 RAY TRACING THROUGH TREE CROWNS

In order to model the interaction of solar and TIR radiation with tree crowns, it is necessary to track the length of the path through tree crown envelopes along the line from the sun and sensor to each surface patch. Specifically, calculation of seen, sunlit and shaded tree crown foliage proportions requires precise information on the path length through tree crowns from both the sensor and solar point-of-view.

2.3.1 Tracing from Sun to Surface Patches

SUM_{VEG} traces a ray from every surface patch to the sun. Tracked rays allow the determination of the shading tendency for each surface patch. For example, if a ray tracked from a surface patch to the sun intersects a building, the surface patch is declared shaded. On the other hand, if the ray from a surface patch to the sun intersects a tree crown, the surface patch is declared 'partially shaded'. The degree of surface patch shading is dependent upon the biophysical properties of the tree crown that intersects the ray path. Detailed accounting of the length of the ray path (S_S) through the tree crown(s) is required to determine the extinction of light before it reaches partially shaded surface patches.

Calculation of a diffuse transmittance coefficient for partially shaded surface patches also requires the tracking of path length through tree crowns. However, since incident downwards diffuse radiation originates from the entire sky hemisphere, it is necessary to track the length of multiple rays through tree crowns in order to integrate the

incoming diffuse radiation over the entire sky. Therefore, SUM_{VEG} divides the upper hemisphere into a number of sky sectors based on user specified azimuth and zenith angular intervals. Subsequently a ray is traced from each partially shaded surface patch to every sky sector. If a tree crown intersects the ray path, the length through the crown is recorded.

2.3.2 Tracing from Sensor to Surface Patches

SUM_{VEG} also traces a ray from every surface patch to the sensor. This ray tracing allows for the classification of surface patches based on their visibility to the sensor. For example, if a ray traced from a surface patch to the sensor is intersected by a building, the surface patch is subsequently declared 'not seen' by the sensor. If the intersecting object is a tree crown, the view of the surface patch will be only partially impeded due to the gap nature of tree crowns. The degree to which the surface patch is obscured from view by the tree crown depends on the probability of gap along the path through the crown, which is a function of the length of path through the crown along a line to the sensor (S_V).

2.4 INTERACTION OF LIGHT WITH HETEROGENEOUS TREE CROWNS

2.4.1 Light Extinction along the Solar Ray Path

As light rays travel from the sun to surface patches, a portion is attenuated by media through which the light passes. When a ray of light hits an opaque built surface such as a building wall or roof, it is fully attenuated. However, gaps within tree crowns allow a portion of direct beam and diffuse radiation to reach unaltered to depth in the crown, visible as sunflecks on the surface that is partially shaded by the tree crown. Since SUM_{VEG} is not an energy budget model, there is currently no attempt to correct for atmospheric attenuation of incoming light radiation or track the receipt of energy within tree crowns. Instead, SUM_{VEG} models the extinction of direct beam and diffuse light radiation by tree crowns in order to determine the relative proportion of radiation that passes unaltered through the crown.

In SUM_{VEG} light attenuation in tree crowns is modelled using a modified Beer-Lambert-Bouguer Law approach that calculates light extinction in envelopes containing a

turbid medium (Campbell and Norman, 1998). Within the model two terms are used to describe the attenuation of light within individual tree crowns. Equation [1.5.6] is used to calculate the light extinction coefficient (K_{be}) for an ellipsoidal leaf angle distribution. The use of an ellipsoidal leaf angle distribution allows Equation [1.5.6] to approximate a range of leaf angle distributions. For the majority of model simulations, a spherical leaf angle distribution is assumed ($\chi = 1$), which is a good approximation for many real tree species (Campbell and Norman, 1998). Additionally, the 'G-factor' (G) of Nilson (1971) uses the mean projection of unit foliage area in a particular direction *r* to describe the attenuation of solar radiation through tree crown envelopes. A G value of 0.5, which approximates a spherical leaf angle distribution indicating independence of off-nadir and azimuth angle, is the SUM_{VEG} default setting used in the majority of simulations.

2.4.2 Probability of Gap in Individual Tree Crowns

K_{be} and G are subsequently used to calculate the gap probability as a function of θ_S and azimuth φ_S angle within individual tree crowns as

$$P_b(\theta_S, \varphi_S) = \exp[-K_{be}(\theta_S) \cdot u_L \cdot S_S(\theta_S, \varphi_S) \cdot \Omega_C \cdot \cos(\theta_S)] \quad (2.4.1)$$

$$P_b(\theta_S, \varphi_S) = exp[-G(\theta_S) \cdot u_L \cdot S_S(\theta_S, \varphi_S) \cdot \Omega_C] \quad (2.4.2)$$

where u_L is the foliage area density and $S_S(\theta_S, \varphi_S)$ represents the path length through the crown along a particular θ_S and φ_S angular direction. Ω_C is the clumping factor, and in this case is an index used to describe the tendency for foliage within individual tree crowns to clump along branches within individual tree crown volumes. For the majority of simulations within this dissertation, a clumping index of unity is assumed, indicating randomly distributed foliage. These calculations describe the potential for direct beam light radiation to pass unaltered through tree crowns. As such, ($1–P_b$) estimates the probability of light being intercepted by tree crown foliage.

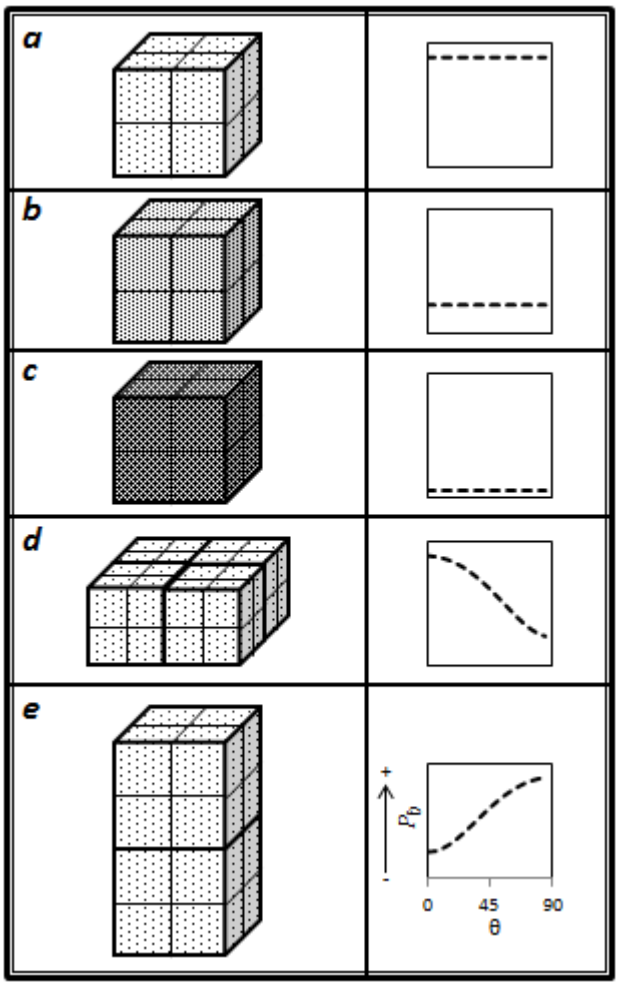


Figure 2.4: Sample of tree crown shapes and the relative influence on gap probability as a function of θ_S. (a), (d), and (e) represent the influence of tree crown shape. (b) and (c) represent the influence of foliage area density (Darker shades indicate increasing u_L).

For simplicity, all tree crowns are assumed to have identical foliage area densities within a given urban configuration. Additionally, no foliage density heterogeneity is simulated within individual tree crowns in order to simplify gap probability calculations. Figure [2.4] illustrates the relative control of tree crown shape on gap probability through individual tree crowns, as a function of incident angle, assuming a spherical leaf angle distribution. It is important to note that, for these simulations, although modelled trees are cuboid shapes, gap probability estimates used for the calculation of foliage proportions assume ellipsoids with equivalent radii (See Section [2.5.2]). When tree crowns are spheres (a), P_b is independent of θ_S since the path length is equal for all θ_S. When tree crowns are wider than they are tall (d), P_b is higher at lower θ_S decreasing with increasing angle. This is due to the increased path length through crowns at higher θ_S. On the other

hand, P_b though tall and thin tree crowns (*e*) is highest at larger θ_S and lowest for small θ_S for the same reason. When the foliage area density is increased (*b* and *c*) for spherical crown shapes, P_b remains independent of θ_S. However, the relative increase in the amount of foliage intercepting area results in a decreased P_b compared to low density foliage crowns.

2.5 LEAF VIEW FACTOR

2.5.1 Equating the Probability of Gap to a Leaf View Factor

In order to estimate a remotely-detected brightness temperature (T_S) for the surface within a remote sensor IFOV, it is necessary to determine the view factor occupied by each surface type to a finite point representing the sensor. SUM_{VEG} does this for each surface patch using a contour integration approach (see Soux *et al*. (2004) for a more detailed description of the view factor computations). This involves computing the view factor occupied by each patch *j* to the differential patch *di,* where the patch *di* is the sensor position.

In order to include tree crowns in the calculation of T_S, it is necessary to determine the view factor occupied by tree crown foliage with the sensor IFOV. However, the gap nature of tree crowns complicates view factor computation. Specifically, tree crowns within the sensor IFOV partially obscure surfaces such that a particular view line may include both tree crown foliage and a portion of the surface underneath. In SUM_{VEG}, the simplifying assumption is made that the portion of view factor occupied by tree crown patch *j* to sensor position *di* is equal to the projection of tree crown foliage upon the underlying surface. SUM_{VEG} does not explicitly calculate the view factor occupied by tree crown foliage within the sensor IFOV. Instead, SUM_{VEG} first computes the view factors for the urban surface without tree crowns elements. Following this, surface patches previously declared 'partially obscured' from sensor view by tree crown foliage are used to approximate the view factor for tree crown foliage based on the degree to which the surface patch is obscured. In this method the total view factor ($\psi_{di,j}$) from patch *j* to sensor position *di* is assumed equal to the sum of the view factor for tree crown ($\psi_{di,jV}$) and the view factor for surface seen through tree crown gaps ($\psi_{di,jS}$):

$$\psi_{di,j} = \psi_{di,jS} + \psi_{di,jV} \quad (2.5.1).$$

SUM_{VEG} uses the probability of gap within tree crowns to weight view factors and determine the relative contribution of tree crowns and surfaces partially obscured by tree crowns to T_S. Equations [2.4.1] and [2.4.2] are modified and subsequently used to determine the relative proportion of ground and tree crown foliage viewed along a line from the sensor to surface patches that intersects one or more tree crowns. In this procedure, $K_b(\theta_S)$, $G(\theta_S)$, θ_S, and φ_S are replaced with their sensor view counterparts, $K_b(\theta_V)$, $G(\theta_V)$, θ_V, and φ_V, in order to estimate the gap probability along a line from the sensor to partially obscured surface patches (P_V); $G(\theta_V)$ remains equal to 0.5 when a spherical distribution of leaf inclination angles is used. Replacing the path length through the crown along a line from the sun to the surface patch (S_S) with the path length through the crown along a line from the sensor to the surface patch (S_V) results in a P_V equal to the proportion of ground seen by the sensor through tree crown gaps. By this logic, (1–P_V) is equal to the proportion of tree crown foliage viewed by the sensor. SUM_{VEG} calculates the view factor for every partially obscured surface patch ($\psi_{di,j}$) as if the patch were not obscured by a tree crown element. The view factor of patch *j* to sensor position *di* is then weighted using P_V to calculate the surface ($\psi_{di,jS}$; Equation [2.5.2]) and tree crown ($\psi_{di,jV}$; Equation [2.5.3]) view factors:

$$\psi_{di,jS} = \psi_{di,j} \cdot P_V \quad (2.5.2)$$

$$\psi_{di,jV} = \psi_{di,j} \cdot (1 - P_V) \quad (2.5.3).$$

This tree crown view factor computation method is based on two primary assumptions: 1) the view factor from an individual leaf to the sensor is directly proportional to the fractional area of the leaf as seen by the sensor and 2) P_V from the sensor position through a tree crown provides a realistic measure of the fraction of foliage 'seen' by the sensor. Colaizzi *et al*. (2010) use similar assumptive reasoning as (1) when estimating the fractions of sunlit and shaded foliage visible to a sensor over a row crop, modelled as continuous ellipses, within a remote sensor IFOV. These fractions are subsequently used to calculate geometric view factors for use in a canopy radiation model (Colaizzi *et al*., 2012). Specifically, when calculating a hemispherical canopy view factor

occupied by a row crop within the IFOV of a downwards facing sensor, Colaizzi *et al*. (2012) note that this is equal to the fraction of canopy visible to the sensor. Similar assumptive reasoning as (2) is used by Chen and Leblanc (2001) for the calculation of multiple scattering within their 4-Scale Geometric Optical model. They use a series of view factors based on the probability of gaps within tree crowns to model multiple reflection events of solar radiation within tree crown elements and to determine estimates of sunlit and shaded foliage based on the sensor and solar geometry. A number of related studies—both modelling and observational—that have investigated the directional variation of radiative surface temperature, have used similar gap probability techniques to characterize the interaction of TIR radiation with tree crown foliage (e.g. Francois *et al.,* 1997; Chehbouni *et al.,* 2001). Based on these simplifying assumptions, the calculation of view factor occupied by tree crown foliage uses the projected area of foliage elements onto the underlying surface along the path from the sensor.

An alternative to this simplified method would be to treat each leaf element as a small patch and run view factor computations for each leaf to the sensor. Such a method would be expected to provide highly accurate view factor estimates. However, this would require detailed information on the number, size, and orientation of every leaf element within all tree crown cells and would be prohibitively computationally intensive. On the opposite end of the spectrum, a very simple method for calculating the view factor occupied by tree crown viewed by the sensor would be to assume solid rectangular shaped crowns and run view factor computation for the patches visible to the sensor. However, this method fails to account for the complex nature of tree crowns that allows sunlit foliage to be viewed on the shaded crown side and shaded foliage to be viewed on the sunlit crown side (Chen and Leblanc, 1997). Additionally, this method would underestimate the view factor for surfaces partially obscured by tree crowns since any surface obscured by tree crown elements would be declared completely ‘not seen’ by the sensor. The current method of view factor calculation based on gap probability and tree crown projected areas is expected to provide a reasonable balance of computational expense and accuracy.

2.5.2 Accounting for the Hot-Spot Effect in Calculation of the Proportions of Seen Foliage

The complex pattern of shading within tree crowns, and deviation between sunlit and shaded leaf surface temperature, further complicates the calculation of T_S by making it necessary to account for the proportion (i.e. view factor) of sunlit (P_T) and shaded (Z_T) leaf elements as 'seen' by a remote sensor. The majority of models that require estimates of the relative proportions of sunlit and shaded leaf foliage viewed by a remote sensor typically rely on a relatively simple approximation that uses solid geometric shapes to represent tree crowns (e.g. Li and Strahler, 1985). The position of the sun and sensor are used to determine the area of the shape surface that is viewed and the patterns of shading on the crown control the proportion of seen, sunlit and shaded foliage. However, these models fail to account for the complex nature of tree crown foliage whereby sunlit foliage may be viewed on the shaded crown side and *vice versa* (Chen and Leblanc, 1997).

SUM_{VEG} uses a modified version of Chen and Leblanc's (1997; 2001) 5-Scale[5] model to determine the relative proportions of sunlit and shaded foliage within individual tree crowns 'seen' at a particular sensor position. 5-Scale is a hybrid geometric optical model that uses a series of probabilities based on tree crown distribution, tree crown dimensions, and biophysical parameters as well as sensor and solar geometry to provide an estimate of P_T and Z_T. This model accounts for both the complex nature of tree crowns and the hot spot effect.

The original model is designed for use in determining the bi-directional reflectance distribution over natural forest canopies. Therefore, estimates of foliage proportions are for a distribution of tree crowns and modifications are required to allow 5-Scale to determine the leaf element proportions on an individual tree crown basis. This is necessary given the sporadic distribution of tree crowns characteristic of urban areas. Appendix [A] details the calculations involved in the modified 5-Scale model incorporated into SUM_{VEG}.

[5] 5-Scale is a combination of 4-Scale and LIBERTY (Dawson *et al.,* 1998) that also accounts for radiative transfer within foliage. This feature is not used in the modified 5-Scale model incorporated into SUM_{VEG}.

It is important to note that, while simulated SUM_{VEG} tree crowns are cubes or cuboids, calculations of seen, sunlit and shaded foliage using the 5-Scale model assume spherical or elliptical tree crown shapes. While it would be possible to modify 5-Scale to calculate these proportions for cuboid tree crowns, this was deemed an unnecessary modification since the majority of real tree crowns are more closely approximated by spherical or elliptical shapes than cuboids. Therefore, the approximations for foliage proportions are expected to be more accurate when simulating actual urban tree crowns with spherical or elliptical crowns. The result of this assumption is a possible slight overestimation of the path length through simulated tree crowns that are subsequently used by the modified 5-Scale model.

The modifications to 5-Scale allow it to calculate P_T and Z_T for an individual tree crown. Since the purpose of 5-Scale is to calculate a bi-directional reflectance distribution, the total viewed surface is assumed to consist of either sunlit and shaded foliage or sunlit and shaded ground such that the sum of all four surface definitions is unity. However, for the purposes of SUM_{VEG}, P_T and Z_T must be redefined as fractions of the total viewed tree crown foliage in order to allow the weighting of tree crown view factors. When normalized, the view factor occupied by tree crown foliage ($\psi_{di,jV}$) can be partitioned into the view factor for sunlit foliage ($\psi_{di,jVs}$) and shaded foliage ($\psi_{di,jVh}$):

$$\psi_{di,jVs} =\cdot \psi_{di,jV} \cdot P_T \quad (2.5.4)$$

$$\psi_{di,jVh} =\cdot \psi_{di,jV} \cdot Z_T \quad (2.5.5).$$

The modified 5-Scale model depends upon the phase angle between the sun and sensor to determine the sunlit and shaded foliage within tree crown patches. In this treatment, a single sensor line-of-sight (LOS) corresponding to the approximate centre of the circular or elliptical projected IFOV, as controlled by the sensor geometry, is used as the sensor angular position for each patch. However, when a sensor with a non-infinitesimal IFOV is used, such as is the case for thermal remote sensing thermometers, assuming a single sensor angular position for each patch may not be appropriate since the actual angle between patches on the peripheral of the IFOV and the sensor may be significantly smaller or larger than the LOS angle. For example, when the sun and sensor are aligned, the hot spot effect causes mostly sunlit foliage or ground to be ‘seen’.

However, if the remote sensor has a relatively large IFOV, tree crowns on the projected IFOV peripheral may actually be viewed at an angle not corresponding to the hot spot.

In order to account for this IFOV dependence, SUM_{VEG} calculates an angular position (θ_V, φ_V) for all surface patches partially obscured by tree crowns along a line to the sensor position. Therefore, rather than use a single sensor angle, each surface patch receives its own θ_V and φ_V relative to the sensor. Subsequently, P_T and Z_T are calculated for tree crowns relative to the patch position within the sensor IFOV projected onto the surface.

2.6 Assigning Radiances to Surface and Tree Crown Patches

2.6.1 General Radiance Assignment

SUM_{VEG} is not an energy budget model and therefore requires input of radiance for each surface type. Current surface types in SUM_{VEG} include: roof, walls, street, alley, intersection, lawn, and tree crown. Additionally, an earlier version of SUM allows for snow cover in model simulations (Nanni, 2010). Based on a surface type declaration and determination of patterns of surface shading using ray tracing methods, SUM_{VEG} assigns a radiance value to every surface within the sensor IFOV. Remotely-detected radiance, computed using Equation [2.1.1], is converted to an equivalent T_S as

$$T_S = \left[\left(\frac{L_S}{1.25x10^{-9}}\right)^{1/4.49}\right] - 273.15 \tag{2.6.1}$$

(Verhoef *et al.*, 1997).

2.6.2 Tree Crown Foliage Radiance Assignment

Radiance values for shaded leaf elements are dependent upon the degree of shading which is a function of location within a tree crown relative to the sun. Thus the degree of leaf shading is expected to increase with depth in the tree crown volume as evidenced by the exponential attenuation of light along a ray path through a tree crown. Calculating the degree of shading for all foliage elements within a crown envelope would be time consuming and computationally expensive due to the use of probabilistic distributions in

SUM_{VEG} such that it is not precisely known where every leaf element is positioned within a crown envelope.

One possible simplification is to create layers within the crown relative to the sun position, with layers deeper in the crown, relative to the solar angle, classified as more shaded then layers 'closer' to the sun. However, this method still suffers from high computational expense. Instead, the modified 5-Scale model of Chen and Leblanc (2001) estimates P_T and Z_T with no separation of the *shaded* foliage category based on the degree of shading. Therefore, in SUM_{VEG}, leaf radiance is simplified through the adoption of two temperature categories: 1) fully sunlit and 2) partially shaded. The model assumes that all partially shaded leaf elements are shaded to the same degree and thus receive the same radiance value. This simplification is necessary due to the use of the 5-Scale model incorporated into SUM_{VEG} which separates foliage into sunlit and shaded categories, also with no separation of shaded foliage based on the degree of shading.

Leaf radiance is also a function of the leaf inclination angle (angle between the sun and normal to the leaf face) such that leaf elements with smaller inclination angles will register higher radiance values than those angled away from the sun's rays (Fuchs, 1990). Within SUM_{VEG} a representative solar radiation incident upon leaf elements is estimated assuming a distribution of leaf inclination angles from 0 to $\pi/2$ with the range of angles separated into equal interval classes. Subsequently, the radiative flux incident upon each class is estimated. A representative radiative flux over all leaf angles is estimated by averaging the radiative flux at each angular class. Sunlit leaf elements are assumed to receive both direct and diffuse radiation while shaded leaf elements receive diffuse and forward scattered direct radiation (See Appendix B).

2.6.3 Partially Shaded Surface Patches

The radiance for surface patches 'partially shaded' from direct solar radiation by tree crown foliage will be between the two extremes of sunlit surface (maximum) and shaded surface (minimum), specific to each surface type. This is due to the gap nature of tree crown foliage that, unlike opaque structures such as buildings, allows a portion of the incoming solar radiation to pass unaltered to the underlying surface (hence 'partially shaded'). For example, a modelled road surface patch partially shaded by a tree crown

will have a radiance value somewhere between the sunlit and shaded road surface radiance.

Since SUM_{VEG} is not an energy budget model, it does not calculate a radiance value for each patch partially shaded from direct solar radiation through solution of the energy budget. This means that temperatures for these surfaces must be provided from observations or energy budget models. However, since few urban energy budget models explicitly treat tree crown vegetation, a weighting routine has been added to SUM_{VEG} that estimates radiances for partially shaded surface patches by weighting between the sunlit and shaded values. Sunlit and shaded surface radiance values are weighted based on the probability of gap through tree crowns to all partially shaded surface patches. Two tree crown gap probabilities are used: 1) the probability of gap for direct shortwave beam radiation and 2) the probability of gap for diffuse shortwave radiation.

The gap probability for direct beam shortwave radiation is calculated for partially shaded surface patches using Equation [1.5.10] and/or [1.5.11]. Incident diffuse radiation originates from all directions and therefore calculating the transmission coefficient for diffuse radiation (P_d, equal to the gap probability for diffuse radiation when leaf elements are assumed black) through a tree crown requires integration over all sky sectors (Equation [2.6.2]; *adapted from* Campbell and Norman, 1998):

$$P_d(\theta) = 2 \cdot \int_{\theta=0}^{\pi/2} P_b(\theta_S) \cdot \sin(\theta) \cdot \cos(\theta)\, d(\theta) \qquad (2.6.2).$$

In this formulation, the diffuse transmittance coefficient is assumed independent of azimuth angle and the diffuse radiation can be thought of as an individual beam originating from every sky sector. In SUM_{VEG} numerical integration is used to estimate a diffuse radiation gap probability, calculated on an individual patch basis as the gap probability for diffuse radiation integrated over all off-nadir angles from 0 to $\pi/2$ and averaged over all azimuth angles from 0 to 2π. Equation [2.6.2] is extended to treat heterogeneous tree crowns with the use of direct beam gap probabilities through individual crown volumes.

The hemisphere for this calculation is divided into contiguous azimuthal and off-nadir angular intervals creating a number of sky sectors similar to the procedure of Abraha and Savage (2010). Increasing the number of sectors by decreasing the sector

angular interval increases computation time. This necessitates finding a balance between the number of intervals and the resultant computational requirements. Abraha and Savage (2010) divided the sky hemisphere into 24 azimuth and 5 off-nadir angles of 15° each, for example. By default, SUM_{VEG} divides the hemisphere into 35 azimuthal intervals of 10° and 30 off-nadir angular intervals of 3° each. SUM_{VEG} subsequently traces a ray from each partially shaded surface patch to every sky sector. In this manner, diffuse radiation is treated as a number of beams emanating from all sky sectors to each partially shaded surface patch.

Since the purpose of this calculation is to estimate a surface radiance for partially shaded surface patches, there is no need to estimate a diffuse radiation gap probability for surface patches that are not shaded by tree crowns. If no surface (e.g. tree crown, building, etc.) is intersected along a particular path, the beam radiant energy from that sky sector is assumed to be fully transmitted to the surface patch (e.g. Figure [2.5] sky sectors A and B). This results in a diffuse transmittance (P_d) from that particular off-nadir angle calculated as

$$P_d(\theta) = 2 \cdot \sin(\theta) \cdot \cos(\theta) \qquad (2.6.3).$$

(Campbell and Norman, 1998). If a tree crown is hit along the ray path to a sky sector, the path length ($S_d(\theta, \varphi)$) through the crown is recorded and used to calculate a beam gap probability (e.g. Figure [2.5] sky sector C). This results in a beam gap probability less than unity and the resultant diffuse transmittance probability is calculated as

$$P_d(\theta) = 2 \cdot P_b(\theta) \cdot \sin(\theta) \cdot \cos(\theta) \qquad (2.6.4).$$

If leaf elements are assumed ‘black’, thereby attenuating all incident radiation, the diffuse transmission through a crown is equivalent to the probability of gap along the ray path through the crown volume. The use of these equations to estimate a diffuse gap probability is contingent on the assumption that the fraction of diffuse radiation transmitted through a crown is equivalent to the fraction of sky hemisphere visible through tree crown gaps (Canham, 1988).

To simplify, if a particular ray path from a partially shaded surface patch to a sky sector intercepts a building feature, the diffuse irradiance from this sector is assumed to be fully transmitted to the surface patch (i.e. as if no building were present). Computation

of the actual diffuse radiation originating from such sectors requires information on both the incoming diffuse radiant energy as well as the radiative properties of building surfaces. This adds a further layer of model complexity that is unnecessary for the intended application of SUM_{VEG}. Should SUM_{VEG} ever be modified to solve the energy budget for surface patches, this assumption may require reconsideration.

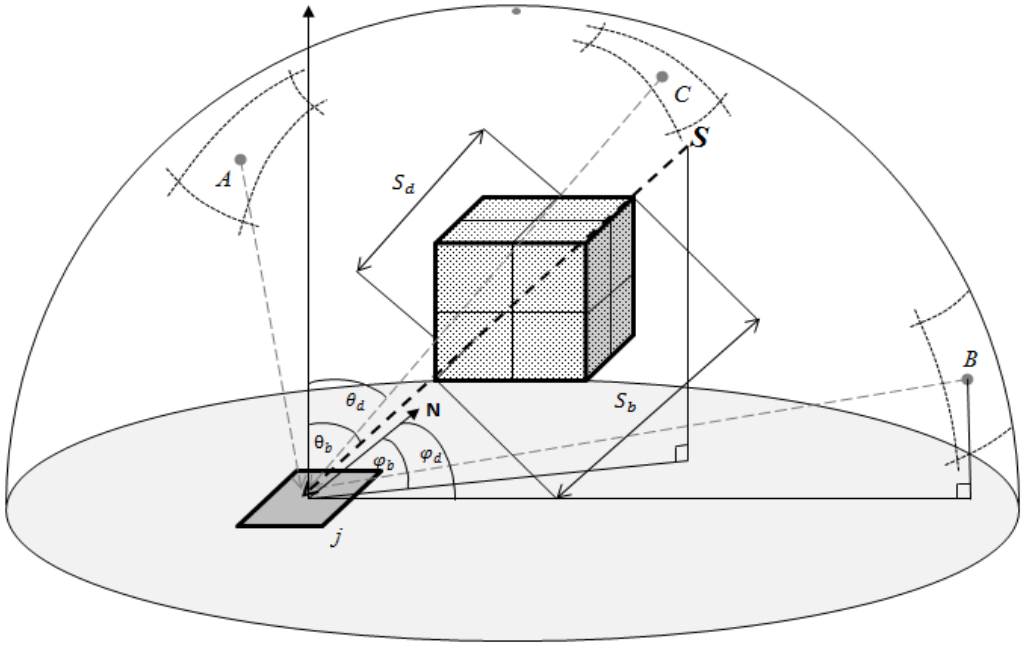


Figure 2.5: Representation of SUM_{VEG} direct and diffuse solar radiation gap probability calculation method. The upper hemisphere is divided into sky sectors based on azimuthal and off-nadir angular intervals. For direct radiation, a single ray is traced from the solar position (*S)* to partially shaded patch *j*. For diffuse radiation, a ray is traced from every sky sector to *j*. Both transmittance calculations require tracking path length through tree crowns (Cube in centre of hemisphere). 'N' indicates North. See text for other variable descriptions.

As well as determining the direct and diffuse transmittance coefficients for each partially shaded surface patch, the relative fraction of both direct (b_{frac}) and diffuse radiation (d_{frac}) to each surface patch is required. If leaf temperatures are calculated, these proportions are estimated from the ratios of the magnitude of downwards diffuse and direct radiation to the total downwelling shortwave radiative flux.

If leaf temperatures are input, the absolute values of direct and diffuse radiation are no longer required and SUM_{VEG} instead approximates diffuse and direct radiation fractions as a function of solar geometry and based on the atmospheric conditions (Campbell and Norman, 1998). The fraction of total radiation that is diffuse is calculated

using an empirical relationship identified by Liu and Jordan (1960) and modified for use within SUM_{VEG}:

$$I_d = 0.3 \cdot (1 - {\tau_{atm}}^m) \cdot I_{po} \cdot \cos\theta_S \quad (2.6.5)$$

where I_d is the magnitude of diffuse radiation received at the Earth's surface and is a portion of the extraterrestrial flux density (I_{po}). In order to estimate a *relative* proportion of diffuse radiation, I_{po} is assumed equal to unity. Therefore the ratio of the diffuse radiation and extraterrestrial radiation represents the relative fraction of diffuse radiation as a function of θ_S. Subsequently, the direct beam fraction is calculated as (1–d_{frac}). τ_{atm} and *m* represent the atmospheric transmittance and optical mass number, respectively. Typical values of atmospheric transmittance for clear days range between 0.6 and 0.7 (Gates, 1980). Atmospheric transmittance values less than 0.4 typically represent overcast sky conditions (Campbell and Norman, 1998). In SUM_{VEG} clear sky and overcast conditions use atmospheric transmittance values of 0.7 and 0.3, respectively. All of the subsequent simulations within this thesis use clear sky conditions. Such conditions enhance differences in solar insolation between sunlit and shaded surface components and are expected to maximize effective anisotropy The optical mass number is calculated as a function of P_a and θ_S from

$$m = \frac{P_a}{101.3 \cdot \cos\theta_S} \quad (2.6.6)$$

which works well for $\theta_S < 80°$ when refraction effects in the atmosphere can be neglected with minimal impact (Campbell and Norman, 1998).

The radiance (L_j) for every partially shaded surface patch (*j*) is subsequently calculated as

$$L_j = L_{MIN_j} + [\left(L_{MAX_j} - L_{MIN_j}\right) \cdot \left(\left(d_{frac} \cdot P_d\right) + \left(b_{frac} \cdot P_b\right)\right)] \quad (2.6.7)$$

where L_{MAX_j} and L_{MIN_j} are the maximum (sunlit) and minimum (shaded) radiance, respectively, for surface patch *j* and are dependent on surface type. The resultant calculated radiance will fall between the maximum and minimum extremes, with the weighting controlled by the relative fractions and gap probabilities for direct and diffuse radiation. Appendix [B] presents results for the evaluation of the partially shaded surface temperature algorithm incorporated into SUM_{VEG}.

2.6.4 Summary of SUM_{VEG} Remotely-Detected Radiance Calculation

Incorporation of tree crown elements into SUM_{VEG} using the preceding methodology results in three possible general categories of surface patches to consider when calculating the sensor-detected radiance for patch *j* (L_{S_j}). Firstly, if a patch *j* is not partially shaded from the sun and not partially obscured from the sensor view by tree crown elements, the original SUM weighting of radiance to surface patch view factor ($\psi_{di,j}$) is used:

$$L_{S_j} = L_j \cdot \psi_{di,j} \tag{2.6.8}$$

where L_j is the patch radiance dependent upon surface type and shading class. Secondly, if a surface patch is partially shaded from the sun but not obscured by tree crown from the sensor, [2.6.8] is modified to use radiance values for partially shaded surface patches calculated using [2.6.7] and the view factor occupied by the patch does not change.

Lastly, if a surface patch is partially shaded from the sun and partially obscured from the sensor by one or more tree crown elements, the patch essentially contributes three separate weighted radiance values which sum to provide L_{S_j}: 1) the weighted radiance of the partially shaded surface seen through gaps in the tree crown by the sensor (Equation [2.6.9]), 2) the weighted radiance of sunlit foliage (Equation [2.6.10]), and 3) the weighted radiance of shaded foliage (Equation [2.6.11]):

$$L_{S_{j1}} = L_{j1} \cdot \psi_{di,jS} \tag{2.6.9}$$

$$L_{S_{j2}} = L_{j2} \cdot \psi_{di,jVs} \tag{2.6.10}$$

$$L_{S_{j3}} = L_{j3} \cdot \psi_{di,jVh} \tag{2.6.11}$$

where $\psi_{di,jS}$, $\psi_{di,jVs}$, and $\psi_{di,jVh}$ represent the view factor occupied by surface seen through crown gaps, sunlit foliage, and shaded foliage, respectively.

2.7 SUMMARY OF MODEL METHODOLOGY

In summation, SUM_{VEG} is a vegetated sensor view model that treats either relatively simple surface geometries comprised of regularly-spaced, block structure buildings surrounded on all sides by tree crowns or more complex GIS-based surfaces with variable building footprint, height, spacing, and tree crown placement. Tree crowns are represented as cuboid shapes containing a turbid medium with crown dimensions and foliage biophysical parameters controlled by the user. Any combination of tree crown shape and foliage parameters is possible within the current build framework.

Radiation transfer through tree crown foliage is approximated using a gap probability approach. The hot spot effect and complex nature of tree crowns is accounted for by incorporation of a modified 5-Scale model to estimate sunlit and shaded foliage proportions based on surface-sensor-sun geometrical relations (Chen and Leblanc, 1997; 2001). Subsequently, gap probabilities are used to weight view factors occupied by foliage and surface patches within the sensor IFOV. Additionally, gap probabilities for direct beam and diffuse solar radiation are used to weight temperatures for surface patches partially shaded from direct solar radiation by tree crown foliage. Sunlit and shaded leaf surface temperatures are estimated using the leaf temperature model of Campbell and Norman (1998), modified to approximate temperatures for leaf elements with a distribution of inclination angles from 0 to $\pi/2$. The following chapter deals with the validation and testing of the modified leaf surface temperature and proportion routines incorporated into SUM_{VEG}.

Chapter 3

TESTING THE LEAF SURFACE TEMPERATURE AND PROPORTION SUB-MODELS

This chapter deals with the main modifications to the SUM model of Soux *et al*. (2004) that allows it to treat tree crowns when investigating thermal anisotropy for treed urban surfaces (i.e. SUM_{VEG}). Two important additions are made: a leaf temperature model to calculate sunlit (T_{ls}) and shaded leaf surface temperatures (T_{lh}) and a leaf proportion model to estimate P_T and Z_T based on solar-sensor-surface geometry. These sub-models provide the two primary sources of information for tree crown foliage required by SUM_{VEG} to estimate T_S for the surface within a remote sensor IFOV: 1) view factors occupied by sunlit and shaded foliage components and 2) T_{ls} and T_{lh}.

The leaf temperature model is adapted from Campbell and Norman (1998) and is based on the humid operative temperature. It includes modifications in an attempt to scale up from a single leaf temperature to temperatures representative of the sunlit and shaded leaf elements within an individual tree crown that have a distribution of leaf inclination angles. The leaf proportion routine is a modified version of the 5-Scale model of Chen and Leblanc (1997; 2001) that estimates foliage proportions for an individual tree crown rather than a forest canopy.

The leaf temperature model is evaluated using temperatures derived from TIR images for three dates and two locations: 1) TIR images of *Parthenocissus tricuspidata* (Boston ivy) and *Metasequoia glyptostroboides* (dawn redwood) acquired on May 30th, 2013 and June 3rd, 2013 on the Western University, Ontario campus and, 2) airborne TIR images of the Sunset residential neighbourhood of Vancouver, B.C. acquired on August 17th, 1992 as part of an observational campaign conducted by Voogt and Oke (1997; 1998). The purpose of this evaluation is to determine whether the leaf temperature model

can provide leaf surface temperatures, in lieu of measurements, for the assessment of thermal anisotropy.

The 5-Scale model has previously been validated and shown to compare well with measurements of bi-directional reflectance distributions over forest canopies (e.g. Chen and Leblanc, 2001; Leblanc *et al*., 1999, White *et al*., 2002). The modified 5-Scale model—incorporated into SUM_{VEG}—is investigated based on its ability to follow expected trends in foliage proportions as a function of a number of tree crown biophysical parameters. While these tests do not constitute an evaluation of the modified 5-Scale model, when combined with the SUM_{VEG} full model evaluation in Chapter 4 they instill confidence in the potential of the model to provide reasonable estimates of leaf proportions in an urban environment.

3.1 LEAF SURFACE TEMPERATURE MODEL TESTS

3.1.1 Leaf Temperature Model Evaluation with TIR images of Boston ivy and dawn redwood

In the following tests, the SUM_{VEG} leaf temperature model is only evaluated for clear sky situations and for a relatively small sample size of meteorological conditions. However, thermal anisotropy is expected to be maximized under clear sky conditions when the contrast between sunlit and shaded urban facets is highest. All subsequent full SUM_{VEG} tests within this thesis use forcing data acquired from days characterized by minimal cloud cover. Therefore, validation under clear sky conditions is the most relevant for the current research.

Thermal Imaging of Sunlit and Shaded Leaf Elements

The leaf temperature model in SUM_{VEG} is evaluated upon its ability to replicate T_{ls} and T_{lh} extracted from TIR images of Boston ivy and dawn redwood leaves (e.g. Figure [3.1]). Images were acquired on June 3rd, 2013 for both vegetation types and May 30th, 2013 for dawn redwood using an FLIR A320 Tempscreen TIR camera developed by FLIR Systems, Inc. This camera operates in the 7.5–13µm spectral range with a measurement accuracy of ±2°C and 25° x 18.8° FOV (1.36 mrad IFOV). It has a thermal

sensitivity of <0.05°C at +30°C and operating temperature range of -15°C to +50°C. The resultant TIR images have a resolution of 320 x 240 pixels. Several TIR images were acquired for both plant species from various viewing positions with the camera positioned on the roof of Talbot College on the campus of the Western University, Ontario. Both measurement dates are characterized by clear skies and low θ_S with images acquired from 10:28am–10:38am (EDT; May 30th, 2013) and 12:54pm–1:02pm (EDT; June 3rd, 2013).

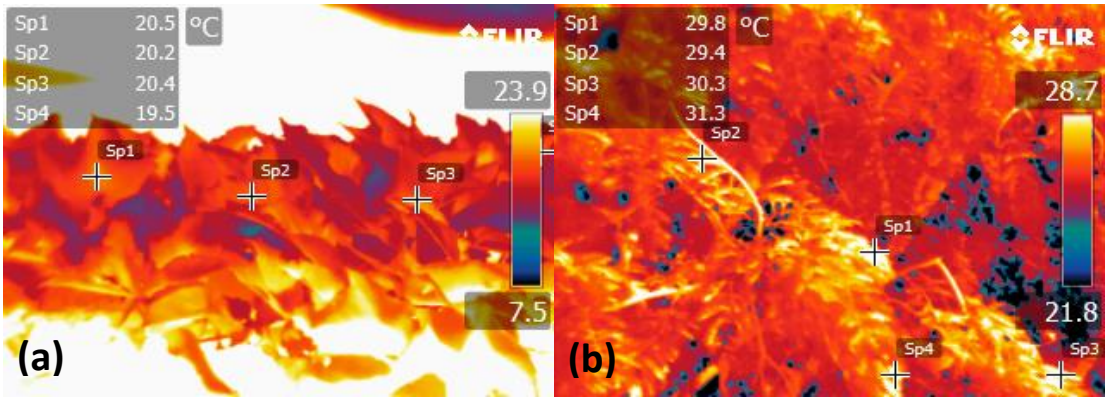


Figure 3.1: Example TIR images of (a) Boston ivy (June 3, 2013) and (b) dawn redwood (May 30, 2013) from which sunlit or shaded leaf surface temperatures are extracted. Points indicated by Sp(#) indicate pixels chosen to represent sunlit leaf elements.

The leaf temperature model estimates the kinetic leaf surface temperature based on solution of the leaf energy budget. The FLIR A320 operates on the Stefan-Boltzmann Law equating the amount of TIR radiation (7.5–13 µm) originating from surfaces within the instrument IFOV, and subsequently absorbed by the thermal camera sensing element, to a radiometric surface temperature. Therefore, when evaluating the leaf temperature model using temperatures extracted from TIR images, it is necessary to account for atmospheric and emissivity influences on leaf surface temperature.

Leaf surfaces are not perfect emitters in the thermal infrared spectral range with an emissivity less than unity. Thus, image pixel values include thermal radiation emitted from leaf elements yet also incorporate radiation from ambient sources reflected by leaf surfaces. Additionally the volume of air between the sensor and leaf surface absorbs and re-emits a portion of the radiant flux, emitted from leaf surfaces, towards the sensing element. Inclusion of reflected radiation and radiation emitted from the volume of air between the camera and leaf elements, if not properly accounted for, may lead to error in the estimation of leaf surface temperature. For example, if air temperature is lower than

leaf element surface temperature, radiation originating from the air volume and reflected by leaf elements towards the thermal camera will result in a lower sensed radiometric leaf surface temperature than the true value.

Post processing of TIR imagery using FLIR software corrects for this potential bias. This requires precise knowledge of the distance from the camera to the objects of interest, estimates of leaf emissivity, and accurate measurement of air temperature during imaging. While an emissivity specific to Boston ivy and dawn redwood leaf surfaces could not be found, a value of 0.97 is assumed based on common values for similar tree species (Campbell and Norman, 1998). Inclusion of these parameters allows the FLIR software to make an estimate of leaf temperature as

$$U_{tot} = \left[\varepsilon_L \tau_{atm} U_{obj}\right] + \left[(1-\varepsilon_L)\tau_{atm} U_{refl}\right] + \left[(1-\tau_{atm})U_{atm}\right] \qquad (3.1.1)$$

where U_{obj}, U_{refl}, U_{atm}, and U_{tot} are the voltages representing the incoming radiation components; specifically, emission by the object (i.e. leaf elements), reflection by the object of ambient source radiation, emission by the atmosphere, and total scene radiance, respectively (FLIR Systems, 2012). ε_L and τ_{atm} represent the leaf emissivity and atmospheric transmittance, respectively. Voltages are calculated by the software as the product of radiant flux density (Wm^{-2}) and an instrument specific constant. Equation [3.1.1] is rearranged to solve for U_{obj}. U_{obj} is then used to provide an estimate of radiometric surface temperature based on the Stefan-Boltzmann law. Processed images are displayed using FLIR R&D software. Several pixels on each image, visually chosen to represent sunlit or shaded leaf elements, are subsequently used to determine image averages of T_{ls} and T_{lh}.

Comparison of Modelled and Measured Leaf Surface Temperature

Talbot College hosts an experimental green roof assembly that provides 5 minute averages of several measured meteorological parameters required as input by the SUM_{VEG} leaf temperature model, including: air temperature (T_a), downwelling shortwave (K_{dn}) and longwave (L_{dn}) radiation, relative humidity (RH), and wind speed (U_a).

Measurements of T_a are used to estimate a saturation vapour pressure (e_s) as

$$e_s = 0.611 \cdot \ exp((17.502 \cdot T_a)/(T_a + 240.97)) \qquad (3.1.2)$$

(Campbell and Norman, 1998). Measurements of relative humidity and estimates of e_s are used to calculate a water vapour pressure (e_a), where $e_a = (RH \cdot e_s)/100$. Air pressure (P_a) is assumed equal to concurrent observations from the London International Airport.

The leaf temperature model requires a characteristic dimension (d), defined as the length of the object in the direction the wind is flowing (Campbell and Norman, 1998). Determining this value for leaf shapes is difficult given the variation of width along the length of the leaf. Campbell and Norman (1998) note that for forced convection, the characteristic dimension is computed as

$$d = \left\{ \frac{\int_0^{f_{width}} d(y) \cdot dy}{\int_0^{f_{width}} \sqrt{d(y)} \cdot dy} \right\} \tag{3.1.3}$$

where *d(y)* indicates the variation in leaf width along the length *y* of the leaf. For the estimation of the characteristic dimension for Boston ivy and dawn redwood, it is assumed that leaf elements are shaped like intersecting parabolas. Based on this simplifying assumption, the characteristic dimension can be approximated as $d = 0.72 \cdot f_{width}$ (Campbell and Norman, 1998), where f_{width} is the leaf element maximum width. Leaf samples were collected for both tree species and their maximum width recorded to determine an average species specific representative leaf element width; these widths are subsequently used to calculate the characteristic dimension for each tree species.

Stomatal conductance for water vapour is a measure of the ability of leaf elements to diffuse water vapour through stomatal pores and is controlled by the leaf surface boundary-layer and concentration gradient of water between the leaf and surrounding air layer (Campbell and Norman, 1998). Calculation of g_{vs} is difficult and time consuming and requires precise information on stomatal density and size (Campbell and Norman, 1998). g_{vs} measurements are not available so this parameter must be estimated for the tree species in question. Table 7.2 in Campbell and Norman (1998) provides g_{vs} values for open and closed stomata for several plant species. Based on the common values provided in Campbell and Norman (1998), a range of *reasonable* g_{vs} values were tested and the value chosen that offers the closest fit to the leaf surface temperatures derived from the TIR imagery. This best fit selection was only attempted after all other necessary parameters were determined in order to minimize bias resulting from its selection.

Resultant g_{vs} match values characteristic of closed stomata, with $g_{vs} < 0.01$mol m^{-2} s^{-1} (Campbell and Norman, 1998). Indeed, a stomatal conductance of approximately 0.001mol m^{-2} s^{-1} offered a reasonable fit for the majority of TIR extracted sunlit and shaded leaf surface temperatures for both tree species and on both dates. This value for stomatal conductance is low, even for closed stomata, and suggests that the best fit methodology may be aggregating errors in the stomatal conductance term. However, only relatively substantial changes in g_{vs}—such as the difference between open and closed stomatal conductance—results in significant changes in modelled sunlit and shaded leaf temperatures. For example, increasing and decreasing g_{vs} one order of magnitude (i.e. $g_{vs} = 0.01$ mol m^{-2} s^{-1} and $g_{vs} = 0.0001$ mol m^{-2} s^{-1}) results in less than a 1% difference between modelled T_{ls} and T_{lh} with g_{vs} equal to 0.001 mol m^{-2} s^{-1}. The influence on remotely-detected brightness temperature is negligible.

Table [3.1] lists the parameters, required by the model, and their corresponding range as used for the calculation of leaf temperatures for the two measurement periods.

Table 3.1: Inputs used in the leaf temperature model to estimate T_{ls} and T_{lh}. Values in a range indicate slight variation during the time of imaging.

Vegetation Type	**DAWN REDWOOD**		**BOSTON IVY**
Date	30/05/2013	03/06/2013	03/06/2013
Time (EDT)	10:28am–10:38am	12:54pm–1:02pm	12:54pm–1:02pm
RH (%)	63.14–63.56	51.64–53.87	51.64–53.87
$\boldsymbol{e_a}$ $\boldsymbol{(kPa)}$	2.04–2.13	0.78–0.81	0.78–0.81
$\boldsymbol{T_a}(°\boldsymbol{C})$	25.3–25.9	13.0–13.1	13.0–13.1
$\boldsymbol{K_{dn}}(\boldsymbol{Wm^{-2}})$	653–764	982–989	982–989
$\boldsymbol{L_{dn}}(\boldsymbol{Wm^{-2}})$	385–401	299–300	299–300
$\boldsymbol{U_a}(\boldsymbol{ms^{-1}})$	1.3–1.7	1.9–2.3	1.9–2.3
$\boldsymbol{P_a}(\boldsymbol{kPa})$	99	101	101
$\boldsymbol{g_{VS}}$ $(\boldsymbol{molm^{-2}s^{-1}})$	0.001	0.001	0.001
***d* (m)**	0.0216		0.0612
$\boldsymbol{\alpha_L}$ | $\boldsymbol{\varepsilon_L}$	0.20 | 0.97		0.20 | 0.97

Figure [3.2] presents the comparison between leaf surface temperatures extracted from TIR images and those estimated using the SUM_{VEG} leaf temperature model. The leaf temperature model is able to predict both T_{ls} and T_{lh} with high accuracy and precision. In

particular, the modelled T_{lh} estimates are highly correlated ($r^2 = 0.99$) with observations (Figure [3.3]). Net absorbed radiation and air temperature are the main controls on the modelled surface temperatures. Thus, precise knowledge of these terms is required in order to have confidence in modelled leaf surface temperatures. There is a general tendency for the leaf surface temperature model to slightly underestimate T_{ls} with a mean absolute error (*MAE*) of 2.27°C (Table [3.2]). In nature, leaf surface temperature responds quickly to changes in forcing conditions such as insolation, wind speed, vapour pressure deficit, etc (Jones, 1999). The model uses 5 minute averages of forcing conditions that may smooth fluctuations to which leaf elements respond. This may explain the inability of the model to resolve the variations in leaf surface temperature between images acquired within a short time frame.

The difference between sunlit leaf temperatures extracted from images taken within a short time period of the same plant species is also potentially the result of variation in leaf inclination angle relative to the solar zenith angle. Leaf elements oriented perpendicular to the incoming solar rays will register a higher apparent temperature than leaf elements whose normal is at a larger angle from the θ_S. This is evident in the variation in TIR derived T_{ls} from image 12 to 16 (Figure [3.2]). Over the time period that these TIR images were acquired, only minimal variation in the meteorological variables—required as input to the leaf surface temperature model—were observed. Thus, the modelled T_{ls} are approximately constant around 16.9°C. However, temperatures extracted from these TIR images show large variation in T_{ls} up to a maximum difference of 5.55°C.

Preferably, validation of the leaf temperature model would use a sample of sunlit leaf temperatures over all inclination angles from 0 to $\pi/2$. However, when extracting leaf surface temperatures from the TIR images, no attempt was made to sample a representative range of leaf inclination angles relative to the sun position. As a result, a bias in the sample will introduce bias into the evaluation. This is expected to underestimate the surface temperature of leaf elements oriented perpendicular to the sun and overestimate the temperature of leaf elements oriented parallel to the solar rays.

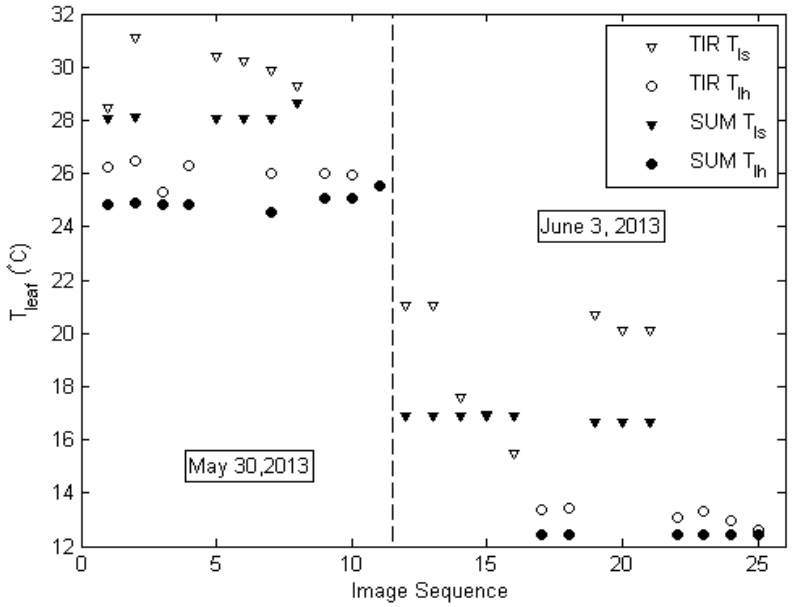


Figure 3.2: Comparison of T_{ls} and T_{lh} derived from TIR images of Boston ivy and dawn redwood acquired on May 30, 2013 and June 3, 2013 and the those estimated using the SUM_{VEG} leaf temperature model. Images are numbered chronologically.

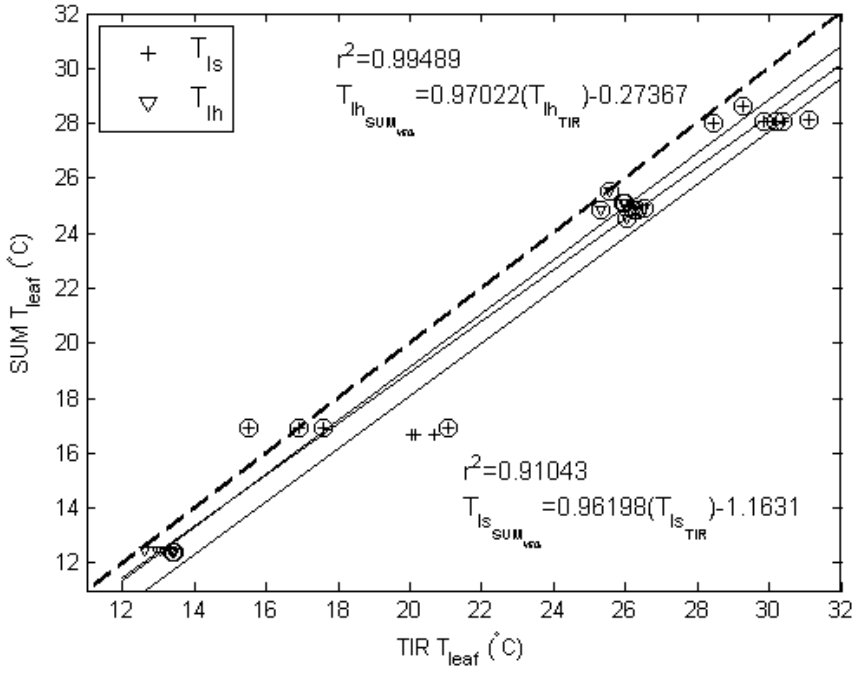


Figure 3.3: Linear regression of T_{ls} and T_{lh} derived from TIR images of Boston ivy and dawn redwood acquired on May 30, 2013 and June 3, 2013 and estimated by the SUM_{VEG} leaf temperature model. Symbols representing dawn redwood temperatures are circled. The dashed line indicates the 1:1 line.

Table 3.2: Time and date information for TIR images acquired on the roof of Talbot college and statistics for modelled leaf temperatures. Plant species A and B represent dawn redwood and Boston ivy, respectively.

Image	Date	Time (EDT)	ΔT_{ls} (°C)*	ΔT_{lh} (°C)	Plant Species
1	30/05/2013	10:28am	-0.44	-1.41	A
2	30/05/2013	10:32am	-2.99	-1.60	A
3	30/05/2013	10:33am	—	-0.49	A
4	30/05/2013	10:33am	—	-1.49	A
5	30/05/2013	10:34am	-2.36	—	A
6	30/05/2013	10:34am	-2.16	—	A
7	30/05/2013	10:34am	-1.83	-1.50	A
8	30/05/2013	10:36am	-0.66	—	A
9	30/05/2013	10:37am	—	-0.91	A
10	30/05/2013	10:37am	—	-0.83	A
11	30/05/2013	10:38am	—	-0.01	A
12	03/06/2013	12:54pm	-4.16	—	A
13	03/06/2013	12:54pm	-4.16	—	A
14	03/06/2013	12:55pm	-0.69	—	A
15	03/06/2013	12:55pm	-0.01	—	A
16	03/06/2013	12:55pm	+1.41	—	A
17	03/06/2013	12:57pm	—	-0.96	A
18	03/06/2013	12:57pm	—	-1.04	A
19	03/06/2013	1:01pm	-4.00	—	B
20	03/06/2013	1:01pm	-3.45	—	B
21	03/06/2013	1:01pm	-3.40	—	B
22	03/06/2013	1:02pm	—	-0.61	B
23	03/06/2013	1:02pm	—	-0.86	B
24	03/06/2013	1:02pm	—	-0.51	B
25	03/06/2013	1:02pm	—	-0.14	B
		$\boldsymbol{MAE}$	2.27	0.88	
		$\boldsymbol{MAE_A}$	1.90	1.02	
		$\boldsymbol{MAE_B}$	3.62	0.53	
		$\boldsymbol{r^2}$	0.91	0.99	
		$\boldsymbol{b}$ #	0.96	0.97	
		$\boldsymbol{a}$	-1.16	-0.27	

* Positive values indicate leaf temperature overestimation and *vice versa*

'b' and 'a' represent the slope and y-intercept of the linear regression trendline, respectively

The leaf temperature model also has a tendency to underestimate T_{lh} with a *MAE* of 0.88°C for both species (Table [3.2]). The assumption of a distribution of leaf angles also controls the magnitude of shortwave radiation incident upon shaded leaf elements; in this

case the magnitude of diffuse and forward scattered shortwave radiation incident upon leaf elements is a function of the leaf element angle. This assumption could cause the underestimation of T_{lh} exhibited by the leaf surface temperature model. However, the model is able to estimate T_{lh} more accurately than T_{ls}.

3.1.2 Leaf Temperature Model Evaluation with Airborne TIR Images of the Sunset Residential Neighbourhood

Thermal Imaging of the Sunset Residential Neighbourhood, Vancouver, B.C.

As a further test of the ability of the SUM_{VEG} leaf temperature model to estimate T_{ls} and T_{lh}, foliage brightness temperatures extracted from airborne TIR images acquired during an observational campaign over the Sunset residential area, Vancouver, B.C., Canada, are compared to SUM_{VEG} leaf temperature estimates. The Sunset residential area of Vancouver, B.C. is characterized by single, detached dwellings arranged in N–S and E–W block orientations (Voogt and Oke, 1997). There is extensive vegetation as ground level lawns, trees, and shrubs. TIR images of the Sunset area are also used for evaluation of the full SUM_{VEG} model (Chapter 4).

During an observational campaign intended to investigate the directional nature of urban surface temperature as measured from airborne remote sensors, an AGEMA 880 LW thermal scanner (8–14μm) was mounted to a helicopter and used to obtain thermal images of the Sunset residential area on August 17, 1992 (Voogt and Oke, 1997; 1998). Three separate flights were flown over the course of the day, subsequently labelled flight 6 (0858–0923 LMST), flight 7 (1303–1333 LMST), and flight 8 (1623–1648 LMST). Each flight consists of several lines in an attempt to image the 'complete' urban surface. Specifically, each flight involved four lines at nadir and two from each cardinal viewing direction at $\theta_V = 45°$. Brightness temperatures extracted from the TIR images have been corrected for atmospheric influences using LOWTRAN 7 with input derived from atmospheric soundings.

Comparison of Measured and Modelled Leaf Surface Temperature

The Sunset urban climate research tower (49.2261°N and 123.0784°W) provides 15 minute averages of several variables required as input into SUM_{VEG}, including T_a, RH,

U_a, and K_{dn} and L_{dn}. P_a is retrieved from hourly measurements made at the Vancouver International Airport, available as Environment Canada historic weather data. f_{width} is estimated as 10cm by calculating a mean leaf diameter based on observations from Voogt and Oke (1997). A similar procedure, as applied for the Talbot College leaf temperature model evaluation tests, is used to estimate a representative g_{vs} whereby a range of potential values is investigated and used to determine the value that offers the best fit to the leaf surface temperature measurements, once all other parameters have been selected. Once again, a single value is used to model T_{ls} and T_{lh} for every TIR frame.

Since forcing conditions are estimated based on 15 minute averages from the Sunset urban climate research tower, modelled leaf surface temperatures are constant within each 15 minute interval. Thus, comparisons between measured and modelled leaf surface temperatures can only be made based on a single modelled value from each 15 minute interval corresponding to the timing of the TIR images. TIR images from the three flights are separated into groups based on the 15 minute averaged Sunset climate tower meteorological forcing data such that the temperatures extracted from each frame are compared to a single modelled estimate.

The relatively low resolution of the TIR images makes it difficult to extract temperatures for tree crown foliage and even more challenging to separate this based on sunlit and shaded components. In order to increase the *likelihood* of extracting either T_{ls} or T_{lh}, the TIR frames are further segregated into groups based on view direction. Specifically, in order to estimate T_{ls} and T_{lh} values from the TIR images, pixels are extracted from TIR images at view angles expected to 'see' the sunlit or shaded crown side based on φ_S. For example, pixels used to estimate average T_{ls} values for flight 6 (0858–0923 LMST) are extracted from TIR images acquired with the sensor facing north and west—i.e. sensor viewing the sunlit south and east crown side. For each view direction, two TIR frames are randomly chosen and a number of pixels—visually chosen to represent tree crown foliage—are extracted and averaged to estimate a mean T_{ls} and T_{lh}.

Table [3.3] and [3.4] compare the modelled and observed estimates for T_{lh} and T_{ls}, respectively, and provide simple summary statistics regarding the ability of the leaf temperature model to predict leaf surface temperature measurements. For the most part,

Table 3.3: Statistics of the comparison between modelled and measured T_{lh}.

TIME (LMST)	DIRECTION[1]	T_{lh} (TIR) (°C)	T_{lh} (SUM_{VEG}) (°C)	$\lvert\Delta T_{lh}\rvert$ (°C)
0909	S	18.68	17.64	1.04
0909	S	17.83	17.64	0.18
0913	E	18.04	17.64	0.40
0913	E	17.85	17.64	0.21
1321	S	22.50	21.80	0.70
1321	S	22.49	21.80	0.69
1317	W	23.05	21.80	1.25
1317	W	23.24	21.80	1.44
1637	S	24.95	24.01	0.94
1637	S	25.54	24.01	1.53
1634	W	25.03	24.01	1.02
1634	W	25.01	24.01	1.00
			MAE	0.87
			r^2	0.99
			b [#]	0.89
			a	1.50

[1] V, N, S, E, W – nadir, north, south, east, and west (Indicates direction sensor is facing)
[#] 'b' and 'a' represent the slope and y-intercept of the linear regression trendline, respectively

Table 3.4: Statistics of the comparison between modelled and measured T_{ls}.

TIME (LMST)	DIRECTION[1]	T_{ls} (TIR) (°C)	T_{ls} (SUM_{VEG}) (°C)	$\lvert\Delta T_{ls}\rvert$ (°C)
0857	V	22.12	21.79	0.33
0857	V	23.16	21.79	1.37
0910	W	23.74	22.03	1.71
0910	W	24.09	22.03	2.06
0915	N	22.33	22.03	0.30
0915	N	23.08	22.03	1.05
1304	V	25.89	26.24	0.35
1304	V	26.33	26.24	0.09
1315	E	25.96	26.14	0.18
1315	E	26.50	26.14	0.36
1323	N	28.56	26.14	2.42
1323	N	27.46	26.14	1.32
1622	V	26.96	26.50	0.46
1622	V	26.56	26.50	0.06
1636	E	27.73	26.27	1.46
1636	E	26.24	26.27	0.03
1639	N	26.53	26.27	0.26
1639	N	26.10	26.27	0.17
			MAE	0.78
			r^2	0.84
			b [#]	0.99
			a	-0.54

[1] V, N, S, E, W – nadir, north, south, east, and west (Indicates direction sensor is facing)
[#] 'b' and 'a' represent the slope and y-intercept of the linear regression trendline, respectively

the leaf temperature model estimates compare well with measurements (*MAE* of 0.78°C and 0.87°C for T_{ls} and T_{lh}, respectively) and the leaf temperature model is able to replicate the general trend in T_{ls} and T_{lh} over the course of the three flights (Figure [3.4a] and [3.4b]). Differences between modelled and measured values are probably the result of a combination of input error and inherent problems in the sampling methodology used to extract values of T_{ls} and T_{lh} from TIR images.

Firstly, as previously noted, modelled estimates for leaf temperature based on meteorological forcing from the Sunset climate tower can only be calculated for each 15 minute averaged time interval. This means that variations in meteorological forcing conditions are smoothed as a result of this averaging. For example, when estimating a T_{lh} value during flight 6, TIR frames acquired with a south and east facing sensor are used. Since these TIR frames were acquired approximately 4 minutes apart, the same modelled T_{lh} value is used—for comparison purposes—while the measured value deviates as much as 5.85°C.

Secondly, the relatively low resolution of the TIR frames makes it unfeasible to infer any detailed information of tree crown biophysical parameters and a number of necessary simplifications and assumptions must be made (e.g. spherical leaf angle distribution, stomatal conductance, etc.). The assumption of a distribution of leaf angles in particular is potentially problematic. The amount of shortwave radiation incident upon sunlit and shaded estimates is estimated by averaging the incident shortwave radiation over all leaf inclination angles from 0 to $\pi/2$. However, within each pixel chosen to represent either T_{ls} or T_{lh}, it is possible that the leaf inclination angles are not represented by this distribution; this could result in modelled leaf temperature estimates underestimating or overestimating actual leaf surface temperatures dependent on the actual distribution of leaf angles. This may explain the relatively large difference between a number of T_{ls} estimates extracted from the two test frames for the same flight and view direction (e.g. nadir T_{ls} estimates for flight 6, north-facing T_{ls} estimates for flight 7) (Figure [3.4a]).

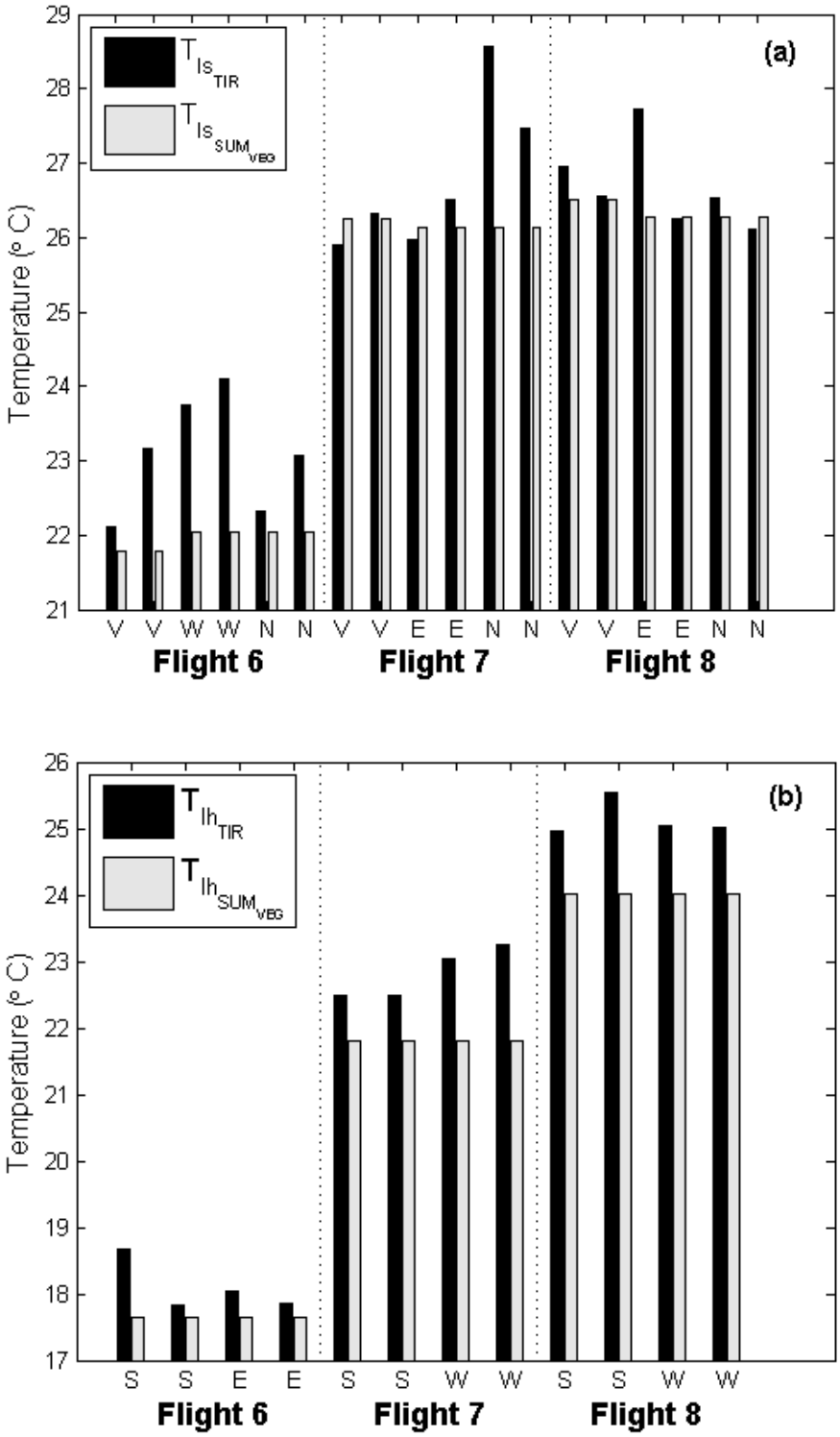


Figure 3.4: Comparison of modelled estimates of (a) T_{ls} and (b) T_{lh} with measurements extracted from TIR images acquired on August 17, 1992 of the Sunset residential neighbourhood of Vancouver, B.C. 'V', 'N', 'S', 'W', and 'E' represent nadir, north, south, west, and east viewing directions, respectively.

Similar to the leaf temperature model evaluation using TIR images acquired from the Western University campus, there is a tendency for the model to underestimate T_{lh} (Figure [3.4b]). Within the leaf temperature model, T_{lh} estimates are made by assuming all shortwave radiation is diffuse and forward scattered direct. It is possible this may be underestimating the insolation for shaded leaf elements. This is further complicated by the possible presence of sunlit leaf elements within the pixel values used to estimate T_{lh}. The low resolution of the TIR images and gap nature of tree crowns probably results in a mix of sunlit and shaded foliage and ground within each pixel.

3.2 LEAF PROPORTION MODEL TESTS

3.2.1 Investigating the Influence of Foliage Clumping and Density on Sunlit and Shaded Foliage Proportions

The 5-Scale model of Chen and Leblanc (1997; 2001) and Leblanc *et al*. (1999) has been evaluated and found to compare well with bi-directional reflectance measurements made during the Boreal Ecosystem Atmosphere Study (BOREAS) (Leblanc *et al*., 1999). A paucity of available validation data—which would require datasets of view factors occupied by sunlit and shaded foliage within a sensor IFOV for individual tree crowns—precludes direct evaluation of the modified 5-Scale model incorporated into SUM_{VEG}. Instead, the following tests evaluate the ability of the modified 5-Scale model to predict anticipated trends in the proportion of foliage visible to a remote sensor as a function of tree crown biophysical parameters. These tests, combined with the full SUM_{VEG} model evaluation in the following chapter indirectly evaluate the potential of the modified leaf proportion model to estimate P_T and Z_T required by SUM_{VEG} in order to estimate T_S for treed urban domains.

It is important to note that the leaf proportion routine incorporated into SUM_{VEG} does not calculate the total vegetation proportion or view factor occupied by tree crown foliage within a sensor IFOV. These are calculated using a combination of contour integration based on Stokes theorem (to estimate view factors) and radiative transfer techniques (to model the interaction of shortwave and longwave radiation within tree crowns and weight surface view factors). Instead, the modified 5-Scale model is used to

apportion the total foliage view factor into sunlit and shaded fractions based on sensor and solar geometry and a number of tree crown biophysical parameters.

Figure [3.5] illustrates the setup for the following simulations with a sensor centred on a single tree crown, where the tree crown outer boundary essentially corresponds to the conical projection limit of the IFOV. The purpose of this setup is to limit ground proportions, visible to the sensor, to those 'seen' through gaps within the tree crown. As a result, foliage proportions estimated using this setup represent proportions for individual tree crowns rather than as a canopy. Based on this sensor configuration, four surface types are possible within the sensor IFOV: 1) P_T, 2) Z_T, 3) sunlit ground, and 4) shaded ground. Ground components are those visible to the sensor through gaps within the tree crown volume. Since the modified 5-Scale model is used to determine relative proportions of sunlit and shaded foliage visible to the sensor, only the first two are of importance for the current research. Here, P_T and Z_T are normalized to the total amount of foliage (i.e. P_T and Z_T sum to unity).

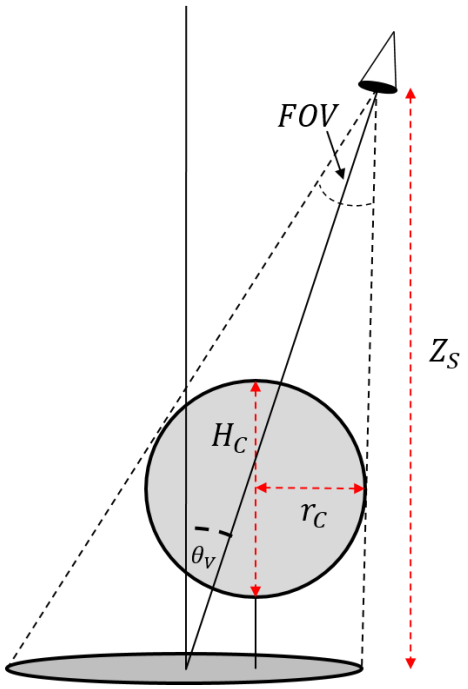


Figure 3.5: Illustration of the test used to investigate the trend in P_T and Z_T—for a single tree crown—over a range of Ω_C and μ_L.

The clumping index (Ω_C) indicates the tendency for foliage to clump along branches and ranges from 0 (highly clumped) to 1 (randomly dispersed) (Chen and

Cihlar, 1995). Increasing the clumping index results in a relative increase in Z_T at all θ_V, except for a sensor with θ_V corresponding to θ_S (Figure [3.6]). Except for a small angular range around the solar zenith angle ($\theta_S \pm 5°$), the increase in Z_T with increasing leaf dispersion is largely independent of θ_V. For all of these tests, the density of foliage within each tree crown volume is held constant at $1m^{-1}$. As leaf elements become increasingly dispersed within the crown volume, the size of gaps within the crown decreases. While the actual density of foliage within the volume does not change, increasing leaf dispersion decreases the occlusion that occurs between leaf elements at lower Ω_C and increases the actual proportion of foliage visible to the sensor.

The maximum of P_T and minimum of Z_T occur at a 45° sensor off-nadir angle for all Ω_C values. This corresponds to the hot spot where the sensor and sun are aligned ($\theta_S = \theta_V, \varphi_S = \varphi_V$) and exclusively sunlit foliage is visible to the sensor. As the sensor and sun angle diverge, the opposite occurs, with mainly shaded foliage and ground visible to the sensor. At the hot spot, changing Ω_C has no influence on the relative proportion of sunlit and shaded foliage since all foliage is sunlit. Ω_C does, however, modify the total view factor occupied by foliage; increasing leaf dispersion (increasing Ω_C) within crown volumes increases the total view factor occupied by foliage within the sensor IFOV.

For all θ_V angles—except where $\theta_V = \theta_S$—the relative increase in $Z_T$with increasing Ω_C coincides with a necessary decrease in the relative proportion of P_T. However, since increasing Ω_C is accompanied by an actual increase in the view factor occupied by total foliage, the view factor occupied by sunlit foliage experiences only marginal changes with increasing Ω_C. Similarly, at the hot spot, while the relative proportion of sunlit foliage does not change, the increase in foliage view factor with increasing Ω_C indicates an increase in the actual view factor occupied by sunlit foliage (i.e. since the majority of foliage at the hot spot is sunlit).

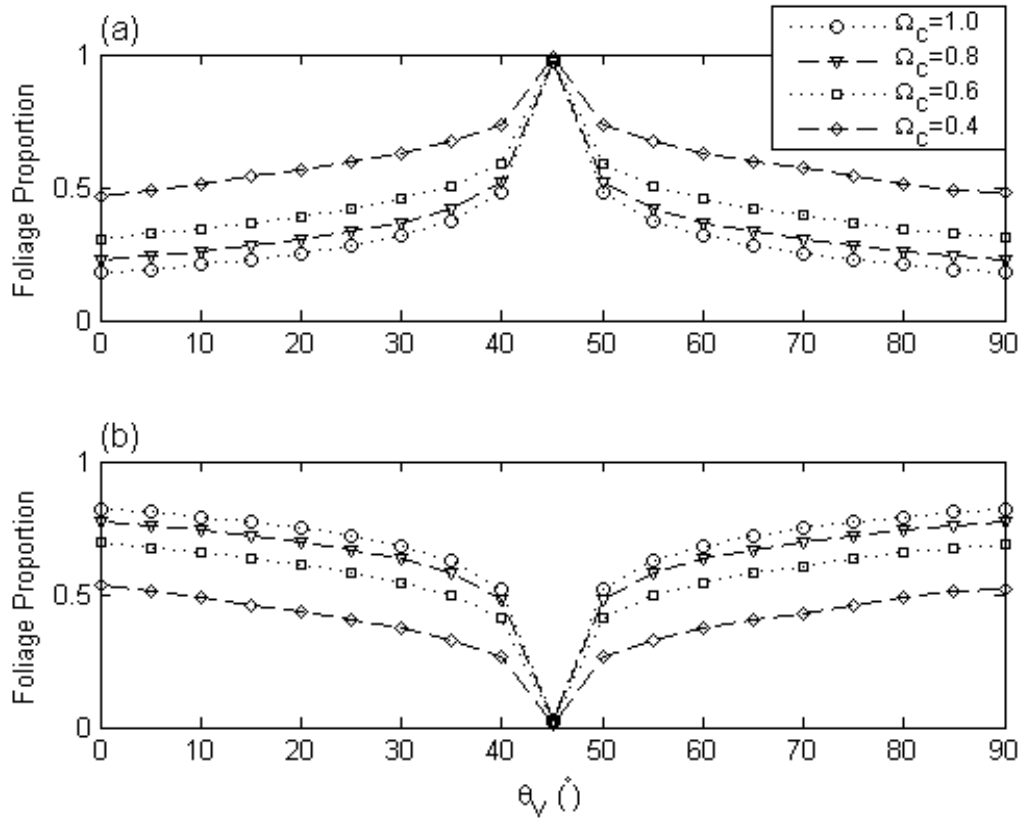


Figure 3.6: Proportion of (a) sunlit and (b) shaded foliage as a function of Ω_C over a range of θ_V with the sun at $\theta_S = 45°$.

Foliage area density (μ_L) is a measure of the total leaf surface area (m^2) within each tree crown volume (m^3). In SUM_{VEG}, all tree crowns have identical μ_L with no intra-crown variability. The density of foliage within crown envelopes controls the interaction of foliage with shortwave radiation (i.e. the temperature of surfaces shaded from direct shortwave radiation). Within SUM_{VEG} μ_L also controls both the view factor occupied by vegetation, as well as the distribution of P_T and Z_T. Increasing μ_L within each tree crown volume results in an increase in the view factor occupied by total foliage.

Similar to the change in foliage proportions with increasing Ω_C, increasing μ_L indicates decreasing size of gaps within the crown volume as the added foliage fills gaps within the crown volume (Figure [3.7]). At the hot spot, changes in μ_L have no effect on P_T and Z_T. When $\theta_V \neq \theta_S$, increases in μ_L result in an increase in the relative proportion of shaded foliage at the expense of sunlit foliage. This results from the increase in leaf-leaf shading that occurs with an increase in μ_L.

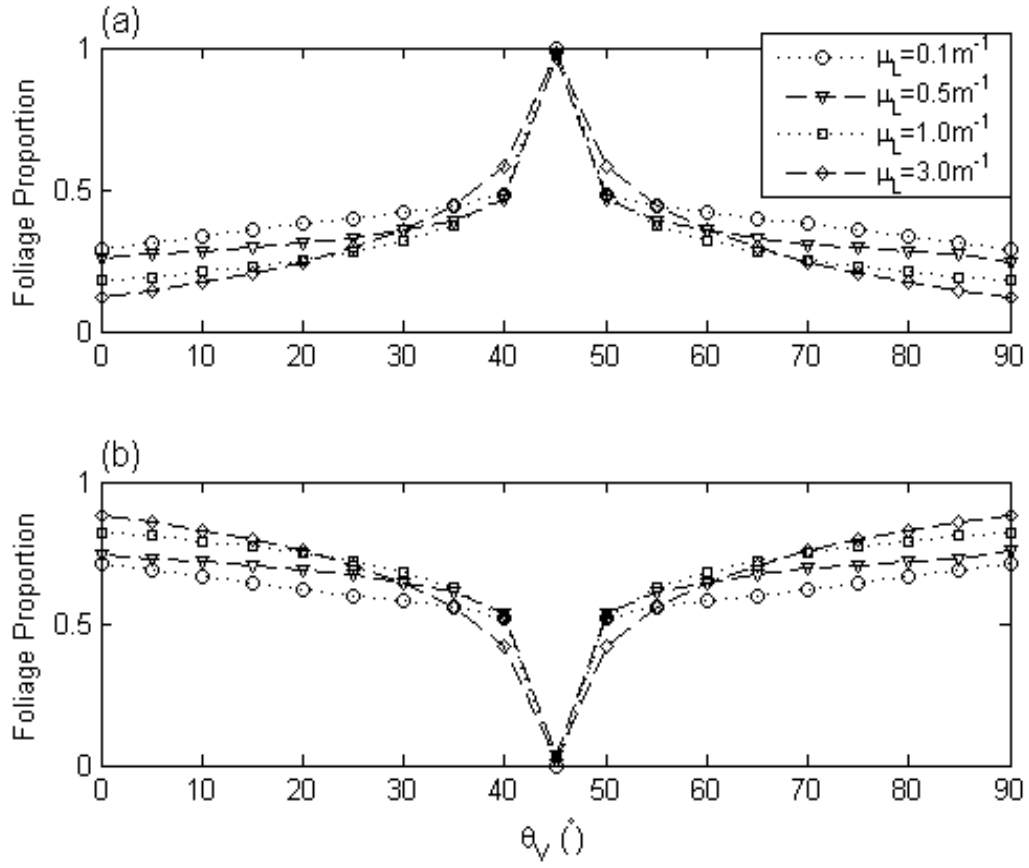


Figure 3.7: Proportion of (a) sunlit and (b) shaded foliage as a function of μ_L over a range of θ_V with the sun at $\theta_S = 45°$.

In general, the foliage proportions predicted by the modified 5-Scale leaf proportion model incorporated into SUM_{VEG} follow expected trends based on physical processes and parallel those patterns found in the original 5-Scale model for a forest canopy. While these tests do not constitute an evaluation of the leaf proportion routine within SUM_{VEG}, when combined with the previous 5-Scale full model evaluation and the SUM_{VEG} full model evaluation in the following chapter, they instill confidence in the ability of the routine to estimate the foliage proportions required by SUM_{VEG}.

3.3 Summary of SUM_{VEG} Leaf Temperature and Proportion Routines

In general, trends in the relative proportions of sunlit and shaded foliage behave as expected as evidenced in several tests involving the manipulation of a number of crown biophysical parameters. When combined with the full model evaluations of the original 5-

Scale model (Leblanc *et al.*, 1999) and SUM_{VEG} (Chapter 4), the leaf proportion routine incorporated into SUM_{VEG} is expected to provide reasonable and realistic estimates of sunlit and shaded foliage proportions, accounting for the hot spot effect and complex nature of tree crown foliage (Chen and Leblanc, 1997) —i.e. shaded foliage visible on the sunlit crown side and *vice versa*.

The leaf temperature model used in SUM_{VEG} is a simple approximation in which T_{ls} and T_{lh} are calculated based on a number of leaf biophysical parameters and radiative fluxes incident upon leaf elements oriented with a distribution of leaf angles. The result is a single T_{ls} and T_{lh} averaged over all leaf inclination angles from 0 to $\pi/2$. In order to evaluate its efficacy for the current research, the leaf temperature model of Campbell and Norman (1998), modified to treat a distribution of leaf inclination angles, is validated using leaf surface temperatures derived from two TIR image datasets: 1) TIR images of two tree species (Boston ivy and dawn redwood) acquired using a handheld TIR camera and, 2) TIR images obtained from a helicopter-mounted TIR camera over the Sunset residential area of Vancouver, B.C., Canada.

With proper consideration of inputs and necessary assumptions, model estimates of T_{ls} and T_{lh} compare well with observations extracted from TIR images. The evaluation using Sunset TIR images is particularly relevant since the same image dataset is also used in Chapter 4 to evaluate the full SUM_{VEG} models' ability to estimate T_S and conduct a case study investigation of thermal anisotropy over the Sunset domain.

Chapter 4

SUM_{VEG} EVALUATION AND SUNSET CASE STUDY RESULTS

This chapter presents the procedure and results of the SUM_{VEG} full model evaluation using remotely-detected brightness surface temperature measurements from the Sunset residential neighbourhood of Vancouver, B.C., Canada (Section [4.1]). The primary goal of this evaluation is to determine the ability of SUM_{VEG} to replicate T_S for the surface within an airborne TIR remote sensor IFOV. If the model is able to satisfactorily estimate T_S at any given individual sensor view position (θ_V and φ_V), it implies that SUM_{VEG} can also accurately quantify the thermal anisotropy over a treed urban surface since this is calculated based on an assemblage of individual T_S over a range of sensor positions. Following this model evaluation, the Sunset residential surface is used as a case study to investigate the influence of tree crowns on thermal anisotropy (Section [4.2]). Additionally, in Section [4.2.3] SUM_{VEG} estimates of thermal anisotropy are compared to measurements from TIR images over the Sunset surface obtained by Voogt and Oke (1998). Finally, Section [4.3] summarizes the results of the full model evaluation and Sunset case study and provides general conclusions regarding the influence of tree crowns on thermal anisotropy in the Sunset residential neighbourhood.

4.1 VANCOUVER SUNSET RESIDENTIAL AREA: *AUGUST 17TH, 1992*

4.1.1 Site Description

The Sunset area of Vancouver, B.C. (49.2255°N 123.0827°W) is a residential neighbourhood characterized by detached dwellings typically 1 to 2 stories tall. The main study area included within this investigation is bounded by 45th Avenue to the North, 53rd Avenue to the South, Fraser Street to the West, and Dumfries Street to the East. Dwellings are typically arranged in blocks with the block long axes aligned either N–S or

E–W (Figure [4.1]). In this orientation, dwellings are set far back from the street with narrow spacing between houses within each block. Roofs are typically hip or gabled roofs with small pitch angles. The area is characterized by extensive vegetation of all forms (Voogt and Oke, 1997).



Figure 4.1: VanMap orthophoto (2002) of a section of the Sunset neighbourhood with the two dominant block orientations (N–S and E–W). Buildings within a block are spaced close together and tree crowns generally line streets with sporadic distribution around residential lots.

4.1.2 Evaluation Data

In order to investigate the influence of the three-dimensional urban surface on brightness surface temperature measurements made by TIR remote sensors, Voogt and Oke (1997; 1998) pursued an observational campaign that involved using a combination of airborne and vehicle mounted TIR sensors to characterize the "complete surface temperature" for the Sunset residential area of Vancouver.

In order to characterize the temperature distributions for vertical surface facets (e.g. building walls, vegetation with vertical extent, etc.), Voogt and Oke (1998) mounted a series of Everest Interscience Model 4000A infrared transducers (15° IFOV) onto a pickup truck at a range of angles relative to the horizontal. Vehicle traverses across the

Sunset area were subsequently used to produce surface temperature distributions spatially averaged over the traverse. During the traverses the IRT IFOV will generally contain a mix of surface types (e.g. wall facet, mixed vegetation, sky) requiring separation of the temperature distribution into the various surface components. Distribution truncation and mixed distribution modelling were used to separate distributions into their constituent components and the result are temperatures for the vertical facet surfaces, including directional wall facets, averaged over the sampling interval. Surface temperature measurements averaged over a spatial area have been partially corrected for surface emissivity by modelling the canyon radiative exchange (Voogt and Oke, 1998).

An AGEMA Thermovision 800 BRUT system with a model 880 LWB scanner was mounted onto a helicopter and used to produce TIR images of the Sunset residential neighbourhood during three flights on August 17th, 1992, corresponding to 0858–0923 LMST, 1303–1333 LMST, and 1623–1648 LMST, in order to complement surface temperature distributions obtained from the vehicle traverses. For each flight, four lines at nadir and eight lines at 45° off-nadir in each of four viewing azimuths aligned with the block structure were used to image the Sunset surface with a large overlap between consecutive TIR frames. Radiance values for surfaces within each frame are corrected for atmospheric effects using the LOWTRAN 7 Atmospheric Transmittance/ Radiance model (Kneizys *et al.*, 1988) with atmospheric profiles measured by radiosondes (lower atmosphere) and upper air reporting stations (upper atmosphere). However, there is no correction for surface emissivity in the conversion of surface radiance values to brightness temperatures. Voogt and Oke (1997) use ellipsoids and truncated ellipsoids to represent tree crowns and accounts for gaps within crowns using field based estimations for each of the general tree type categories (Table [4.1]).

Here, the objective is to evaluate the ability of the SUM_{VEG} model to replicate T_S from individual airborne TIR frames (e.g. Figure [4.4a]). This evaluation uses a realistic urban form digitized from orthophotos and component surface temperatures derived from the airborne (horizontal surfaces) and automobile (vertical surfaces) TIR measurements of Voogt and Oke (1997; 1998).

4.1.3 Representation of the Sunset Urban Surface

In order to investigate the thermal anisotropy over the Sunset neighbourhood of Vancouver, the urban surface was digitized from VanMap orthophoto imagery and used to create GIS layers of building footprints and heights, as well as street and alley surfaces. Figure [4.2] presents the plan view raster image of the digitized Sunset surface where building values indicate the height in metres and the streets and alleys are coded to match their type declaration in SUM_{VEG}. Following digitization of all building footprint, street, and alley surfaces, the residual ground level surface is categorized as grass vegetation.

Since temperatures for the component surfaces within the Sunset domain are derived from TIR images obtained on August 17th, 1992, it is desirable to digitize the surface from imagery obtained as close to this date as possible. While VanMap provides orthophoto imagery from 1994, the resolution is too low to extract building and street dimensions and tree crown locations with a high degree of confidence. Instead orthophotos from 2002 were used to create the surface GIS layers for built surfaces and 2011 orthophotos used for tree crown locations.

While it is probable that houses built after 1992 are included in the analysis, it is unlikely that building dimensions have deviated significantly from those in 1992. Visual comparison of 1994 and 2002 VanMap orthophoto imagery reveals that at least 51 houses out of approximately 2233 houses within the Sunset domain (2.3%) have been significantly altered—generally enlarged—or added with most of the difference concentrated in the 12 block southwest sub-domain. Additionally, visual comparison of tree locations in the northwest Sunset sub-domain between 1992 and 2011 reveals that at least 75 trees have been added since 1992 (9.9% increase), though at least 44 have also been removed. Most of the additions appear to be in the form of smaller street trees while the removals have been made generally in order to add or renovate homes. Based on this, the results from the use of Sunset TIR images to evaluate and test the model, with a surface generated from more recent aerial imagery, may slightly overestimate the contribution of tree crowns to remotely-detected brightness temperatures. However, investigating this is convoluted in the current model configuration since the identical nature of tree crowns is also expected to cause an under- or overestimation of T_S.

Building heights are determined using Google Street View© to estimate the height in number of stories (to the nearest 0.25 stories) for all houses within the study domain, with 1 story = 3.05 m. Garage and auxiliary structures, typically located on the alley side of building lots, are assigned a constant height of 3.05 m (1 story) following the procedure of Voogt and Oke (1997). VanMap orthophotos are also used to generate a GIS layer of points to indicate the location of tree crowns within the Sunset domain, taking care to avoid low level shrub vegetation.

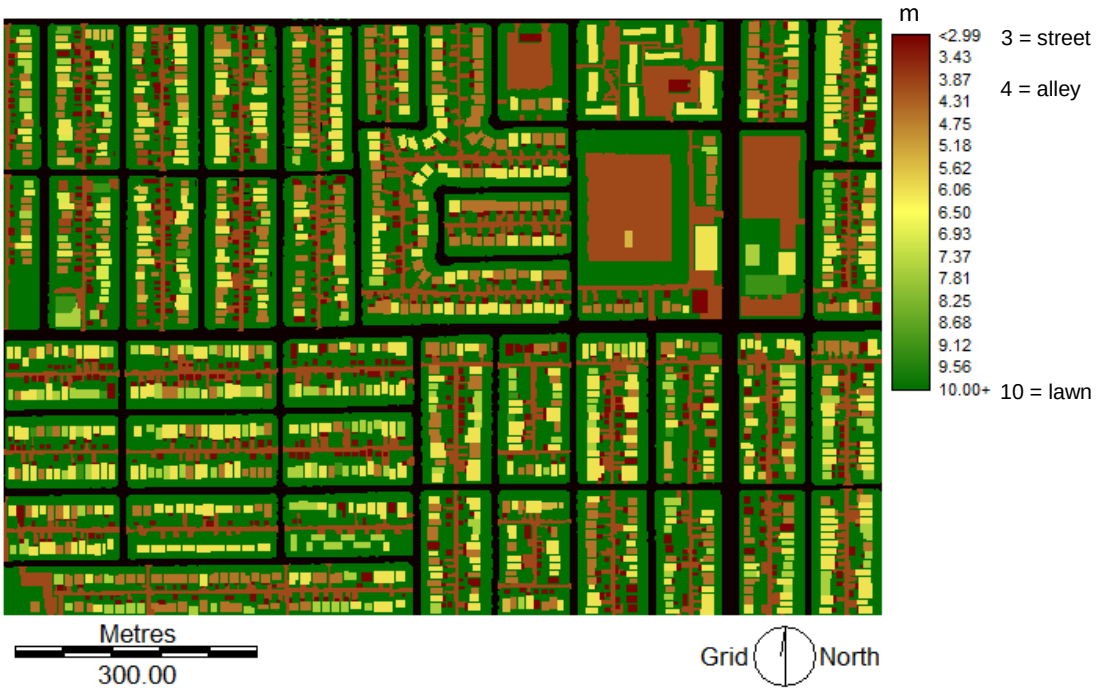


Figure 4.2: Plan view of the digitized Sunset residential domain used for the SUM_{VEG} full model evaluation and case study. For buildings, values indicate the height in metres while ground level surface values match their declaration type in SUM_{VEG}.

Table [4.1] indicates the most common tree types within the northwest corner 8 block sub-domain including their frequency, mean tree height (H_T), trunk height (H_{tk}), and crown radius (r_c). In order to determine a single set of representative dimensions for tree crowns within the Sunset domain, as required by SUM_{VEG}, the dimensions for each tree type in Table [4.1] are weighted according to the relative tree crown frequency (excluding shrubs/bushes) and rounded to the nearest integer resulting in a H_T, H_{tk}, and r_c of 8, 3, and 3 metres, respectively. Assuming that the northwest sub-domain presents a representative sample of tree crowns within the Sunset area, these dimensions are applied

to every tree crown within the simulated domain. It is also assumed, in absence of detailed measurements of leaf angular distributions, that the tree crowns within this domain exhibit a spherical distribution of leaf angles as this offers a close fit to many actual tree crown species (Campbell and Norman, 1998).

Table 4.1: Frequency (*n*), tree height (H_T), trunk height (H_{tk}), and crown radius (r_C) for the general tree types present in the Sunset northwest sub-domain (*adapted from* Voogt and Oke (1997)).

Tree Type	n	H_T	H_{tk}	r_C
Shrubs/Bushes	81	2.47	0.09	1.07
Coniferous	78	8.55	1.77	3.09
Deciduous	289	7.73	3.16	3.41
Flowering Deciduous	43	6.24	2.74	3.00

Visual approximations of μ_L for tree crowns within the Sunset northwest sub-domain made by Voogt and Oke (1997) are used to estimate a representative μ_L of 2.4m^{-1}, assumed to be randomly distributed within the crown envelopes (i.e. Ω_C = 1.0). Figure [4.3] presents a plan view horizontal slice of the Sunset northwest sub-domain showing the locations and size of tree crowns relative to building structures.

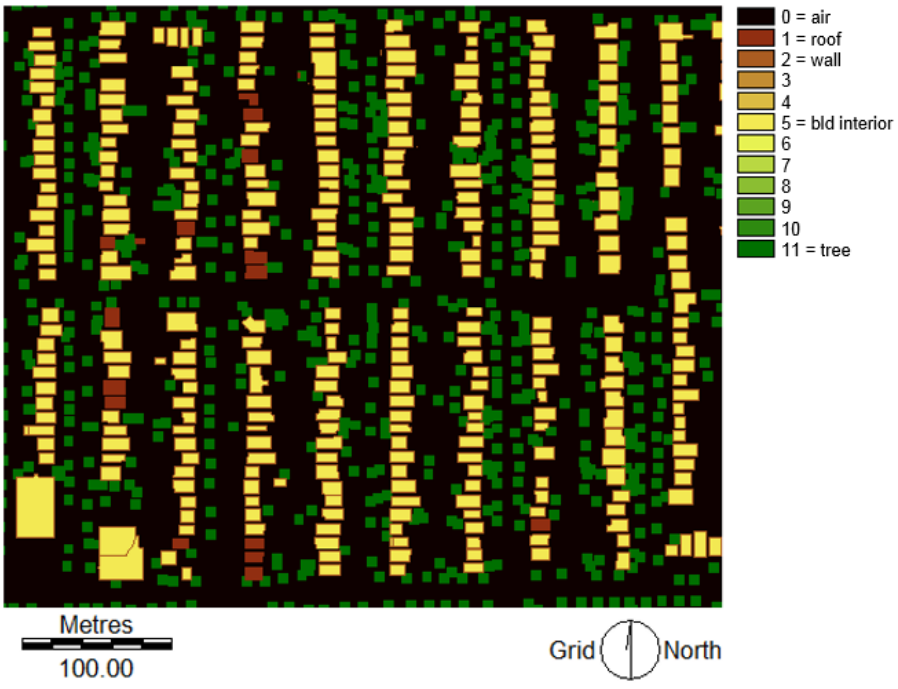


Figure 4.3: Plan view 'slice' of the Sunset northwest sub-domain at a height of 4m with ground level surfaces excluded in order to compare tree crown size and location relative to buildings. Values indicate SUM_{VEG} surface codes.

4.1.4 Full Model Validation using Surface Temperature Observations

To evaluate SUM_{VEG}, several airborne TIR frames obtained during the observational campaign of Voogt and Oke (1997) are chosen from each flight on August 17th, 1992 such that four frames from nadir and two from each cardinal viewing direction (N-S-W-E) at 45° off-nadir are included in the evaluation (3 flights x 12 frames/flight = 36 frames in total). Figure [4.4] illustrates the validation procedure used. Figure [4.4a] presents a typical TIR frame obtained from nadir (Flight 6, Line 2, Frame 40) at an approximate sensor height of 975m and Figure [4.4b] represents the attempt to match the surface within the sensor IFOV using SUM_{VEG} and the digitized Sunset surface. Figure [4.4b] does not show the ground level surface types (e.g. grass, street, alley, etc.) but these are included within the analysis.

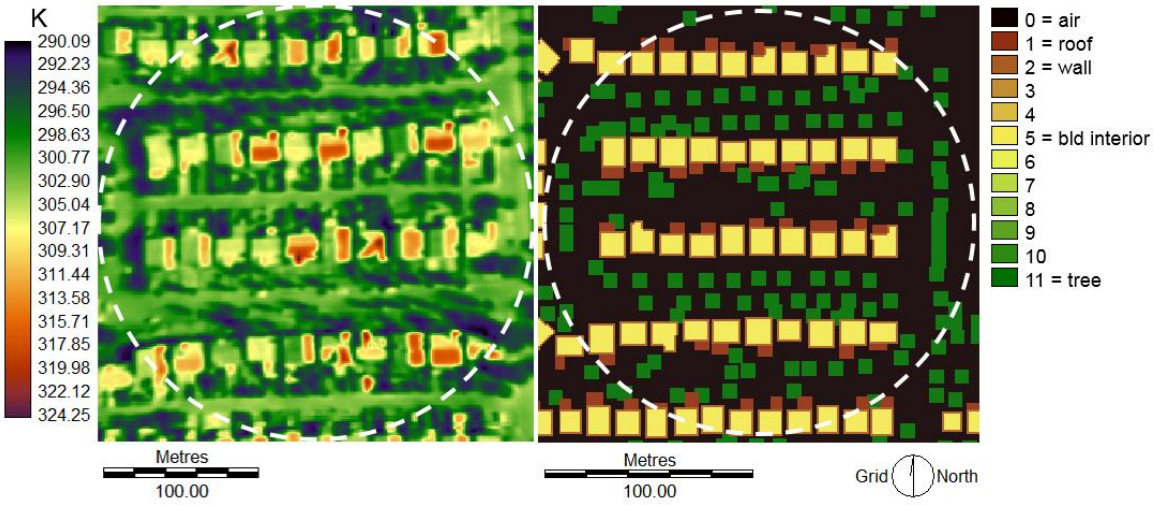


Figure 4.4: Visualization of the SUM_{VEG} model evaluation procedure using TIR images from Voogt and Oke (1997; 1998). (a) TIR frame with sensor at nadir and (b) the digitized surface (at 4m) with matching sensor geometry. The dashed circle on the TIR frame is an example of the mask applied to produce a circular IFOV and the dashed circle on the digitized surface indicates the modelled IFOV. Values on the TIR frame indicate surface temperature, in Kelvins, corrected for atmospheric effects. Values on the digitized surface indicate the surface codes within SUM_{VEG}.

Temperatures for the horizontal component surfaces (e.g. sunlit and shaded roof and ground) are extracted and averaged from one TIR frame on either side of the frame being replicated. For example, for the evaluation of frame 40 from flight 6, line 2, horizontal surface temperatures are extracted from TIR frames 39 and 41, both of which display at least 75% overlap with frame 40. Temperatures for vertical surface components are

extracted from remotely-detected temperatures obtained via truck-mounted infrared thermometers (IRT) during traverses through the residential streets performed concurrently with the airborne flights (Voogt and Oke, 1997). While the locations of the surface temperatures obtained by the truck mounted IRTs may not correspond precisely to the surfaces within the sensor IFOV for a particular frame of interest, traverse averages of vertical surface facet temperatures ensures a representative sample of the various facet types corresponding approximately to the time of airborne imaging.

T_{ls} and T_{lh} are modelled using the leaf temperature model of Campbell and Norman (1998) incorporated into SUM_{VEG}. The relatively low resolution of TIR images combined with the gap nature of tree crowns makes it difficult to extract surface temperatures for leaf elements and even more difficult to separate this into T_{ls} and T_{lh} as SUM_{VEG} requires. Section [3.1.3] details the evaluation of the leaf temperature model using the same TIR image dataset as the current full model evaluation and Sunset case study. Favourable results from this leaf temperature model evaluation inspire confidence in its ability to accurately provide temperatures for the sunlit and shaded leaf surfaces in the TIR frames.

Meteorological forcing data required by the model to estimate leaf surface temperatures were obtained from the Sunset urban climate research tower located at 49.2261°N and 123.0784°W. Data provided by this tower has been used extensively in urban climate studies dating back to the 1970's (e.g. Oke, 1979; Oke, 1988; Christen *et al.*, 2011). α_L, ε_L, and g_{vs} are estimated using the same values employed for the validation of the leaf temperature model with Sunset temperature observations (Section [3.1.3]).With these measurements and estimates and assuming a distribution of leaf angles for radiation interception, the leaf temperature model provides estimates of T_{ls} and T_{lh} and their evolution over the course of the three flight times on August 17$^{\text{th}}$, 1992.

Temperatures for surfaces shaded from direct shortwave radiation by tree crown foliage are calculated by SUM_{VEG} based on a weighting between the maximum (sunlit) and minimum (shaded) surface temperatures, dependent upon surface type. The weighting is calculated based on the transmission of direct and diffuse solar radiation to the shaded surface beneath tree crowns (Section [2.7.3]). As with tree foliage temperatures, the

resolution of the airborne TIR images of Voogt and Oke (1997) is too low to extract with confidence the temperature of surfaces shaded from the sun by tree crowns.

Figure [4.5] presents the comparison of T_S between: 1) the TIR image subset chosen for the evaluation of SUM_{VEG}, 2) SUM_{VEG} without tree crown vegetation (equivalent to the original SUM but with the addition of a simple ground-level vegetation), and 3) SUM_{VEG} with tree crowns present. In this comparison, both SUM_{VEG} configurations include ground-level vegetation (i.e. grass) in order to isolate the influence of tree crown vegetation. Vertical dotted lines divide the three flight times with the sensor view direction on the x-axis[6]; each x-axis point indicates a single TIR frame. L_S estimates are made by masking the TIR frames to produce a circular IFOV and averaging the value of each TIR image pixel radiance. Assuming a surface emissivity equal to 1.0, L_S can be converted to an equivalent T_S using Equation [2.6.1] for TIR radiation within a wavelength range of 8–14μm (Verhoef *et al.,* 1997).

In the absence of tree crowns SUM_{VEG} overestimates T_S for all frames with a *MAE* of 3.56°C. Tree crown foliage, specifically T_{lh}, is close to T_a and generally several degrees cooler than built facet surface temperatures. Therefore, adding tree crowns reduces T_S for every frame, though spatial heterogeneity of tree crown distribution in the Sunset domain results in an unequal reduction for each frame. As a result, SUM_{VEG} tends to both under and overestimate T_S. This spatial heterogeneity also increases the variability of T_S estimates with tree crowns present, reducing the correlation coefficient from 0.98 to 0.96 (Figure [4.6]). Nevertheless, the addition of tree crowns increases the accuracy of T_S estimates for every frame, reducing the *MAE* by 2.69°C and the root mean square error (*RMSE*) by 2.59°C. Table [4.2] presents results for statistical tests comparing SUM_{VEG} and SUM estimated T_S and directional differences in T_S (i.e. ΔT_S) to observations (Willmott *et al.*, 1985). Relative to SUM, SUM_{VEG} demonstrates a substantial reduction in error for the estimation of T_S. Similar to the reduction in correlation coefficient, the increase in unsystematic RMSE is probably due to the increased model complexity resulting from the inclusion of tree crowns.

[6] Sensor view direction indicates the direction the sensor is facing, e.g. a north facing sensor will view mainly south facing building walls.

The tendency for SUM_{VEG} to both under- and overestimate T_S for individual TIR frames is probably the result of the identical nature of tree crown elements modelled using SUM_{VEG}. From VanMap orthophotos and Google Street View © imagery, it is obvious that the Sunset residential neighbourhood is characterized by a wide diversity of tree species and range of size and biophysical parameters (e.g. μ_L). Care has been taken to approximate tree dimensions and biophysical parameters with a representative set of values. Nonetheless, the TIR frames used for the validation come from several of the Sunset regions and it is probable that the representative set of tree crown biophysical parameters may not match the configuration of trees within every TIR frame.

Table 4.2: Validation statistics for the SUM_{VEG} evaluation with Sunset airborne T_S and ΔT_S.

Statistic	T_S		ΔT_S
	SUM_{VEG}	SUM	SUM_{VEG}
RMSE	1.06	3.65	1.06
# $RMSE_S$	0.41	3.57	0.49
$RMSE_U$	0.98	0.77	0.83
MAE	0.87	3.56	0.88
b (slope)	0.95	1.05	1.00
a (intercept)	1.93	1.92	0.54
d (index of agreement)	0.99	0.88	0.97
r^2	0.96	0.98	0.92
N (# of images)		36	

$RMSE_S$ and $RMSE_U$ represent the systematic and unsystematic RMSE, respectively

For example, there is a tendency for the Sunset streets to be lined with relatively small, short trees with sparse foliage. Alternatively, back lawns, and to a certain extent front lawns, tend to contain larger, more mature tree crowns. If a TIR frame captures a surface area characterized by mainly street trees, the representative set of biophysical dimensions may overestimate the influence of trees on T_S. The opposite may occur if large, mature trees dominate the sensor IFOV in which case SUM_{VEG} may underestimate the influence of trees on T_S.

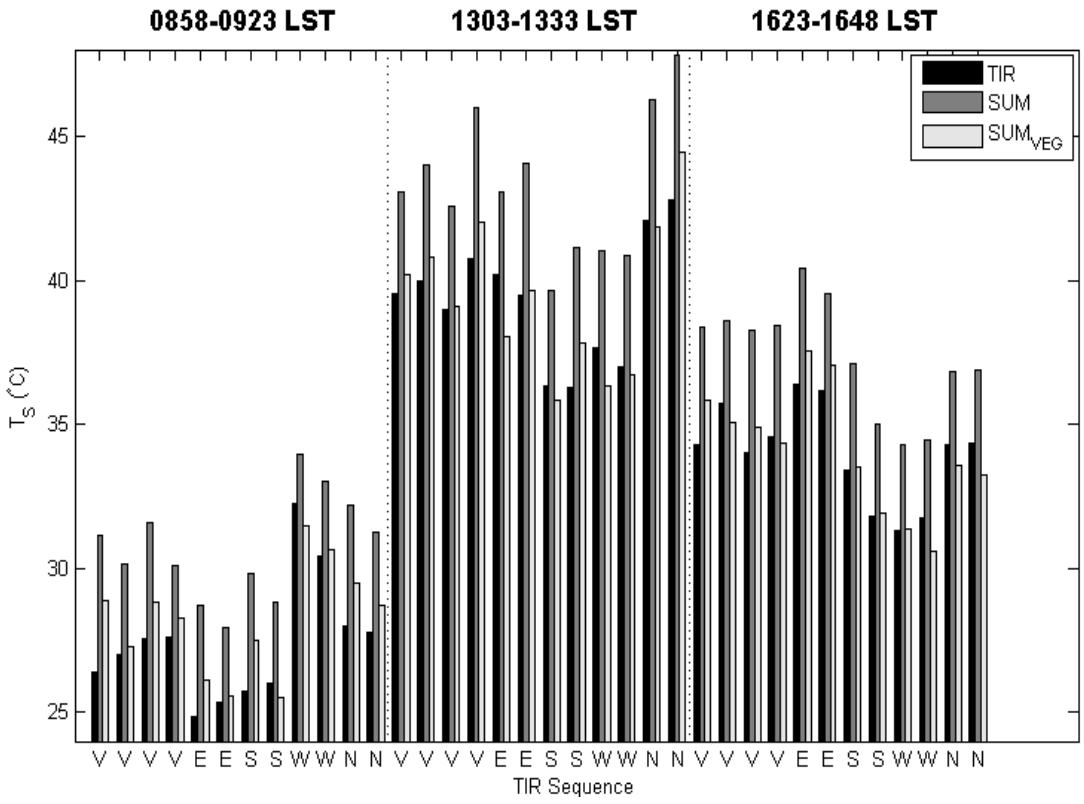


Figure 4.5: Comparison of T_S with (SUM_{VEG}) and without (SUM) tree crowns to the remotely-sensed temperature for all TIR frames used in the SUM_{VEG} evaluation. V-Nadir, E-East, W-West, N-North, S-South indicates direction sensor is facing relative to North = 0°.

The inclusion of tree crowns into the simulated TIR frames influences T_S in a number of ways. Firstly, tree crown foliage occludes building or ground level surfaces from the sensor and replaces them with foliage surfaces which are typically cooler than the built surfaces they are replacing. Secondly, due to the gap nature of tree foliage, crowns partially shade surfaces from the sun. The overall influence of both effects is a decrease in T_S. For all frames used in the SUM_{VEG} evaluation, the inclusion of tree crowns, on average, decreases T_S by 3.23°C. With a *MAE* (overestimation) of 3.56°C in the absence of tree crowns, the inclusion of trees into SUM_{VEG} substantially increases the accuracy of modelled T_S estimates.

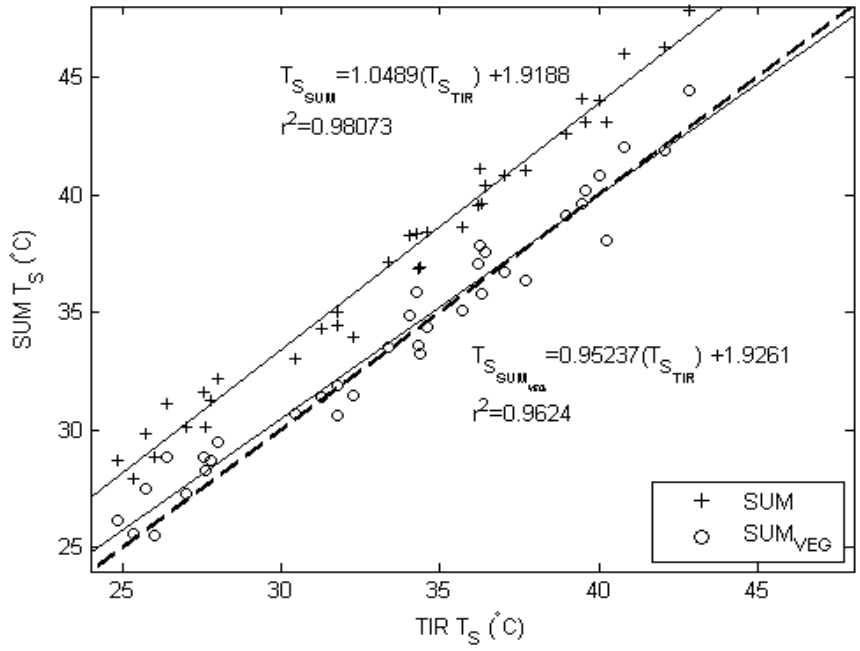


Figure 4.6: Linear regression of T_S with (SUM_{VEG}) and without (SUM) tree crowns to TIR-derived surface temperature for all sensor view angles. Dashed line indicates the 1:1 line.

4.2 Influence of Tree Crowns on Thermal Anisotropy over the Sunset Neighbourhood

4.2.1 Component Surface Temperatures and Sensor Geometry

Effective thermal anisotropy is investigated over the Sunset residential area using digitized GIS surface layers and mean facet surface temperatures from the TIR observations of Voogt and Oke (1997; 1998). Presented here are mainly results from analysis of thermal anisotropy over the 8-block northwest Sunset sub-domain at 0900 LMST and 1200 LMST. This analysis was also performed for other Sunset sub-domains at 1200 LMST including the approximately 12 block southwest sub-domain and the entire Sunset domain using a different sensor configuration. Both the southwest sub-domain and full domain tests result in minimal difference in the degree of thermal anisotropy relative to the northwest sub-domain results.

As in the SUM_{VEG} evaluation, foliage temperatures and temperatures for surfaces shaded from the sun by tree crowns are calculated within the model. Temperatures for the remaining surfaces are extracted from the airborne (horizontal) and automobile (vertical)

remotely-detected estimates based on the measurement time (Voogt and Oke, 1997). Rather than trying to extract surface temperatures from airborne TIR images corresponding precisely to the subset of surfaces chosen for the modelled domain, temperatures are chosen that correspond most closely to the simulation time. This is not expected to have a large influence on the magnitude of effective thermal anisotropy given the relative spatial homogeneity of building structure and, in all likelihood, surface fabric within the Sunset domain. For the temperature of vertical wall facets extracted from automobile traverses this is less of a concern due to their spatial averaging.

Determination of the thermal anisotropy over the Sunset area is accomplished by positioning the sensor over the simulated Sunset surface and varying the sensor view angle in order to characterize the distribution of T_S. For the current investigation, the sensor off-nadir angle is restricted to $\theta_V \leq 60°$ with a 12° IFOV. In order to maintain an approximately equal surface area within the sensor projected IFOV, the sensor height is reduced as θ_V increases; for the Sunset simulations, at nadir the sensor is at 1000m varying along a smooth curve to 500m at $\theta_V = 60°$. Maintaining an approximately equal surface area as a function of θ_V is important for two reasons. Firstly, since T_S reported at each θ_V is produced by summing the temperatures for each surface component (weighted by the view factor each surface occupies), maintaining an equal area is required to ensure a similar sampling of surface structural variability at all θ_V. Secondly, assuming the sensor at nadir captures a majority of the surface variability, not adjusting the sensor height at oblique θ_V would be inefficient since the increase in surface area would substantially increase computation time with relatively minimal change in the reported magnitude of thermal anisotropy.

Consideration of an appropriate surface area for estimating the magnitude of thermal anisotropy requires consideration of sensor geometry—including height of the sensor above the surface (z_S) and IFOV—and surface fabric and structural inhomogeneity. Since, in the current configuration, all surfaces of the same type and with the same shading regime (i.e. sunlit or shaded) receive the same temperature, consideration of surface area requirements is generally concerned with variations in surface structure and the ability of a remote sensor, with a given IFOV, to capture sufficient surface structural heterogeneity. The decision was made to use approximately

the same sensor geometry used by Voogt and Oke (1997) to obtain TIR images over the Sunset residential neighbourhood for two reasons: 1) this allows for comparison with Voogt and Oke's findings regarding the magnitude of thermal anisotropy over the Sunset neighbourhood, and, 2) this offers a reasonable balance between computational time and surface area requirements, ensuring a representative sample of the surface structural variability within the sensor IFOV. With this sensor configuration, the sensor IFOV samples slightly more than a neighbourhood 'block' which is expected to capture most of the surface variance over this residential land use (Schmid *et al.*, 1991).

Results are visualized in polar co-ordinate plots where concentric circles indicate θ_V and radii lines indicate φ_V. Values at each sensor view angle indicate T_S for the surface within the sensor IFOV. Interpolation within each polar co-ordinate plot is based on a θ_V angular range of 0° to 60° in 5° increments and a φ_V range of 0° to 360° in 10° increments (481 sensor view angles).

There are several ways to express the magnitude of thermal anisotropy, and the method of reporting the magnitude of thermal anisotropy may be dependent on the type of surface temperatures used to populate SUM_{VEG} (e.g. facet mean values versus inclusion of intra-facet variability). The following results present the '*maximum effective anisotropy*' (Λ_{MAX}) calculated as the maximum sensor-detected brightness temperature ($T_{S_{MAX}}$) minus the minimum temperature ($T_{S_{MIN}}$) over an assemblage of θ_V (Voogt and Oke, 1998). Use of Λ_{MAX} is acceptable when spatial variability of surface thermal and radiative properties is generally homogeneous (or regular) and when facet mean temperatures are used since we can reasonably expect a smooth distribution of results. For example, the relatively smooth distributions of surface temperatures within the Sunset case study polar co-ordinate plots result from the use of mean surface temperatures for all urban facets and the averaging across the sensor IFOV (Voogt, 2008).

It is important to note that Voogt (2008) found that the SUM model (devoid of vegetation) tends to underestimate the full surface anisotropy when facet mean temperatures are used. While a micro-scale 3d urban energy budget model has been coupled to SUM in order to investigate thermal anisotropy accounting for intra-facet temperature variability (Voogt and Krayenhoff, 2005; Krayenhoff and Voogt, 2007b), the inability of the energy budget model to represent tree crown vegetation precludes its

direct use for the current research. Ideally, future coupling of SUM_{VEG} with a *vegetated* micro-scale energy budget model will account for the influence of micro-scale temperature variability. In particular, Lagouarde *et al*. (2004) suggested, and Voogt (2008) confirmed, that in open urban geometries (i.e. low building height and canyon aspect ratio) accurate thermal anisotropy estimation may be more dependent upon accounting for micro-scale temperature variability than on urban geometry.

DART EB could potentially provide sub-facet scale temperatures for built surfaces, as well as tree canopy foliage temperatures (Gastellu-Etchegorry *et al.*, 2008). Asawa *et al.* (2008) describe a heat balance model paired with a 3d-CAD system that could also potentially provide sub-facet scale surface temperatures necessary to populate SUM_{VEG}, including temperatures for surfaces constructed using GIS input. The combination of surface structural variability (i.e. GIS surface) with sub-facet scale surface temperatures may require a different method to characterize the distribution of thermal anisotropy. However, such investigation is beyond the scope of the current research where facet mean values are used.

4.2.2 Thermal Anisotropy over the Sunset Urban Surface

This section presents the results of the Sunset simulations at 0900 LMST and 1200 LMST for the northwest 8-block sub-domain of the simulated Sunset surface. The northwest sub-domain is characterized by dwellings arranged in blocks with the block long axis typically oriented N–S. There is extensive ground level and tree crown vegetation (low level shrubs/ bushes not included) and the urban geometry is relatively open ($\lambda_P \approx 0.10$). The timing (i.e. 1200 LMST) is chosen because airborne and automobile TIR surface temperatures are available close to this time and effective anisotropy is typically maximized near solar noon due to the large contrast in component surface temperatures generated by differences in insolation (Krayenhoff and Voogt, 2007b). Table [4.3] details the relevant SUM_{VEG} input parameters and surface geometrical relationships for the Sunset northwest sub-domain case study.

Table 4.3: Tree crown biophysical parameters and sensor geometrical specifications for the Sunset residential case study.

Parameter	Units	Value
Sensor and Surface Geometry		
YD	—	230
LMST	hr	0900 and 1200
ϕ	decimal degrees	49.25
Z_S	m	500–1000
IFOV	°	12
λ_P	—	0.10
Tree Crown Biophysical		
LAD	—	Spherical
μ_L	m^{-1}	2.4
Ω_C	—	1.0
α_L	—	0.20
ε_L	—	0.97
H_T	m	8
H_{tk}	m	3
r_C	m	3
f_{width}	m	0.1
λ_V	—	0.06

The inclusion of tree crowns decreases T_S at every sensor position (Figure [4.7]). As with the evaluation of SUM_{VEG} using Sunset temperature observations, this is due to the decreased temperature of tree crown foliage and surfaces shaded by tree crowns that replace warmer and potentially sunlit built surfaces within the sensor IFOV. However, even though the approximate same surface region is 'seen' at all sensor view angles, tree crowns do not reduce T_S equally at every sensor view angle. Figure [4.8a] shows the difference in T_S (ΔT_S) at every sensor view angle between the treed and treeless scenarios. T_S for surfaces corresponding to the hot spot have decreased the least with the largest temperature decrease corresponding to sensor angles far from the hot spot and at large θ_V. Λ_{MAX}—defined as the difference between $T_{S_{MAX}}$ and $T_{S_{MIN}}$—increases due to a larger decrease in $T_{S_{MIN}}$ than $T_{S_{MAX}}$.

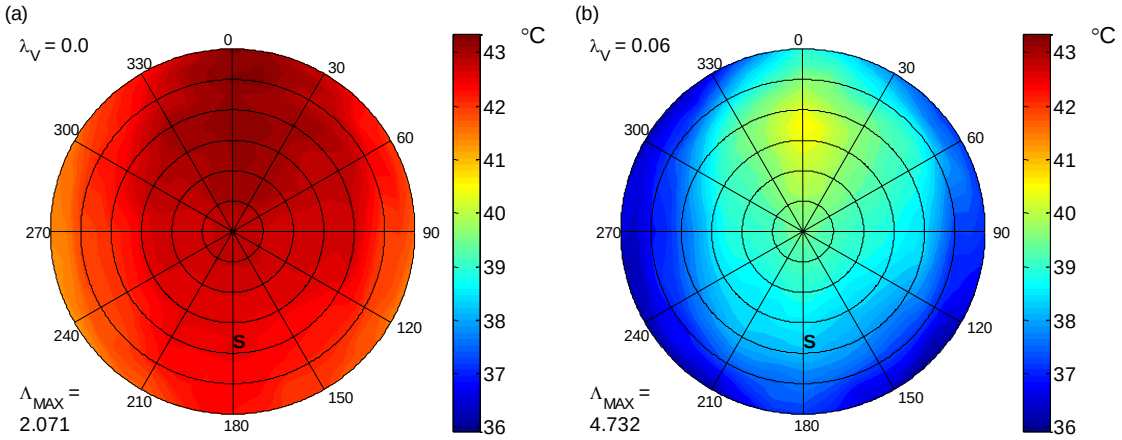


Figure 4.7: Polar co-ordinate plots of T_S at 1200 LMST for the Sunset northwest sub-domain (b) with and (a) without tree crowns.

Figure [4.8b–d] present the view factor occupied by foliage for every sensor view angle, including: total foliage [4.8b], sunlit foliage [4.8c], and shaded foliage [4.8d]. Total foliage view factor values are the sum of the sunlit and shaded foliage view factors. The colour scale range is optimized to highlight differences in view factor between sensor view angles. Together these three polar co-ordinate plots explain the unequal influence of tree crowns on T_S over the range of sensor view angles. The sensor IFOV occupied by foliage is lowest at nadir rising with increasing θ_V and largely independent of φ_V (i.e. symmetrical about nadir). This occurs for two reasons: 1) Sunset tree crowns are slightly wider (6m) than they are tall (5m), and 2) oblique θ_V increase the probability of sensor view intersecting multiple tree crowns. Both of these occurrences increase the path length through tree crowns at high θ_V. This results in a decreased probability of gap and subsequent increased view factor occupied by foliage.

Similar to the unequal angular view factor of total foliage, the view factor occupied by sunlit and shaded foliage varies as a function of sensor view angle, though is also dependent on the hot spot. At the hotspot, the foliage is predominantly sunlit while shaded foliage dominates at sensor view angles far from the hot spot. T_{lh} is generally several degrees lower than T_{ls} and built facet temperatures. T_{ls} is typically closer to built facet temperatures than is T_{lh}. As a result, the 'cooling' effect of tree crowns on T_S is greatest where shaded foliage dominates the sensor IFOV. Therefore, in this simulation the largest influence of foliage occurs at oblique θ_V corresponding to predominantly shaded foliage.

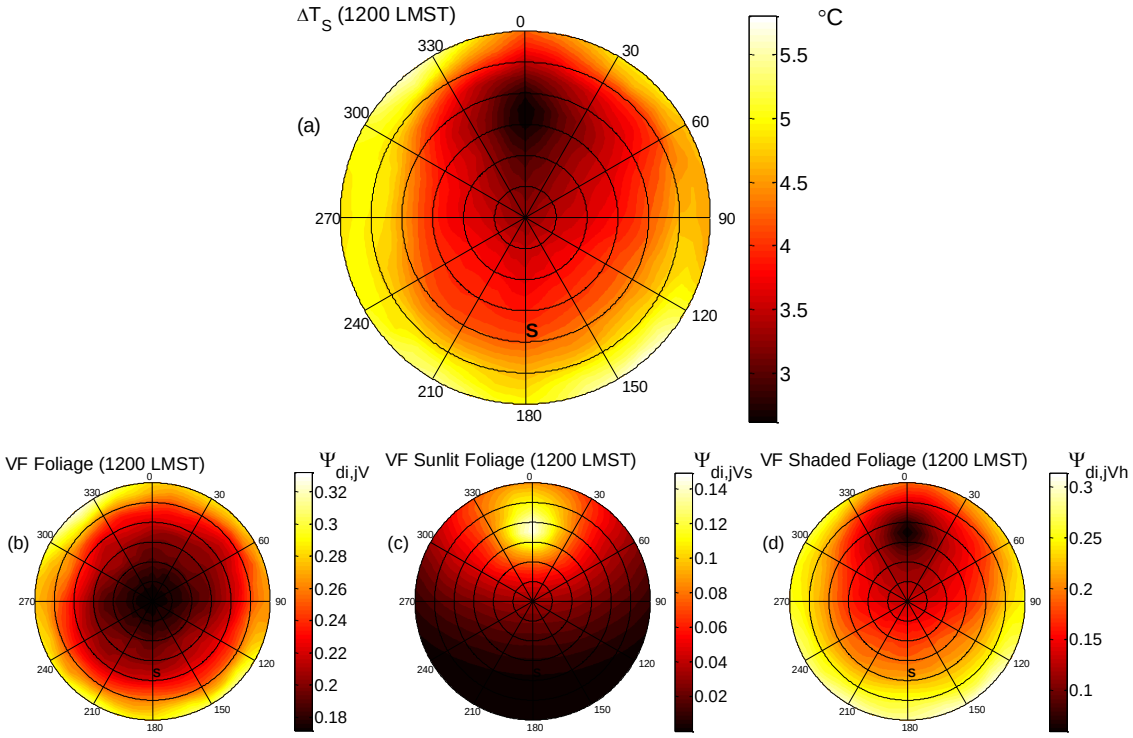


Figure 4.8: Polar co-ordinate plots at 1200 LMST for the Sunset northwest sub-domain. (a) ΔT_S between the treed and treeless scenario at each sensor angular position. (b–d) View factors (Ψ) for foliage at each sensor angular position with $\lambda_V = 0.062$.

The inclusion of tree crowns at 1200 LMST increases Λ_{MAX} by 2.7°C (compared to the treeless simulation). $T_{S_{MAX}}$ coincides with the hot spot and $T_{S_{MIN}}$ coincides with a θ_V far from the hot spot ($\theta_V \approx 60°$). Tree crowns decrease $T_{S_{MAX}}$ from 43.3°C to 40.6°C (-2.7°C) and decrease $T_{S_{MIN}}$ from 41.3°C to 35.9°C (-5.4°C). This unequal treatment of $T_{S_{MAX}}$ and $T_{S_{MIN}}$ by tree crowns is due mostly to the hot spot effect related to the relative proportions of sunlit and shaded foliage visible to the sensor.

The Sunset residential area is a relatively open geometry ($\lambda_P \approx 0.10$) characterized by low building heights and wide streets. Tree crowns tend to shade a portion of sunlit wall and ground surfaces and occlude sunlit surfaces from sensor view, both of which generate temperature contrasts that increase the magnitude of Λ_{MAX}. In more compact urban geometries, it is expected that tree crowns *may* reduce Λ_{MAX} by decreasing the contrast in T_S with sensor view angle. Additionally, at a certain critical value, increasing λ_V *may* reduce Λ_{MAX} magnitude in open geometries as foliage begins to 'saturate' the sensor IFOV and shade or occlude a majority of sunlit built surfaces, thus reducing the

contrast in T_S between opposing sensor view angles. The influence of tree crowns in compact urban geometries and potential existence of a value of λ_V corresponding to maximum Λ_{MAX}, for a given λ_P, in open geometries is investigated in Chapter 5.

Figure [4.9] presents polar co-ordinate plots of T_S as a function of sensor view angle at 0900 LMST for the northwest Sunset sub-domain with [4.9b] and without [4.9a] tree crowns.

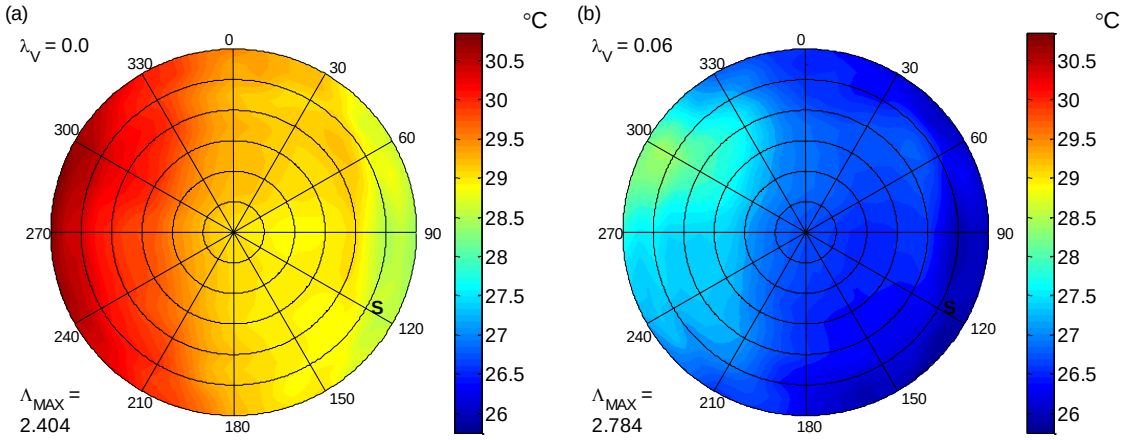


Figure 4.9: Polar co-ordinate plots of T_S at 0900 LMST for the Sunset northwest sub-domain (b) with and (a) without tree crowns.

As with the 1200 LMST simulation, including tree crowns decreases T_S for every sensor view angle. Figure [4.10] details ΔT_S, resulting from the inclusion of tree crowns in the Sunset northwest domain at 0900 LMST, at every sensor view angle. The hot spot influence (i.e. influence of sensor IFOV occupied by sunlit and shaded foliage) is again evident with the minimum decrease in T_S corresponding to $T_{S_{MAX}}$ and larger differences evident far from the hot spot where shaded foliage is a higher proportion of the 'seen' total foliage. With the inclusion of tree crowns, $T_{S_{MAX}}$ decreases 2.3°C and $T_{S_{MIN}}$ decreases 2.7°C. As a result, Λ_{MAX} increases by 0.4°C. This increase is substantially less than in the 1200 LMST simulation due to the relatively minimal contrast between component surface temperatures (e.g. sunlit and shaded surfaces)—and hence reduced contrast in T_S between opposing sensor view angles—that occurs in the early morning hours before insolation has generated substantial surface temperature variability.

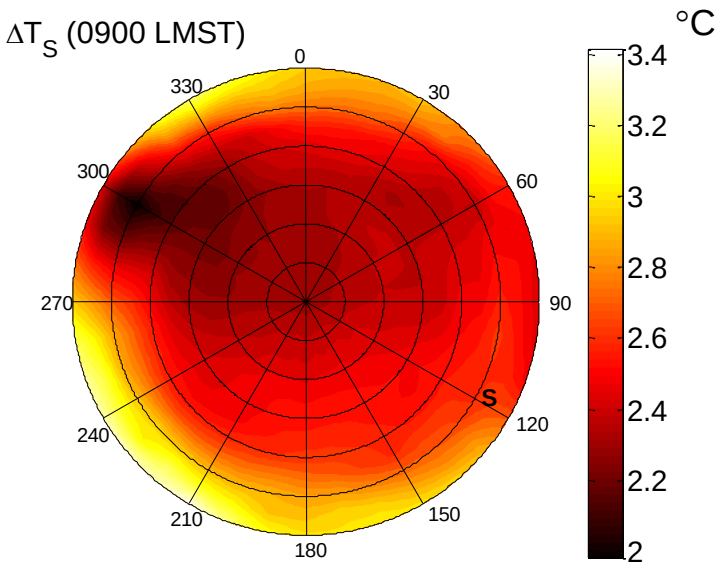


Figure 4.10: Polar co-ordinate plot of ΔT_S between the treed and treeless scenario at each sensor view angle for the Sunset northwest sub-domain at 0900 LMST.

Figure [4.11] presents polar co-ordinate plots of modelled T_S at 1200 LMST over the southwest 12 block Sunset sub-domain [4.11b] and full Sunset domain [4.11a]. The southwest sub-domain is characterized by blocks oriented with an E–W long axis while the full Sunset domain consists of a mixture of blocks with their long axis orientated either N–S or E–W as well as some more mixed land-use (i.e. apartment buildings, electrical substation, open paved area, etc.).

Table [4.4] describes the surface and sensor geometry used for the southwest sub-domain and full domain tests. Simulation of the full domain uses a different sensor geometry from that used in the sub-domain tests. Compared to the northwest sub-domain, the 12 block southwest sub-domain has a λ_P of approximately 0.122 and λ_V of 0.075 indicating a slightly more compact urban geometry (though still relatively open) and more tree canopy cover than in the northwest sub-domain. Adding approximately 7.5% canopy cover increases Λ_{MAX}, relative to the domain without tree crowns, by 3.1°C. As in the northwest sub-domain, the inclusion of tree crowns results in a decrease in T_S at every sensor view angle. The increase in Λ_{MAX} results from a larger decrease of $T_{S_{MIN}}$ than $T_{S_{MAX}}$ due to the angular variation in view factor occupied by sunlit and shaded foliage within the sensor IFOV as a function of sensor view angle.

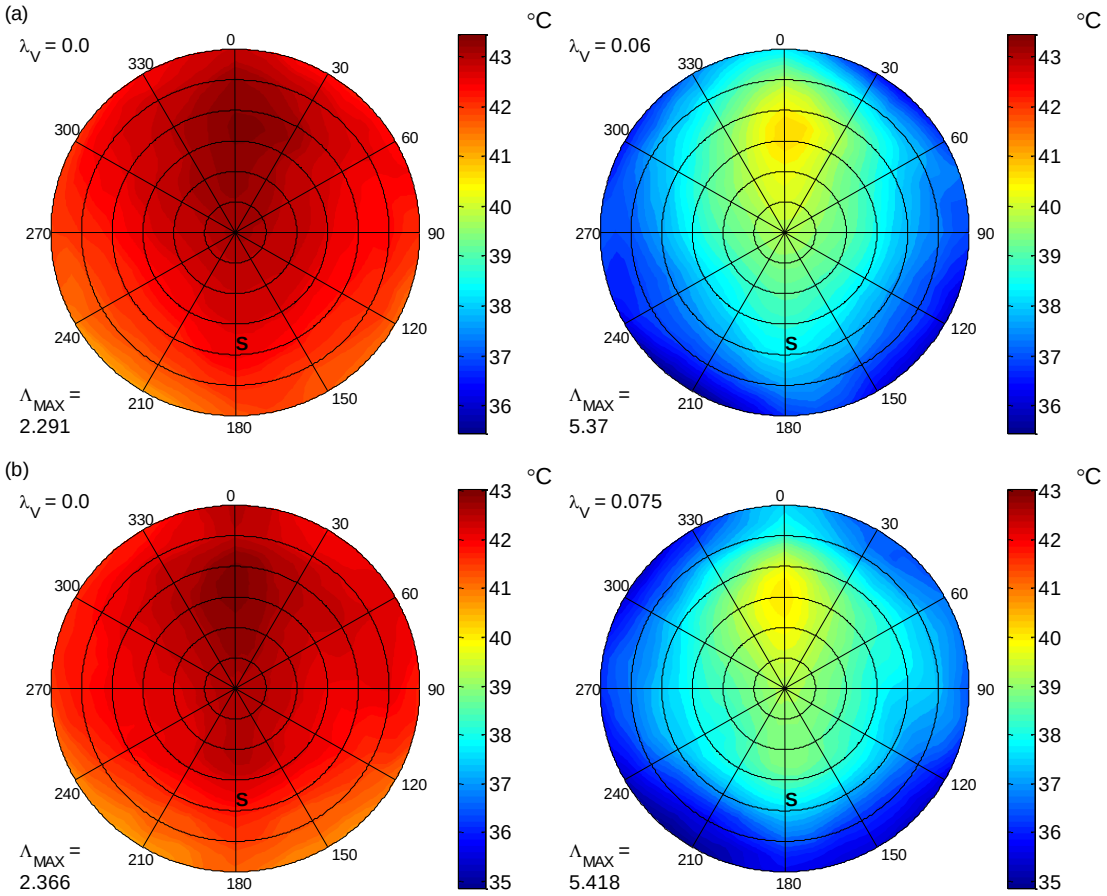


Figure 4.11: Polar co-ordinate plots of T_S at 1200 LMST for (a) the full Sunset domain and (b) for the 12 block southwest sub-domain with (RIGHT) and without trees (LEFT).

Determining Λ_{MAX} for an urban surface requires a sufficiently large surface area within a remote sensor IFOV to view the surfaces that contribute most of the temperature variance (Voogt and Oke, 1998). In order to ensure the sensor geometry used for the northwest and southwest sub-domain tests captures sufficient surface structural heterogeneity, and in order to examine the representativeness of the northwest and southwest sub-domains for the full Sunset domain, a third test of SUM_{VEG} using the full Sunset domain was conducted with a higher z_S and wider IFOV (though still relatively narrow to avoid the possible effective thermal anisotropy dampening effect of wide IFOV sensors) (Table [4.4]). The full Sunset domain and northwest sub-domain have similar λ_P and λ_V of approximately 10% and 6%, respectively.

Table 4.4: Sensor and surface geometry and component sunlit (S) and shaded (SH) surface temperatures for the southwest sub-domain and full Sunset domain simulations. Surface temperatures are the same as those used to populate facets in the northwest sub-domain.

Parameter	Units	Southwest Sub-Domain	Full Domain
Sensor Geometry			
z_S	m	500–1000	650–1300
IFOV	°	12	15
Surface and Temporal Characteristics			
YD	—	230	230
Time	LMST	1200	1200
λ_P	—	0.122	0.103
λ_V	—	0.075	0.060
Component Temperatures (S | SH)			
Roof	°C	58.76 | 44.08	
Street	°C	45.59 | 25.47	
Alley	°C	45.22 | 26.70	
Grass	°C	34.29 | 22.08	
NW	°C	32.56 | 26.42	
SW	°C	32.56 | 26.42	
EW	°C	29.29 | 27.05	
WW	°C	29.29 | 27.05	
Tree	°C	26.34 | 21.68	
T_a	°C	24.8	

Figure [4.11a] presents results for the full Sunset domain with the sensor geometry specified in Table [4.4]. Λ_{MAX} for the Sunset domain roughly corresponds to the results from the northwest sub-domain anisotropy investigation with (11.9% increase) and without (9.6% increase) tree crowns. In general, relatively minimal change in the magnitude of thermal anisotropy occurs with changing sensor spatial position which suggests the current sensor configuration captures the majority of the surface variability (with the use of facet mean surface temperatures).

4.2.3 Comparison of SUM_{VEG} Calculated Directional Temperature Differences with Observations

The preceding validation of SUM_{VEG} (Section [4.1.4]) evaluated its ability to predict T_S extracted from a circular IFOV imposed on TIR images obtained during

airborne traverses with a TIR remote sensor over the Sunset residential neighbourhood. SUM_{VEG} was subsequently used to calculate neighbourhood scale Λ_{MAX} magnitude with the inclusion of tree crown vegetation in the model domain. The following tests evaluate the ability of SUM_{VEG} to predict temperature differences (ΔT_S) between opposing sensor view directions using T_S values extracted from TIR images of the Sunset residential neighbourhood.

Voogt and Oke (1998) calculated mean T_S for each sensor view direction, from the three flights over the Sunset residential neighbourhood, by averaging extracted T_S values from every TIR image. Differences between mean temperatures for each viewing direction can provide information on the degree of effective thermal anisotropy. This is not the same as Λ_{MAX} reported in Section [4.2.2] which is the maximum difference in T_S accounting for *every sensor view angle*. Instead, estimates of thermal anisotropy reported here are differences between any two sensor view angles, where the sensor is restricted to one of five orientations: V-nadir, N-North, S-South, W-West, E-East[7]. Thus, these estimates constitute image-scale estimates of thermal anisotropy over the Sunset residential neighbourhood.

Replicating ΔT_S estimates identified by Voogt and Oke (1998) with SUM_{VEG} is not feasible given the large number of TIR images used to calculate each directional mean T_S for the three Sunset flights. Instead the following analysis uses the same subset of TIR frames used in the evaluation of SUM_{VEG} (Section [4.1]), though the values of ΔT_S reported by Voogt and Oke (1998) are included for comparison purposes. For each of the three Sunset residential flights, nadir values of T_S are the mean of four TIR frames while T_S for each cardinal viewing direction is the mean of two TIR frames. Since the frames used to calculate these mean T_S values with SUM_{VEG} constitute a small fraction of the total number of frames for each viewing direction, large deviations may exist between ΔT_S values reported by Voogt and Oke (1998) and those estimated using SUM_{VEG}, due to spatial variations in surface structure (and facet surface temperatures) across the Sunset residential domain. A more accurate determination of the ability of SUM_{VEG} to replicate

[7] For each cardinal viewing direction, the sensor is angled at approximately 45° off-nadir and indicates the direction the sensor is facing.

ΔT_S estimates can be made by comparison of SUM_{VEG} with the small subset of TIR images that were previously used to evaluate SUM_{VEG}.

Comparisons of ΔT_S and T_S—between estimates derived from the TIR image subset and values calculated using SUM_{VEG}—are made using two sample T-tests. At the 0.01 level, there is not a significant difference between means of ΔT_S from the TIR image subset ($\bar{x} = 0.4°C$, $\sigma = 3.2°C$) and SUM_{VEG} ($\bar{x} = 0.9°C$, $\sigma = 3.4°C$); t(58) = -0.636, p = 0.53. Additionally, there is not a significant difference between means of T_S from the subset of TIR images ($\bar{x} = 33.5°C$, $\sigma_X = 5.3°C$) and SUM_{VEG} ($\bar{x} = 33.7°C$, $\sigma_X = 5.2°C$); t(28) = -0.125, p = 0.90[8].

Figure [4.12a] shows the comparison of ΔT_S using: (1) mean T_S from Voogt and Oke (1998), (2) mean T_S averaged for each view direction from the subset of TIR images, and (3) the SUM_{VEG} modelled estimates of T_S (Figure [4.12b] shows the individual values of T_S, stratified by view direction, used to calculate the values of ΔT_S). Vertical dashed lines divide the three Sunset flights and each x-axis interval corresponds to a difference between view directions (or individual view direction in Figure [4.12b]).
SUM_{VEG} modelled ΔT_S estimates generally compare well with those extracted from the subset of TIR images (*MAE* =0.88°C and *RMSE* = 1.06°C) though less favourably with the values reported by Voogt and Oke (1998) (*MAE* =1.13°C and *RMSE* = 1.47°C). The larger error in comparison to the values of Voogt and Oke (1998) are probably the result of spatial surface variability not resolved by the relatively small subset of TIR images used with SUM_{VEG} to estimate ΔT_S. Since the degree of thermal anisotropy reported here is simply the difference between any two sensor view directions, the accuracy of SUM_{VEG} estimates depend entirely upon the ability of SUM_{VEG} to successfully estimate T_S from each of the directions. Therefore, as anticipated, the *MAE* and *RMSE* for these thermal anisotropy estimates are close to those reported for the full model evaluation of SUM_{VEG}, which used the same subset of TIR images (*MAE* and *RMSE* of 0.87°C and 1.06°C, respectively) (Table [4.2]).

[8] $\bar{x}$ and σ_X represent the mean and standard deviation of the sample, respectively.

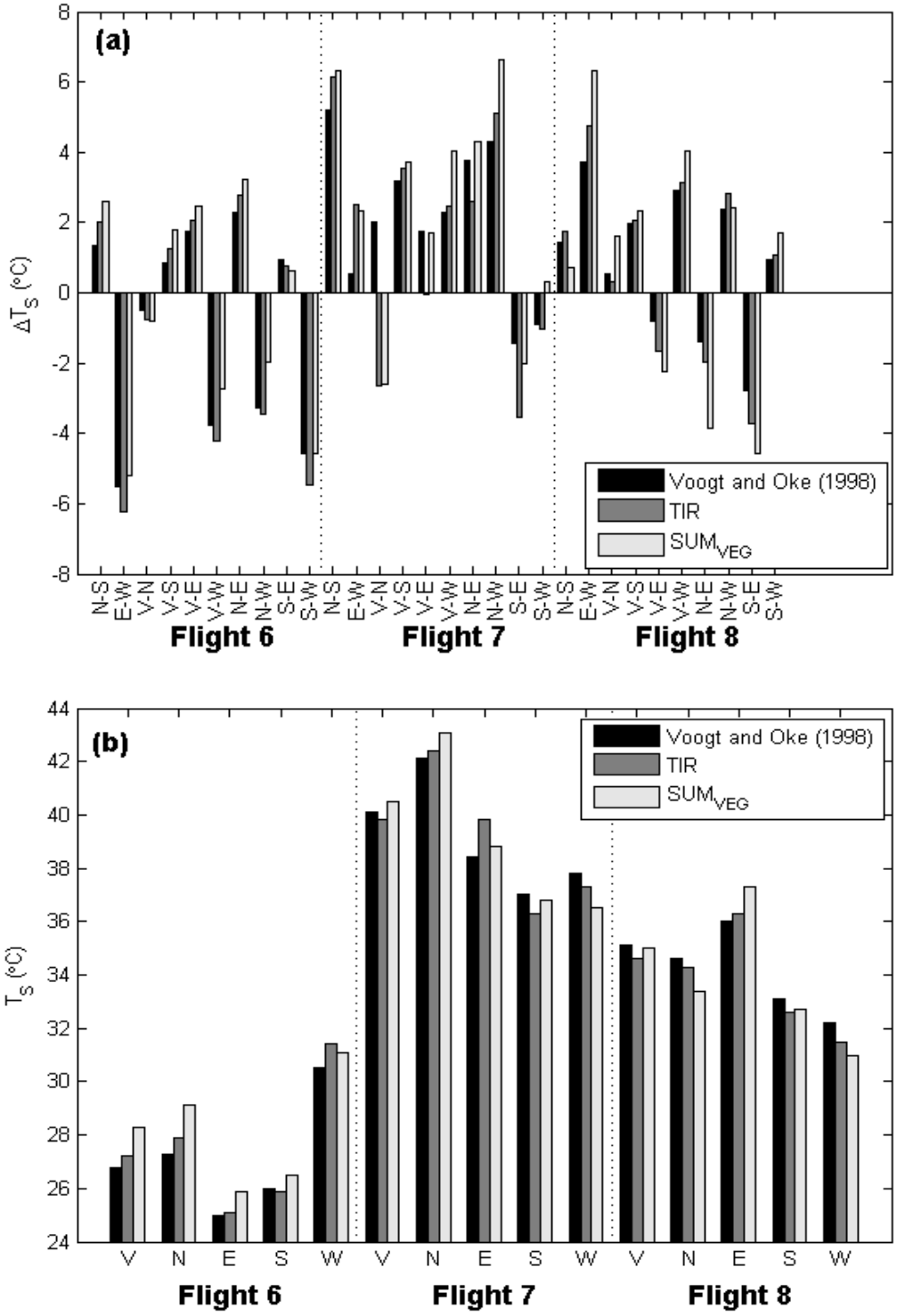


Figure 4.12: (a) Bar plot of thermal anisotropy (ΔT_S) over the Sunset residential surface measured as the difference in T_S between view directions (x-axis) using: (1) all TIR images obtained during the three flights (Voogt and Oke (1998)), (2) using the same subset of TIR images used for the SUM_{VEG} model evaluation, and (3) using SUM_{VEG} for the subset of TIR images. (b) Mean T_S from the same sources used for (a) separated based on view direction. 'V', 'N', 'E', 'S', and 'W' indicate nadir, north, east, south, and west view directions, respectively.

SUM_{VEG} is, for the most part, able to reproduce the trends in opposing view direction identified by Voogt and Oke (1998), including: strong temperature differences between east/west off-nadir viewing directions during the morning and later afternoon flight, a maximum temperature difference between north/south viewing directions during the early afternoon flight and somewhat diminished temperature differences during the morning and later afternoon flights. The underestimation of north/south differences during the late afternoon flight is probably the result of the lack of sloped roofs in SUM_{VEG}. As a result SUM_{VEG} does not resolve the portion of thermal anisotropy generated by the difference in insolation between opposing roof facets.

Relatively large discrepancies between the SUM_{VEG} and TIR derived ΔT_S estimates are found when comparing north/south view directions to east/west view directions during the early afternoon (flight 7). SUM_{VEG} appears to both overestimate north and south view direction and underestimate east and west view direction T_S estimates during the early afternoon. Comparison of the same directional differences (i.e. N–E, N–W, S–E, S–W) between the subset of TIR images and the SUM model *without* tree crowns—though with ground-level vegetation—proves that, in the absence of tree crowns, SUM_{VEG} substantially overestimates T_S from all viewing directions. Interestingly, since the overestimation of each directional T_S is on the same order of magnitude, ΔT_S estimates with the treeless SUM_{VEG}, during flight 7, are actually closer to the values calculated from the subset of TIR images. This suggests that it is the identical nature of tree crowns within SUM_{VEG} that is leading to the over- and underestimation of ΔT_S. Evaluation of SUM_{VEG} using the same subset of TIR images showed that SUM_{VEG} tends to over- or underestimate T_S because the single set of tree crown dimensions applied to all trees is not necessarily representative of the subset of trees within each TIR frame.

Here, the SUM_{VEG} full model evaluation, and comparison to observed ΔT_S, use mean sunlit and shaded facet temperatures for each surface facet (e.g. sunlit and shaded roof, west wall, east wall, etc.). Voogt (2008) found that the use of mean facet temperatures caused SUM to underestimate the total thermal anisotropy for two urban land uses in Vancouver, B.C. Lagouarde *et al*. (2010) also reported a systematic underestimation of modelled urban thermal anisotropy and cited the use of mean facet surface temperatures and simplified surface geometry as potential causes. Interestingly,

with the inclusion of tree crowns, though still using mean sunlit and shaded temperatures for surface facets, SUM_{VEG} tends to both over- and underestimate the degree of thermal anisotropy for the Sunset residential area of Vancouver B.C. (Figure [4.12a]). This implies that at least a portion of the model underestimation reported by Voogt (2008) may be due to the inability of SUM to account for the influence of tree crowns on thermal anisotropy. However, Voogt's analysis was restricted to a light industrial and downtown commercial area in Vancouver, B.C., both of which exhibit low vegetation cover. Further research is required in order to separate the relative error attributable to the use of mean sunlit and shaded facet surface temperatures from the potential bias resulting from the identical nature of tree crowns properties in the current manifestation of SUM_{VEG}. Ideally future coupling of SUM_{VEG} with a vegetated micro-scale urban energy budget model will permit such investigation.

4.3 Summary of SUM_{VEG} Evaluation and Sunset Residential Case Study

The digitized Sunset neighbourhood building and tree surface, with surface temperatures derived from the temperature observations of Voogt and Oke (1997; 1998), is used as a case study to examine the influence of tree crowns on the angular variation of T_S as measured using narrow IFOV TIR remote sensors. At 0900 LMST and 1200 LMST, the inclusion of a 6% surface cover of tree crowns—the average amount of tree crown vegetation determined by analysis of the study area—to the northwest Sunset 8 block sub-domain had several significant influences on T_S and resultant Λ_{MAX}. At 0900 LMST and 1200 LMST, tree crowns increase Λ_{MAX} by 0.4°C and 2.7°C, respectively. The influence of tree crowns on T_S varies with sensor view angle due to the unequal angular distribution of view factor occupied by sunlit and shaded foliage.

Similar results are found in the southwest sub-domain of the Sunset area where buildings are arranged in blocks with the long axis oriented mostly E–W. Here, a 3.1°C increase in Λ_{MAX} is modelled at 1200 LMST with the addition of 7.5% canopy cover (over the treeless simulations). Using SUM_{VEG} over the full Sunset domain and increasing the sensor height (+150m) and IFOV (+3°) yields a similar increase in Λ_{MAX} due to tree crowns (+3.1°C with 6% addition of tree canopy cover). For the full Sunset domain and both sub-domains, the addition of tree crowns decreases T_S at every sensor view angle.

The increase in Λ_{MAX} is due to a larger decrease in $T_{S_{MIN}}$ than $T_{S_{MAX}}$ that arises due to the unequal distribution of sunlit and shaded tree crown foliage as a function of sensor view angle.

The following general conclusions can be made based upon the case study results:

- Tree crowns, by presenting a surface cooler than the built components and by shading of sunlit surfaces, decrease T_S at every sensor view angle. However, due to the hot spot effect generating differences in the view factor occupied by sunlit and shaded foliage with a remote sensor IFOV, the influence of tree crowns varies as a function of sensor view position.
- For the relatively open Sunset urban geometry ($\lambda_p \approx 0.10$), even a relatively low cover of tree crowns ($\lambda_V \approx 0.06$) increases Λ_{MAX} by generating contrasts in surface temperature between opposing sensor view angles. In particular the relative dominance of view factor occupied by shaded foliage at oblique θ_V results in an enhanced 'cooling' influence of tree crowns on $T_{S_{MIN}}$, relative to the sunlit foliage dominated IFOV for the sensor view angle corresponding to $T_{S_{MAX}}$ (i.e. at the hot spot).
- The difference in Λ_{MAX} resulting from the use of the treed and treeless SUM_{VEG} model is large with respect to the actual magnitude of thermal anisotropy. For example, the addition of trees in the northwest sub-domain at 1200LMST on August 17th increases Λ_{MAX} by approximately 2.7°C, which constitutes approximately 58% of the total Λ_{MAX} (4.7°C). This indicates the important influence of tree crown vegetation on thermal anisotropy and supports the use of SUM_{VEG}, as opposed to SUM, for treed urban surfaces.

Previous evaluation of the non-vegetated SUM found it to compare well with remotely-detected city and scale model observations of temperature and surface view factors (Soux *et al.*, 2004; Voogt, 2008). SUM_{VEG} has been evaluated upon its ability to replicate T_S obtained using narrow IFOV TIR thermometers over the Sunset residential neighbourhood of Vancouver, B.C. The main goal of this validation is to determine the improvement associated with the use of SUM_{VEG} over vegetated urban surfaces, using the Sunset residential neighbourhood as a case study.

The following conclusions regarding the SUM_{VEG} full model evaluation are made:

- For the Sunset case study, SUM_{VEG} increases the accuracy of T_S and ΔT_S estimates over the model devoid of tree crown vegetation. Specifically, the inclusion of tree crowns during estimation of T_S for all sensor view angles results in a *MAE* and *RMSE* of 0.87°C and 1.06°C, a decrease relative to the treeless SUM of 2.69°C and 2.59°C, respectively. Two sample Student's T-tests result in no significant difference in the means of samples of T_S and ΔT_S between TIR extracted measurements and SUM_{VEG} estimates.
- Spatial heterogeneity of tree crown biophysical parameters, common in urban areas, necessitates accurate estimation of a representative set of values for the simulated surface domain. Potential error in specification of these values *may* lead to over- or underestimation of the influence of tree crowns on T_S and therefore error in estimates of surface thermal anisotropy. However, further testing is required in order to determine the potential error associated with incorrect specification of tree crown biophysical parameters and to investigate the potential need for modelling tree crown biophysical heterogeneity.

The next chapter presents an analysis of the sensitivity of thermal anisotropy, calculated using SUM_{VEG}, to tree crown cover in a range of urban forms representative of a residential urban land use of varying density. Additionally, the influence of a number of tree crown biophysical parameters on the magnitude of thermal anisotropy is investigated.

Chapter 5

SENSITIVITY OF URBAN THERMAL ANISOTROPY TO TREE CROWN VEGETATION

Several observational studies have noted the high magnitude of urban thermal anisotropy—particularly relative to natural surface covers—for a range of urban land use types (e.g. Voogt and Oke, 1997; Lagouarde *et al.*, 2004; Lagouarde and Irvine, 2008, etc.). The difficulties related to the investigation of this phenomenon are the copious surface parameters, sensor configurations, and meteorological conditions that are known, or are expected, to influence the magnitude of thermal anisotropy. Given the diversity of potential controls on urban thermal anisotropy, emphasis has shifted towards the development of numerical models that allow a flexible manipulation of parameters that may be expected to influence the magnitude of thermal anisotropy (e.g. Soux *et al.*, 2004; Voogt and Krayenhoff, 2005; Lagouarde *et al.*, 2010; Lagouarde *et al.*, 2012). These models have typically been applied to simulate downtown commercial cores or industrial sectors partially in order to avoid the additional complexity of, and in some cases model inability to simulate, tree crown vegetation.

This chapter presents SUM_{VEG} modelled Λ_{MAX}[9] results based on narrow IFOV TIR remote sensors over urban areas with substantial fractions of tree crown vegetation cover. The evaluation and preliminary testing of SUM_{VEG} using the Sunset residential neighbourhood as a case study indicated the high potential of SUM_{VEG} to be used for urban areas with tree canopy cover (Chapter 4). The relatively low coverage of tree crown vegetation in the Sunset residential neighbourhood ($\lambda_V \approx 0.06$) is not necessarily representative of the amount of tree crown cover in many North American residential

[9] Λ_{MAX} results presented here are calculated as the maximum difference of a T_S distribution resulting from range of viewing directions (e.g. Voogt and Oke, 1998).

neighbourhoods, or cities in general, and further investigation is warranted to examine the complete influence of tree crowns on Λ_{MAX}.

Additionally, the Sunset case study represents a single urban geometry; it is hypothesized that the influence of tree crowns on thermal anisotropy is dependent upon the urban geometry, which warrants the examination of their influence in a range of urban geometries. In relatively open urban geometries, such as the Sunset case study ($\lambda_P \approx 0.10$), the inclusion of tree crowns increases temperature contrasts (and thermal anisotropy) by presenting a surface generally cooler than the built facets and shading otherwise sunlit facets (Chapter 4). In compact geometries, the inclusion of tree crowns *may* decrease thermal anisotropy by muting contrasts in temperature between opposing view directions. Additionally, for a given open urban form, sequentially increasing tree crown surface cover may increase thermal anisotropy until a critical value past which adding tree crowns reduces temperature contrasts and lowers thermal anisotropy (i.e. a Λ_{MAX} maximum value effect).

The purpose of this chapter is to apply SUM_{VEG} to examine the sensitivity of Λ_{MAX} over a range of treed urban configurations, represented as regularly-spaced, aligned arrays of square footprint block structure buildings, controlled by building plan fraction (λ_P), tree crown plan fraction (λ_V), and tree height to building height ratio (H_T/BH). Since the influence of urban form on Λ_{MAX} (i.e. λ_P, *BH/BL, BH/SW*) has been previously investigated using a coupled SUM + TUF-3d modelling system (Voogt and Krayenhoff, 2005; Krayenhoff and Voogt, 2007b), the current analysis is restricted to simulations of typical *residential neighbourhood geometries* (i.e. low building heights and moderate building height to building length ratio) with varying densities (λ_P).

5.1 Description of Simulated Urban Surface

5.1.1 Forcing Conditions and Urban Geometry

There is a seemingly endless combination of urban tree crown configurations that could be tested using the SUM_{VEG} model. Here, SUM_{VEG} is used to investigate the sensitivity of daytime Λ_{MAX} to a range of treed residential urban geometries and tree crown biophysical parameters. These tests use a regular urban geometry characterized by

a repeating array of square footprint, block structure buildings separated by equal width streets. Tree crowns line the edge of streets along the building length in order to represent a treed urban surface common to many North American cities (e.g. Figure [5.1]).

Simulations are performed using forcing conditions and solar geometry for the Basel-Sperrstrasse canyon site in Switzerland (47.57°N, 7.58°E) on March 28th and June 21st and the Miami International Airport, Florida (25.79°N, 80.29°W) on June 21st for a number of treed urban geometries. Hourly forcing data are available for both areas and indicate that both dates are characterized by relatively minimal cloud cover. Previous studies using a coupled SUM + TUF-3d model have investigated the influence of urban form and diurnal solar path on thermal anisotropy—in the absence of tree crowns—at the latitude of Basel (Krayenhoff and Voogt, 2007b) which can be used for comparison purposes.

Surface thermal and radiative properties (i.e. construction materials), required for the calculation of surface temperatures using TUF-3d, are held constant between the two latitudinal simulations at values specified by Krayenhoff and Voogt (2007b). Here, only realistic thermal and radiative surface properties are required rather than actual properties for Basel-Sperrstrasse or Miami. Results of this investigation should be interpreted as representative of early spring and early summer clear sky conditions for mid-latitude and lower-latitude residential neighbourhoods.

SUM has previously been coupled to the TUF-3d sub-facet scale energy balance model in order to investigate thermal anisotropy for a diverse set of urban geometrical configurations (Voogt and Krayenhoff, 2005; Krayenhoff and Voogt, 2007b). These tests examined the influence of urban form and diurnal solar path (i.e. latitude, time of year, time of day) on effective thermal anisotropy. The current investigation uses three λ_P that are chosen to broadly represent the range used by Voogt and Krayenhoff (2005) which corresponds to typical values for real cities (Grimmond and Oke, 1999): 0.14, 0.28, and 0.41 with corresponding canyon aspect ratios of 0.53, 1.00, and 1.67, respectively.

For simplicity, buildings are rectangular to maintain a building height to building length ratio (*BH/BL*) and building length to building width ratio equal to unity. Since the *BH/BL* ratio is held constant for all λ_P values, this can be thought of as a single urban land use (residential) where increasing λ_P indicates increasingly dense urban geometries

(i.e. same building size with changing street width). These scenarios are chosen, rather than a more diverse range of urban forms for two reasons: 1) the coupled SUM + TUF-3d has already been used to extensively investigate the influence of urban form on effective thermal anisotropy, and 2) the current geometrical configurations, which can be envisioned as a residential surface with a range of building densities, are expected to present the most obvious influence of tree crown vegetation on thermal anisotropy magnitude. This is because, relative to other land uses, these areas typically display the highest fractions of tree crown vegetation and the buildings are low enough to have substantial wall (and potentially roof) portions shaded from the sun or occluded from the sensor by tree crown foliage.

Oke (1989) reports that, in typical North American cities, residential areas typically exhibit 15–40% tree cover while commercial core and industrial areas generally have less than 10% cover. In commercial cores, typically characterized by high *BH/BL* ratios, trees crowns are generally substantially smaller than buildings (very low H_T/BH) which, given the controlling influence of differential wall facet insolation on thermal anisotropy magnitude (Voogt and Oke, 1997) will in all likelihood limit the influence of tree crowns.



Figure 5.1: Illustration of the regularly-spaced, aligned array of block structure buildings used to investigate the sensitivity of thermal anisotropy to treed residential urban forms. Micro-scale structures illustrated on one building (e.g. sloped roof, ancillary structure) are not currently represented in SUM_{VEG} but are included in this graphic to emphasize the potential influence of such structures on thermal anisotropy.

5.1.2 Tree Crown Coverage and Biophysical Parameters

The influence of tree crowns is investigated based on the total cover of tree crowns (λ_V) rather than on some other tree crown metric (e.g. r_C, f_{width},etc.) since λ_V, as opposed to a single structural dimension, is expected to have a stronger correlation with the magnitude of Λ_{MAX}. Additionally, λ_V can be estimated relatively easily from airborne or satellite imagery or land use land cover (LULC) inventories, whereas individual tree crown metrics may be difficult to extract from lower resolution imagery and require *in situ* measurement.

The Sunset residential case study, using a digitized surface including individual tree crown locations, showed that it has approximately 6% tree canopy coverage (in 2002), though there is some spatial variation (e.g. 7.5% coverage in the Southwest sub-domain). While this number is relatively low compared to the range indicated by Oke (1989), it is not necessarily surprising given the nature of trees in the Sunset neighbourhood; extensive examination using Google Street View© shows that much of the tree crown vegetation in the Sunset residential neighbourhood is generally in the form of smaller street trees with some shrubs, and shrubs were intentionally excluded from consideration in the generation of a tree crown cover map for the Sunset neighbourhood. It is important to note that values of tree crown cover for the Sunset case study are based on a representative set of tree crown dimensions gained from field investigation and could lead to under- or overestimation of the actual cover of tree crowns depending on the tree crown dimensions in a certain area.

Tree crown dimensions are specified in order to control the λ_V ratio within each urban form (λ_P). As a result, tree crown dimensions and spacing for equal λ_V, across the range of λ_P values investigated, are not necessarily equal. This method is used, rather than maintaining equal tree crown dimensions across all urban forms, since it should allow for more direct comparison of the influence of tree crowns between urban forms. For example, the same size tree crowns in two different urban geometries may not produce the same λ_V which would make comparison between the two difficult. For the current investigation, λ_V is varied from approximately 0% to 32%. Five discrete λ_V are simulated, corresponding approximately to 0.0, 0.06, 0.13, 0.25, and 0.32. Figure [2.3] shows an example of the modelled surface for two λ_V ratios.

Specification of a number of tree crown biophysical parameters are necessary to describe the interaction of tree crown foliage with solar radiation and surface radiant energy, including: leaf angle distribution, f_{width}, μ_L, and Ω_C. When testing the influence of tree crowns on Λ_{MAX} magnitude in a range of treed urban forms, all biophysical parameters are held constant. Foliage elements are assumed to be randomly distributed in crown volumes (i.e. no foliage clumping) with a spherical distribution of leaf inclination angles. The influence of Ω_C, f_{width} and μ_L on sensitivity of SUM_{VEG} modelled Λ_{MAX} is investigated for a number of the treed urban geometries from Section [5.2] in Section [5.4].

Given the anticipated control of wall facet shading by tree crowns on the magnitude of Λ_{MAX} it is important to attempt to maintain a similar degree of wall shading by tree crowns for each λ_V and λ_P combination. This is accomplished by maintaining a constant distance of tree crowns from walls (1m) and using tree height to building height ratios. For each λ_P and λ_V combination, three H_T/BH ratios are simulated: 0.50, 1.00, and 1.50. For all simulations, H_{tk} (i.e. the bottom of the crown volume) is held constant at 0.30 times the height of the buildings. As a result, different H_T/BH ratios do not simply indicate shifting the crown upwards within the urban canopy layer. Instead, increasing the H_T/BH ratio also creates a corresponding increase in the vertical extent of tree crowns simulating more wall facet shading and, in the case of $H_T/BH > 1.0$, roof surface shading. Given the control of differential wall facet shading on Λ_{MAX}, results are averaged over street orientations (i.e. domain rotation) from 0° to 67.5° in 22.5° steps which covers the full domain rotation; since walls have identical thermal and radiative properties, a street orientation of 90° is equivalent to a street orientation of 0°.

5.1.3 Estimation of Component Surface Temperatures using TUF-3d

For the following simulations, in the absence of observations, TUF-3d is used to calculate mean facet temperatures for the built surfaces. Previous examination of urban thermal anisotropy with SUM used sub-facet scale surface temperatures calculated using TUF-3d (Krayenhoff and Voogt, 2007a). TUF-3d is a dry, micro-scale urban energy budget model that has been evaluated against observational measurements and found to perform well (Krayenhoff and Voogt, 2007a). However, TUF-3d and SUM do not include

either tree crown or ground-level vegetation and, as a result, the same coupled model cannot be directly employed in the current investigation of Λ_{MAX} in vegetated urban domains.

While a number of energy budget models that treat vegetated urban surfaces have been developed that could potentially provide the necessary component surface temperatures to populate SUM_{VEG} (e.g. see the international urban energy balance model comparison results of Grimmond *et al.*, 2010 and Grimmond *et al*., 2011), TUF-3d output is still superior, for the current purposes, for three reasons: 1) TUF-3d was developed to be compatible with SUM (i.e. same cell array based surface structure) and hence SUM_{VEG}; 2) The intra-facet nature of TUF-3d improves upon facet-average surface temperatures; 3) The same solar geometry routines used in TUF-3d have been implemented into SUM_{VEG} for the calculation of leaf surface temperatures;

SUM_{VEG} is not an energy budget model and therefore does not estimate component surface temperatures based on solution of the energy budget. Since TUF-3d does not currently include tree crown vegetation, temperatures for the built surface facets and canyon air volume do not account for the interaction with tree crown foliage. Similarly the leaf surface temperature model incorporated into SUM_{VEG} does not account for the interaction with the built environment surrounding tree crowns. An alternative to the current method is to use surface temperature measurements, such as those employed for the Sunset residential case study. Such an approach, for the purpose of the current Λ_{MAX} sensitivity investigation, would require detailed observational campaigns beyond the scope of the current study.

Given the relatively sparse number of urban energy budget models that explicitly treat tree crown vegetation (i.e. not a tile-based approach), and in order to allow for the continued use of TUF-3d temperatures to populate the SUM_{VEG} surface, a weighting routine has been incorporated into SUM_{VEG} in an attempt to partially account for the interaction of shortwave radiation with tree crown and built surfaces (Section [2.6.3]). For built surface patches, ray tracing is used to extract surface patches shaded from direct solar radiation by tree crown foliage. Subsequently, the surface temperature for these shaded patches is estimated by weighting between the maximum (were the patch fully sunlit) and minimum (were the patch shaded by an opaque structure such as a building)

surface temperatures based on the probability of gap for direct and diffuse shortwave radiation through the tree crown shading the surface.

Given the inability of TUF-3d to treat tree crown vegetation, SUM_{VEG} simulations are unable to take advantage of the sub-facet scale surface temperatures TUF-3d can provide. Instead TUF-3d is used to estimate mean sunlit and shaded surface temperatures for each facet type. Research is ongoing to incorporate tree crown vegetation into TUF-3d that would potentially allow for a direct coupling of a vegetated TUF-3d with SUM_{VEG} on a patch by patch basis and account for the interaction between foliage and built surfaces in the estimation of temperatures (e.g. Nice *et al.,* 2013; Nice *et al.,* 2014).

5.2 Thermal Anisotropy as a Function of Building and Tree Crown Plan Fractions

5.2.1 Simulation Methods

The purpose of the following simulations is to investigate the influence of tree crowns on Λ_{MAX} in conjunction with other primary controls, including: diurnal solar path (i.e. time of day, time of year, and latitude) and urban form. Component surface temperatures are estimated with TUF-3d (built components) and a relatively simple leaf temperature model (foliage components) using Basel-Sperrstrasse and Miami International Airport forcing conditions. Construction materials, and associated thermal and radiative properties used for the sensitivity tests, are the same as those used by Krayenhoff and Voogt (2007b) for their investigation of the sensitivity of thermal anisotropy to urban form using the coupled SUM + TUF-3d model. Roofs, walls, and street surfaces are comprised of four layers characterized by heat capacity (C), thermal conductivity (k), and layer thickness (Δx) (Table [5.1]).

SUM_{VEG} is initialized using mean sunlit and shaded temperatures of roofs, streets, north walls, south walls, east walls, and west walls as well as sunlit and shaded tree crown foliage temperatures. Table [5.2] provides the relevant sensor and surface geometrical parameters required by SUM_{VEG} for the sensitivity simulations.

Table 5.1: Thermal parameters for surface components used to estimate temperatures with TUF-3d for the sensitivity simulations (Krayenhoff and Voogt, 2007b *through personal communication with* Rene Dupuis, 2003).

Parameter/Facet	**Layer 1**	**Layer 2**	**Layer 3**	**Layer 4**
Δx (m)				
Roofs	0.015	0.015	0.010	0.030
Streets	0.020	0.030	0.100	0.500
Walls	0.009	0.034	0.085	0.017
k (W m^{-1} K^{-1})				
Roofs	1.40	1.40	0.03	1.51
Streets	0.84	0.84	0.93	0.28
Walls	1.12	1.12	1.12	0.28
C (MJ m^{-3} K^{-1})				
Roofs	1.76	1.76	0.04	2.21
Streets	1.92	1.92	1.55	1.35
Walls	1.74	1.93	1.93	1.49

Table 5.2: Sensitivity simulation geometric and tree crown biophysical parameters.

PARAMETER	**UNIT**	**VALUE**
Sensor Geometry		
z_S	m	300
IFOV	°	12.0
Surface Geometry		
λ_P	—	0.13, 0.28, 0.41
λ_v	—	0.0, 0.06, 0.13, 0.25, 0.32
H_T/BH	—	0.5, 1.0, 1.5
BH/BL	—	1.0
η	°	0.0, 22.5, 45.0, 67.5
YD	—	87 and 172
ϕ	Decimal degrees	47.6 (Basel), 25.8 (Miami)
Tree Crown Biophysical		
f_{width}	m	0.05
μ_L	m^{-1}	1.0
LAD	—	spherical
Ω_C	—	1.0
ε_L	—	0.98
α_L	—	0.20
g_{vs}	mmolm^{-2}s^{-1}	0.01

5.2.2 Sensitivity of Thermal Anisotropy to Tree crown Plan Fraction

Figure [5.2] is a surface plot of Λ_{MAX} over the simulated range of λ_P and λ_V and averaged over the full domain rotation (i.e. street orientations η). Each surface plot is interpolated based on 3 $\lambda_P \cdot 5\ \lambda_V = 15$ street orientation averaged simulations and each (λ_P, λ_V) co-ordinate corresponds to a narrow IFOV (12°) remote sensor viewing a treed urban surface over a range of sensor view angles: θ_V of 0° to 60° in 5° increments and φ_V (relative to North = 0°) of 0° to 360° in 10° increments (481 sensor view angles). Figure [5.2] presents the surface plot for the June 21st simulation at 1200 LMST with tree height equal to building height ($H_T/BH = 1.0$) and using Basel-Sperrstrasse forcing conditions, as an example.

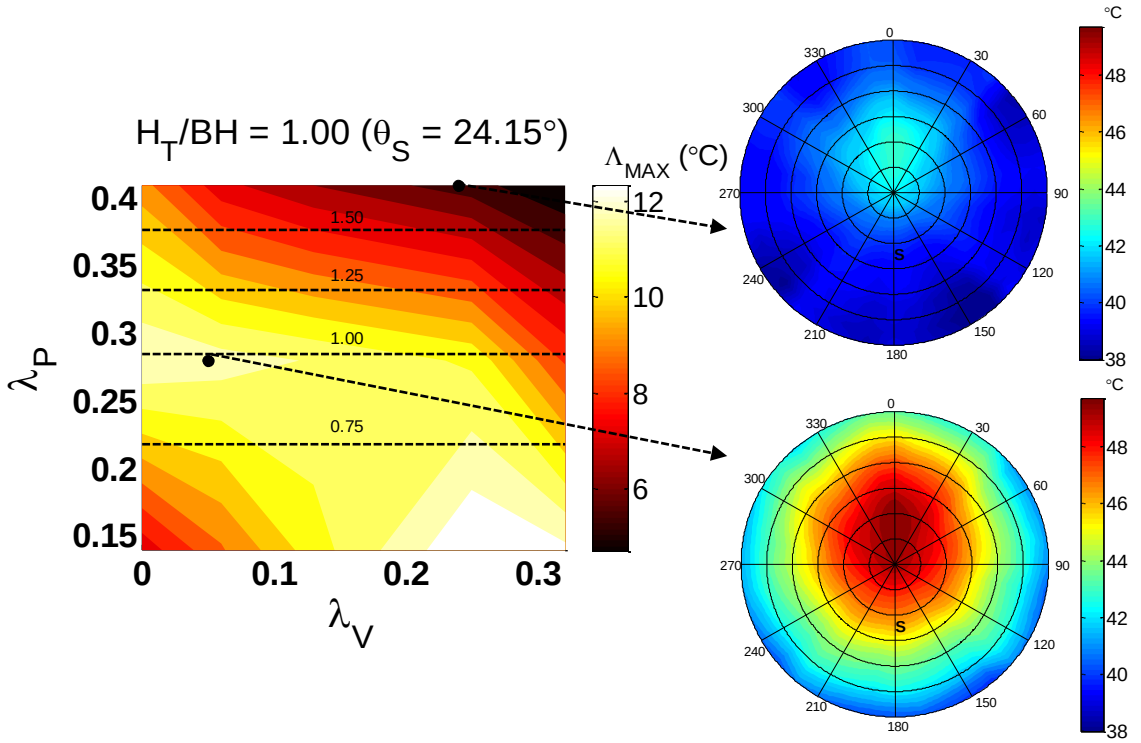


Figure 5.2: Surface plot of SUM_{VEG} modelled Λ_{MAX}, as a function of λ_P and λ_V, for ϕ = 47.6°N on June 21st at 1200 LMST with $H_T/BH = 1$. Dashed lines indicate lines of equal *BH/SW*. Each polar co-ordinate plot corresponds to a single λ_P and λ_V combination. 'S' indicates the θ_S and φ_S.

Krayenhoff and Voogt (2007b), using a coupled SUM + TUF-3d model to study the influence of non-vegetated regularly-spaced arrays of cube structures on effective thermal anisotropy, found that daytime thermal anisotropy on June 21st at a latitude of 47.6°N (Basel) is generally maximized in a moderate to low λ_P range of approximately 0.25–0.33

and high *BH/BL* ratio. They attributed this to the relatively large wall area with high *BH/BL* ratios and the balance that occurs between wall area and mutual shadowing at moderate to low λ_P. Examination of the surface plots ($\lambda_V = 0.0$) in Figures [5.4] and [5.5] confirms this finding for ϕ = 47.6°N on June 21st and March 28th using mean facet temperatures.

For simulations on June 21st and March 28th at ϕ = 47.6°N, the inclusion of tree crowns tends to shift Λ_{MAX} to lower λ_P as a function of λ_V. For example, in the surface plot in Figure [5.2], at $\lambda_V = 0$, Λ_{MAX} is approximately 11.6°C for a surface with a λ_P of 0.28. Increasing the cover of tree crowns while maintaining a $\lambda_P = 0.28$ has two repercussions: 1) the magnitude of Λ_{MAX} decreases with increasing λ_V, and 2) the λ_P corresponding to the maximum Λ_{MAX} decreases with increasing λ_V. The latter is found in all surface plots for June 21st and March 28th at all simulation times (0800, 1000, and 1200 LMST) and H_T/BH ratios for both latitudes investigated (25.8°N and 47.6°N) (Figure [5.4] and [5.5]).

Lower solar elevation angles generally result in reduced magnitudes of Λ_{MAX}. This is due to the lower contrast in component surface temperatures resulting from the reduction in solar insolation. However, the observed trends in Λ_{MAX}, which result from the inclusion of tree crowns, remain largely irrespective of solar angle (Figure [5.3]).

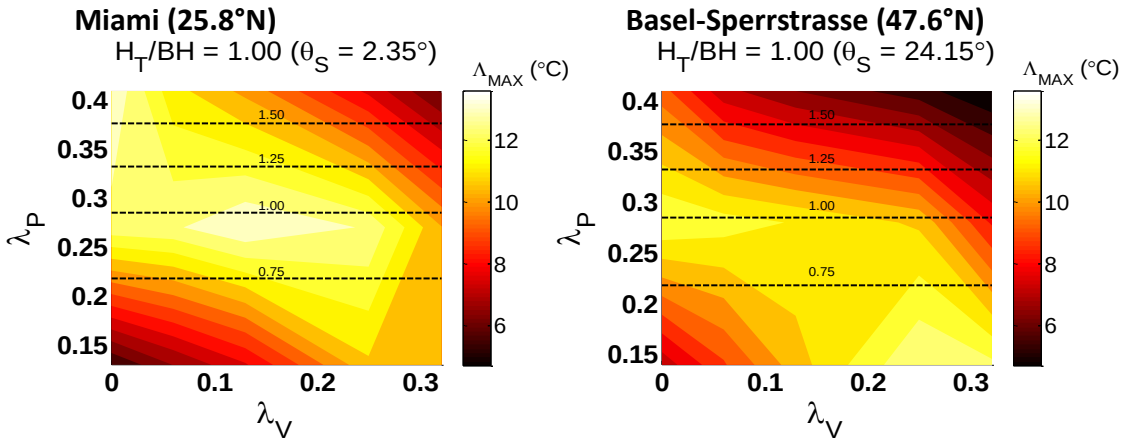


Figure 5.3: Surface plots of Λ_{MAX} on June 21st at 1200 LMST using forcing conditions and solar geometry from the Miami International Airport and Basel-Sperrstrasse canyon. Colour scales are equalized to facilitate comparison. Dashed lines indicate lines of equal *BH/SW*.

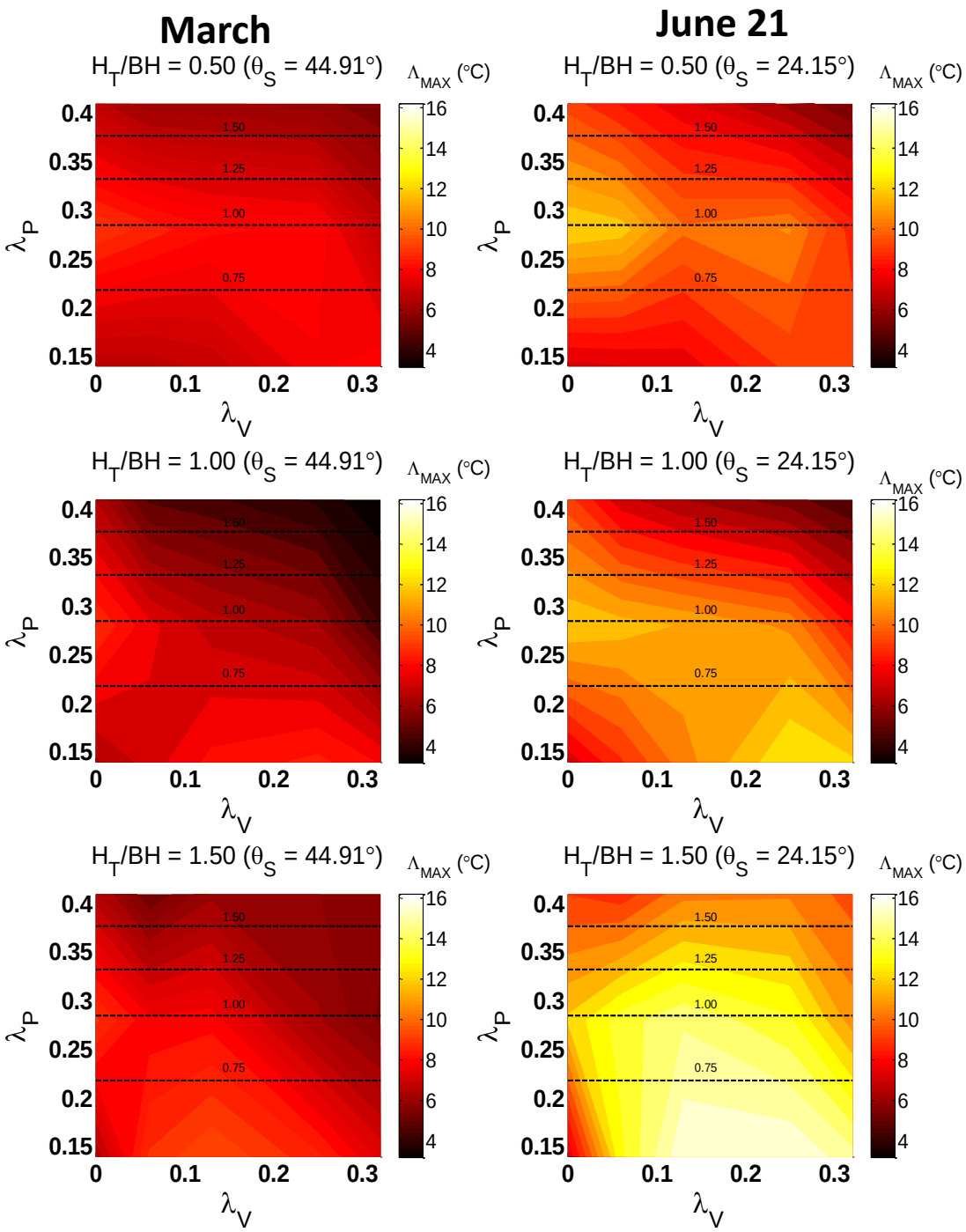


Figure 5.4: Surface plots of Λ_{MAX} for March 28th and June 21st at 1200 LMST using forcing conditions and solar geometry from Basel-Sperrstrasse for several H_T/BH ratios. Dashed lines indicate lines of equal *BH/SW*.

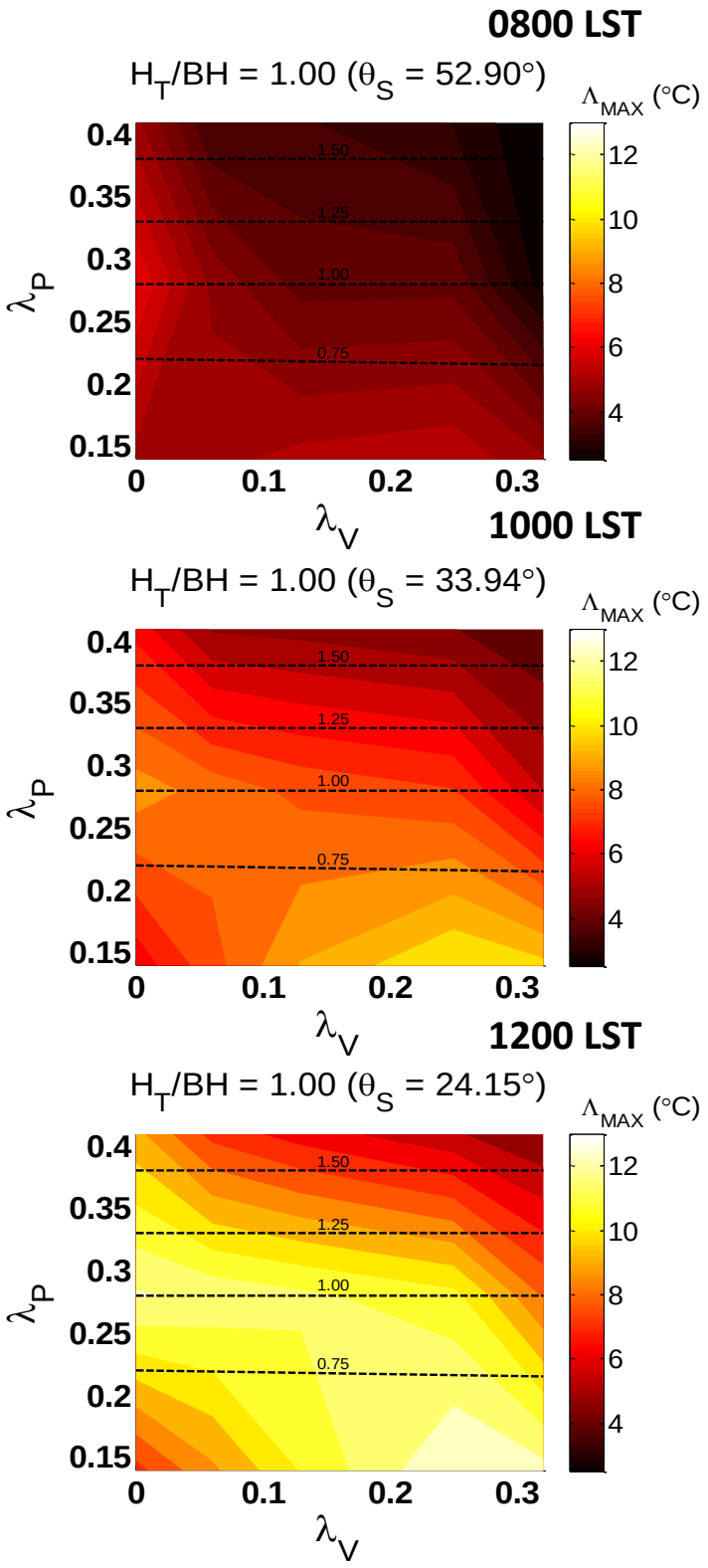


Figure 5.5: Surface plots of Λ_{MAX} for three times on June 21st at 1200 LMST with $H_T/BH = 1.0$ using forcing conditions and solar geometry from Basel-Sperrstrasse. Dashed lines indicate lines of equal *BH/SW*.

The influence of λ_V depends on λ_P, H_T/BH ratio, and solar angle. There tends to be an inflection point (range) corresponding to moderate building plan fractions ($\lambda_P \approx 0.25 - 0.30$) and *BH/SW* = 1.0. For λ_P values above this range, Λ_{MAX} tends to decrease with increasing λ_V while, for surfaces with λ_P fractions below this range, Λ_{MAX} tends to increase with increasing λ_V. This relationship is most evident with high solar elevation angles and does not hold for simulations with $H_T/BH > 1.0$ (Figure [5.4]). This λ_P inflection range tends to shift to lower λ_P with increasing λ_V and with increasing θ_S. There is also generally a broad range of λ_P and λ_V with relatively minimal change in Λ_{MAX}. This region is usually located at low to moderate λ_P (~0.0–0.25) while the λ_V range shifts to higher λ_V with decreasing θ_S. The Sunset case study showed that, in relatively open geometries, Λ_{MAX} increases with the inclusion of tree crowns due mainly to the 'cooling' influence of shaded foliage at oblique θ_V. This broad area of relatively minimal change in Λ_{MAX} probably corresponds to an optimal balance between the 'cooling' influence of tree at oblique θ_V and at the hot spot. For λ_P below this range (i.e. more open geometries), the relatively open canyon results in a substantial view factor occupied by shaded foliage at oblique θ_V which enhances the 'cooling' effect at these θ_V. Conversely, in compact geometries, the narrow canyon limits the view factor occupied by shaded foliage at oblique θ_V.

For simulations with λ_P below the inflection range (i.e. relatively open geometries) there is a maximum value effect evident whereby initial increases in λ_V result in an increase in Λ_{MAX} until a critical value of λ_V is reached after which subsequent increases cause a reduction in modelled Λ_{MAX}. This critical value results from the 'saturation' of the sensor IFOV with tree crown foliage which reduces the contrast between opposing sensor view angles. This value is dependent upon urban form; the λ_V critical value decreases with increasing λ_P. For open geometries, this generally corresponds to moderate λ_V ratios of 0.15–0.25. For compact geometries, this critical value is found at $\lambda_V = 0.0$. In other words, Λ_{MAX} occurs in the absence of tree crowns.

In compact geometries, as a result of the relatively narrow street canyons, the inclusion of tree crowns essentially 'fills' the urban canyon with tree crown foliage. This reduces the substantial contrast in T_S between opposing sensor view angles, such as those between normally sunlit south-facing walls and shaded north-facing walls (in the northern

hemisphere). The λ_V 'critical value' varies with λ_P since λ_P controls the relative canyon size and subsequently the amount of canopy cover needed to 'fill' the canyon.

Figure [5.6] and [5.7] present polar co-ordinate plots of the difference in T_S (i.e. ΔT_S) between $\lambda_V = 0.0$ and 0.32 for $\lambda_P = 0.14$ and $\lambda_P = 0.41$, respectively, on June 21st at 1200 LMST for ϕ = 47.6°N with tree height equal to building height. As is the case of the Sunset case study, the inclusion of tree crowns decreases T_S at every sensor view angle. However, ΔT_S is not equal for every sensor view angle, for either λ_P, which explains the change in Λ_{MAX} that occurs with the inclusion of tree crowns.

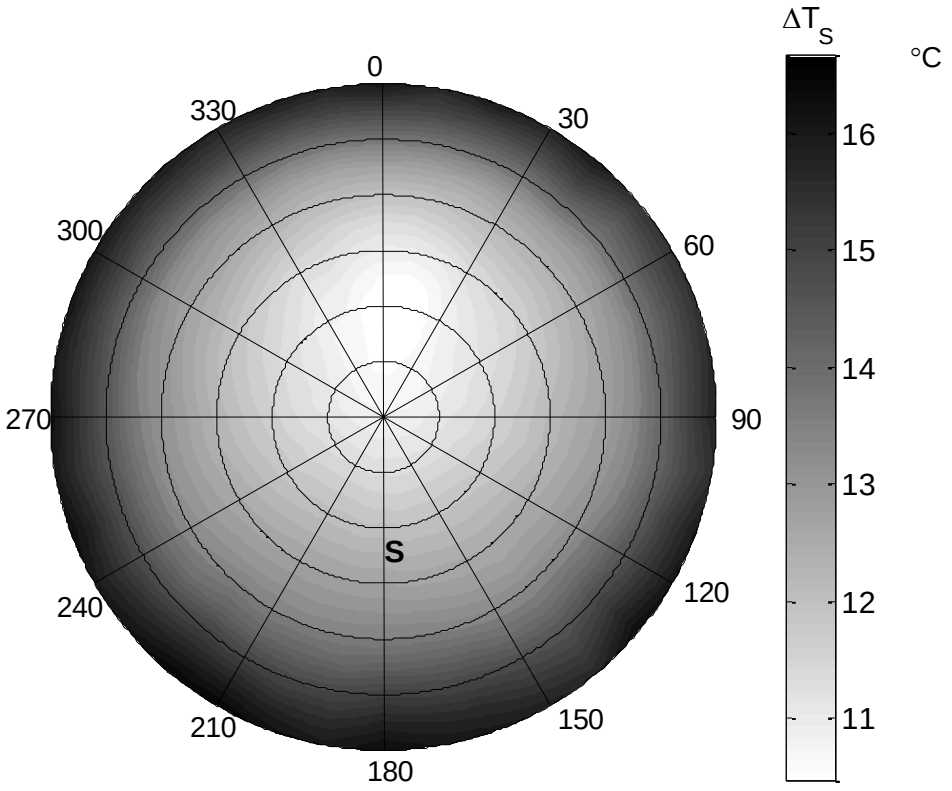


Figure 5.6: Polar co-ordinate plot of ΔT_S between simulations with $\lambda_V = 0.0$ and 0.32, for a surface with $\lambda_P = 0.14$ on June 21st at 1200 LMST for ϕ = 47.6°N.

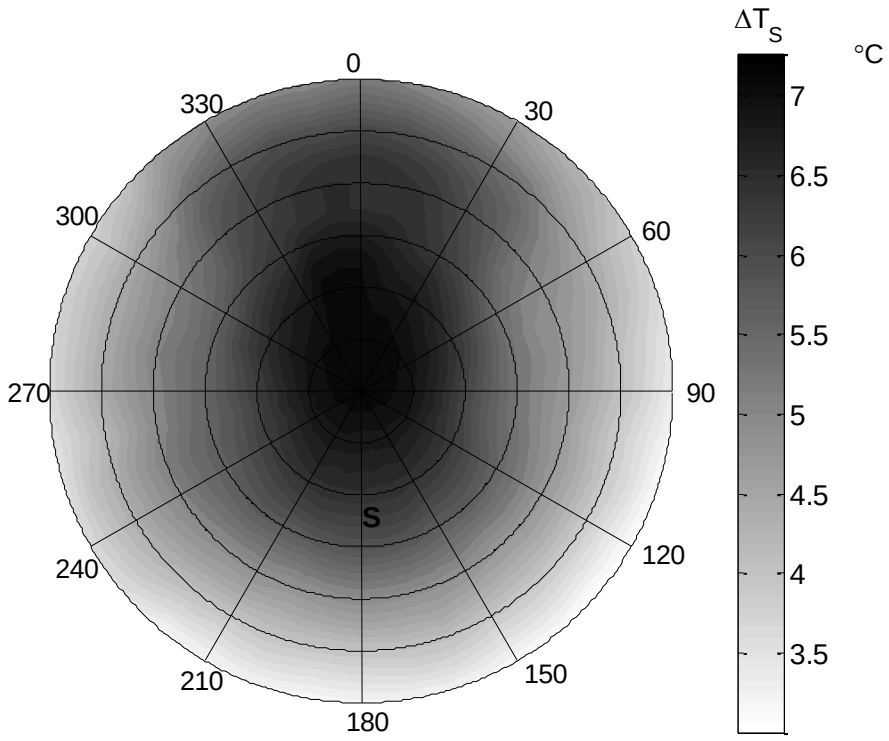


Figure 5.7: Polar co-ordinate plot of ΔT_S between simulations with $\lambda_V = 0.0$ and 0.32, for a surface with $\lambda_P = 0.41$ on June 21st at 1200 LMST for ϕ = 47.6°N.

Figure [5.8] presents the difference in view factor occupied by shaded foliage ($\Delta\Psi_{\text{di,jVh}}$) within the sensor IFOV between simulations with $\lambda_P = 0.14$ and 0.41 on June 21st at 1200 LMST with $H_T/BH = 1.0$. Increases in $\Delta\Psi_{\text{di,jVh}}$ at oblique θ_V indicate that $\Psi_{\text{di,jVh}}$ is higher for more open geometries than relatively compact geometries. Here, the density of the urban form (i.e. λ_P) is varied by changing the street width while buildings maintain constant dimensions. At oblique θ_V, the relatively narrow streets of compact geometries tend to limit the view factor occupied by surfaces within the urban canyon (e.g. ground, wall, etc.). Since tree crowns in SUM_{VEG} are situated within the urban canyon, the view factor occupied by tree crown foliage for a sensor at an oblique θ_V is lower than in open geometries with the same λ_V. This is particularly evident for simulations with $H_T/BH = 1.0$. As a result T_S at oblique θ_V—and coincidentally corresponding to $T_{S_{MIN}}$—are reduced less with the inclusion of tree crown vegetation in compact geometries than in more open urban forms. It is mainly this difference in $T_{S_{MIN}}$ that causes the decrease in Λ_{MAX} magnitude that occurs with the inclusion of tree crown vegetation in compact urban forms.

In relatively open geometries, inclusion of tree crowns initially generates temperature contrasts between opposing view directions. Tree crowns are generally several degrees cooler than sunlit walls (and sunlit ground surfaces) and correspond closely to shaded wall temperatures. When tree crown foliage replaces a portion of the view factor occupied by sunlit wall or sunlit ground surfaces, the magnitude of Λ_{MAX} initially increases (i.e. generates temperature contrasts where, prior to the inclusion of tree crowns, there were none). However, at a certain point increasing λ_V 'saturates' the sensor IFOV. Specifically, the foliage occludes a majority of the view factor previously (i.e. in the absence of tree crowns) occupied by sunlit foliage and replaces it with tree crown foliage close to shaded wall and ground surface temperatures. This reduces the contrast between opposing view directions and lowers the magnitude of Λ_{MAX} which causes the critical value effect evident in all surface plots of Λ_{MAX} on March 28th and June 21st.

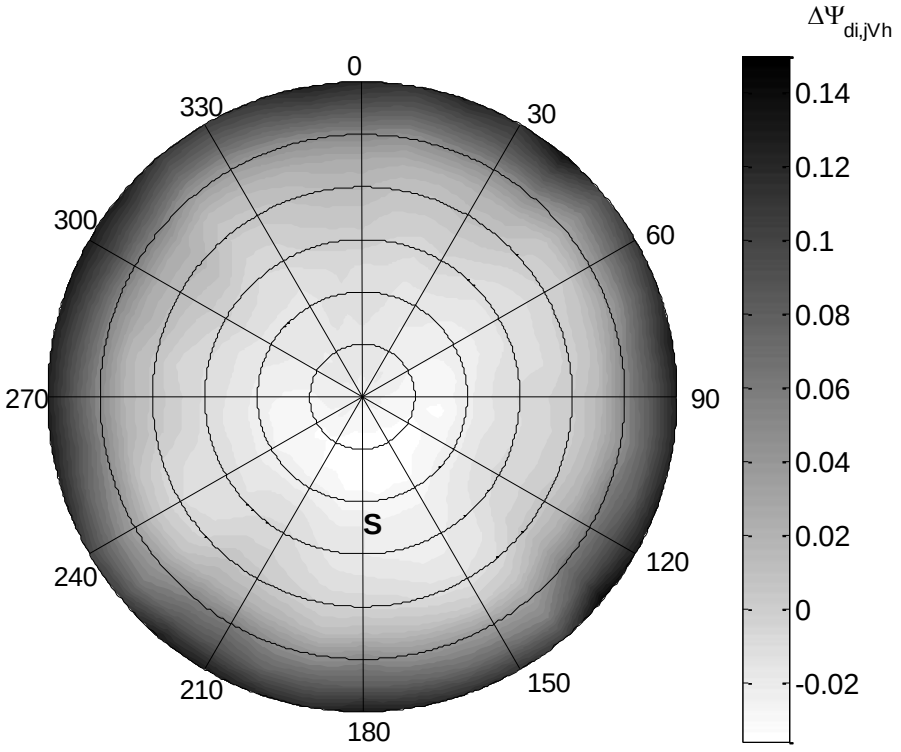


Figure 5.8: Polar co-ordinate plot of $\mathbf{\Delta}\Psi_{\mathrm{di,jVh}}$—with $\lambda_V = 0.32$—between simulations with $\lambda_P = 0.14$ and 0.41 on June 21st at 1200 LMST for ϕ = 47.6°N.

$H_T/BH > 1.0$ indicates roof shading and occlusion of roof surfaces (i.e. reduction of view factor occupied by homogeneously sunlit roof facets within the sensor IFOV) by

tree crown volumes. Increasing H_T/BH has a tendency to lower the λ_V critical value which signifies the crucial role of wall shading/occlusion by tree crowns on the magnitude of thermal anisotropy. When tree crown height is equal or less than building height ($H_T/BH \leq 1.0$), in relatively compact geometries, the magnitude of Λ_{MAX} typically decreases with increasing λ_V because trees tend to mute temperature contrasts between opposing view directions. In particular, sensors at oblique θ_V tend to register lower temperatures—due to the prevalence of cooler walls and shaded surfaces—than a sensor at nadir with an IFOV dominated by sunlit roof surfaces. The relatively closed canyon geometry prevents the sensor from 'seeing' tree crowns, that are within the urban canyon, at oblique θ_V. For a sensor at nadir, since foliage is generally substantially lower in temperature compared to sunlit roofs, tree crowns reduce T_S. Thus, while tree crowns may increase the overall surface temperature heterogeneity within the urban canyon, their introduction to compact urban forms reduces the magnitude of thermal anisotropy.

Since tree crowns are maintained at a constant distance from buildings for every λ_P and λ_V combination, increasing tree height above building height increases Λ_{MAX}. Interestingly, the largest increase in modelled Λ_{MAX} resulting from $H_T/BH > 1.0$ is found in relatively compact urban forms where the inclusion of tree crowns, with $H_T/BH \leq 1.0$, tends to decrease the magnitude of Λ_{MAX} compared to the treeless scenario. This is due to the relative dominance of the view factor occupied by roof surfaces within the sensor IFOV in compact urban forms. Here, all buildings have equal height and, as a result, in the absence of tree crowns are fully sunlit. For a sensor at nadir, and particularly at lower solar elevation angles, tree crowns introduce roof shading. At oblique θ_V, tree crowns also replace a portion of the view factor occupied by roof surface components which, depending on the solar angle may be sunlit or shaded by tree crowns. As a result, in compact geometries, whereas increasing λ_V with $H_T/BH \leq 1.0$ reduced the magntiude of Λ_{MAX} at all times during the day and at both latitudes, increasing λ_V with $H_T/BH > 1.0$ tends to increase the magnitude of Λ_{MAX} (Figure [5.4]). As with the case of open geometries, at a certain point there is a critical value whereby further increases in λ_V act to reduce Λ_{MAX}. The λ_V critical value in compact geometries with $H_T/BH > 1.0$ is similar to the range identified for more open geometries with $H_T/BH = 1.0$ ($\lambda_V \approx 0.15 - 0.25$).

5.3 INVESTIGATING THE DIURNAL TREND OF THERMAL ANISOTROPY

5.3.1 Simulation Methods

Krayenhoff and Voogt (2007b) used the coupled SUM + TUF-3d modelling system to examine the diurnal trend of Λ_{MAX} for several land use zones in Columbus, Ohio using surface geometry, urban construction materials, and radiative properties identified by Arnfield (1982) and thermal properties supplemented by the literature when necessary. Here, we have repeated the simulation using SUM_{VEG} on June 21st and March 28th at ϕ = 47.6°N (Basel) for a residential land use zone (high density detached residential) simulated as a regularly-spaced, aligned array of square footprint block structure buildings. Table [5.3] provides the thermal properties for the surface component layers used in TUF-3d to estimate surface temperatures.

Table 5.3: Thermal parameters used in TUF-3d to estimate facet surface temperatures for the investigation of the influence of tree crowns on diurnal thermal anisotropy (Krayenhoff and Voogt, 2007b).

Parameter/Facet	**Layer 1**	**Layer 2**	**Layer 3**	**Layer 4**
Δx (m)				
Roofs	0.008	0.013	0.032	0.032
Streets	0.015	0.035	0.100	0.300
Walls	0.025	0.043	0.168	0.027
***k* (W m^{-1} K^{-1})**				
Roofs	0.01	0.06	0.03	0.03
Streets	0.65	0.65	0.25	0.25
Walls	0.54	0.20	4.74	0.67
***C* (MJ m^{-3} K^{-1})**				
Roofs	1.76	0.11	0.03	0.03
Streets	1.81	1.81	1.28	1.28
Walls	1.02	0.93	0.99	1.58

Forcing conditions are from the Basel-Sperrstrasse tower site and TUF-3d is used to estimate surface temperatures for the residential facets. T_{ls} and T_{lh} are estimated using the modified leaf temperature model of Campbell and Norman (1998). Since the biophysical parameters (e.g. μ_L, f_{width}, etc.) for all tree crowns are identical here, any differences

between simulations of hourly Λ_{MAX} can be attributed to the relative spatial cover of the urban surface by tree crown foliage (i.e. λ_V).

For both dates, SUM_{VEG} is used to estimate Λ_{MAX} for every hour, on the hour, in local mean solar time, for which the solar elevation angle is greater than zero (0600–1800 LMST for March 28th and 0500–1900 LMST for June 21st). Four tree crown configurations are simulated: 1) no tree crowns (NV), 2) tree crowns with $\lambda_V = 0.11$ and $H_T/BH = 1.0$, 3) tree crowns with $\lambda_V = 0.21$ and $H_T/BH = 1.0$, and 4) tree crowns with $\lambda_V = 0.21$ and $H_T/BH = 1.5$. Comparison of (2) and (3) with (1) describe the influence of λ_V within the urban canyon, while differences between (3) and (4) represent the influence of roof shading from direct solar radiation and reduction of view factor occupied by roof surfaces within a sensor IFOV at oblique θ_V. Table [5.4] provides the surface geometry and biophysical parameters for the three tree crown configurations.

Table 5.4: Geometric and tree crown biophysical parameters used for the high density detached residential case study simulations.

PARAMETER	**UNIT**	$\boldsymbol{\lambda_V = 0.11}$ $\boldsymbol{H_T/BH = 1.0}$	$\boldsymbol{\lambda_V = 0.21}$ $\boldsymbol{H_T/BH = 1.0}$	$\boldsymbol{\lambda_V = 0.21}$ $\boldsymbol{H_T/BH = 1.5}$
Sensor and Surface Geometry				
λ_v	—	0.11	0.21	0.21
H_T/BH	—	1.0	1.0	1.5
f_{width}	m	0.05	0.05	0.05
λ_P	—	0.17		
BH/SW	—	0.40		
z_S	m	250		
IFOV	°	12		
η	°	0.0, 22.5, 45.0, 67.5		
Tree Crown Biophysical				
μ_L	m^{-1}	1.0	1.0	1.0
LAD	—	spherical	spherical	spherical
Ω_C	—	1.0	1.0	1.0
ε_L	—	0.98	0.98	0.98
α_L	—	0.20	0.20	0.20
g_{vs}	$mmolm^{-2}s^{-1}$	0.40	0.40	0.40
H_c	patch units	2	2	4
H_{tk}	patch units	2	2	2
r_c	patch units	1	2	2

5.3.2 Diurnal Thermal Anisotropy for the High Density Detached Residential Case Study

Figure [5.9] presents the trend of street orientation averaged Λ_{MAX} throughout the day of March 28th [5.9a] and June 21st [5.9b] for the residential land use zone. Both days are characterized by mostly clear skies with relatively low wind speeds on June 21st (U_a = 0.97m/s) and moderate wind speeds—and more varied throughout the day—on March 28th (U_a = 2.39m/s). Such atmospheric conditions are expected to maximize thermal anisotropy by enhancing temperature contrasts between sunlit and shaded surface facets (Krayenhoff and Voogt, 2007b).

In the absence of tree crowns, the magnitude of Λ_{MAX} for both dates follows a similar trend characterized by low magnitudes at sunrise, increasing throughout the morning due to surface temperature differences driven by insolation, peaking around solar noon, and falling during the early afternoon until sunset. The maximum daytime anisotropy occurs both days at solar noon with magnitudes of 4.6°C and 5.4°C for March 28th and June 21st, respectively. In the hours before solar noon, Λ_{MAX} increases largely due to the temperature differential between sunlit east- and south-facing walls and shaded west- and north-facing walls. Following solar noon, Λ_{MAX} decreases as west-facing walls become sunlit and solar insolation decreases due to lower solar elevation angles. Both of these influences decrease the disparity between sunlit and shaded surface facets; as the sun heats recently sunlit west-facing wall facets, recently shaded east facing facets begin decreasing in surface temperature. This reduces the temperature difference between west- and east-facing wall facets that developed throughout the morning radiative heating. The slight extended tail in the trend of Λ_{MAX} following solar noon is probably the result of the sustained differential in surface temperature between north- and south-facing wall facets.

Adding 11% surface cover of tree crowns, with $H_T/BH = 1.0$, results in relatively substantial increases in Λ_{MAX} from the later morning through to the later afternoon, with an increase over the treeless simulation at 1200 LMST of 0.7°C and 1.1°C for March 28th and June 21st, respectively. Tree crowns do not alter the relative diurnal trend of anisotropy, though they have a substantially pronounced influence for several hours on either side of solar noon, relative to the hours immediately following sunrise and preceding sunset.

The reduction of Λ_{MAX} on March 28th from 0600 and 0800 LMST and June 21st from 0500–0700 LMST resulting from the inclusion of tree crowns is probably due to the relative similarity in temperatures for leaf and shaded wall surfaces during these times. In the early morning hours, east and south facing walls are primarily sunlit while west and north walls are shaded. Tree crowns replace part of the view factor occupied by sunlit surfaces and replace them with the relatively cooler leaf surface temperatures. Since these temperatures are relatively close to the temperatures for the shaded wall components, this reduces Λ_{MAX}.

As input of solar radiant energy to the surface components increases, tree crowns increase Λ_{MAX} over the treeless simulation due to the sustained lower leaf temperatures relative to the built surfaces, particularly sunlit ground and roof surfaces. This generates temperature contrasts as a function of view direction; tree crowns reduce the surface temperature at every sensor view angle, though they tend to reduce temperatures at the hot spot (i.e. $T_{S_{MAX}}$) less than those associated with the $T_{S_{MIN}}$. As the simulations in Section [5.2] indicate, this is not true for all urban forms; modelled Λ_{MAX} estimates behave as expected given the relatively low building plan fraction for the high density detached residential surface ($\lambda_P = 0.17$). Were the residential surface more compact ($\lambda_P > 0.25$), it would be reasonable to expect the inclusion of tree crowns—with $H_T/BH = 1.0$—to reduce the magnitude of Λ_{MAX}.

Increasing the cover of tree crowns to 21% increases the magnitude of Λ_{MAX} over the simulation with 11% cover for both dates (0.7°C and 1.7°C for March 28th and June 21st, respectively). Eventually, it is probable that a critical value will be reached whereby subsequent increases in λ_V may begin to actually reduce temperature contrasts between opposing view directions and reduce the magnitude of Λ_{MAX}. While this value is not further investigated in these tests, previous use of SUM_{VEG} to investigate thermal anisotropy for regular arrays of block structures—over a range of λ_V and λ_P ratios—suggest that the critical value of λ_V is dependent on the urban form, H_T/BH, and solar angle relative to the domain (Section [5.2]).

For both dates, $H_T/BH > 1.0$ results in an increase in the magnitude of Λ_{MAX} over the treeless scenario and simulations with $H_T/BH = 1.0$. The most pronounced increase occurs at 1200 LMST generally corresponding to the maximum daytime Λ_{MAX}. Relative

to the treeless simulation, adding a 21% cover of tree crowns with $H_T/BH = 1.5$ results in an increase in Λ_{MAX} of 2.2°C and 4.5°C on March 28th and June 21st, respectively. Increasing tree height above building height also results in an increase in Λ_{MAX} over the $H_T/BH = 1.0$ simulation, with $\lambda_V = 0.21$, of 0.8°C and 1.7°C on March 28th and June21st, respectively.

Since these simulations use a regular array of identical block buildings with equal building height, roof surfaces in the absence of tree crowns are completely sunlit. The increase in Λ_{MAX} associated with the inclusion of tree crowns taller than buildings is due to the temperature contrasts generated by the presence of tree crowns. The $H_T/BH = 1.5$ simulation introduces shaded roof surfaces (though relatively minimal due to the high solar angle at 1200 LMST) as well as replacement of the continuously sunlit roof surfaces with substantially cooler tree crown foliage within the sensor IFOV at oblique θ_V. It is important to remember that H_{tk} remains the same so that increasing H_T/BH also simulates increased vertical extent of tree crowns and hence increased wall surface shading/occlusion.

Krayenhoff and Voogt (2007b) found that the residential land use zone—in the absence of tree crown vegetation—resulted in substantially lower magnitudes of thermal anisotropy compared to simulations representing modern high-rise commercial (22 storeys) and built-up commercial (6 storeys) areas. For example, the maximum modelled daily thermal anisotropy on June 21st was approximately 8.3°C and 9.7°C for modern high-rise and built-up commercial, respectively, at solar noon. However, inclusion of 21% surface cover of tree crowns 1.5 times building height increases the maximum daily Λ_{MAX} for the residential land zone above the values that Krayenhoff and Voogt (2007b) report for the modern high-rise commercial and built-up commercial zones (Λ_{MAX} = 9.9°C). Therefore, while tree crowns do not generally change the diurnal trend or timing of Λ_{MAX}, these results indicate the importance of accounting for tree crown vegetation in the estimation of thermal anisotropy magnitude for treed residential land use zones, particularly when making comparisons to other urban land uses.

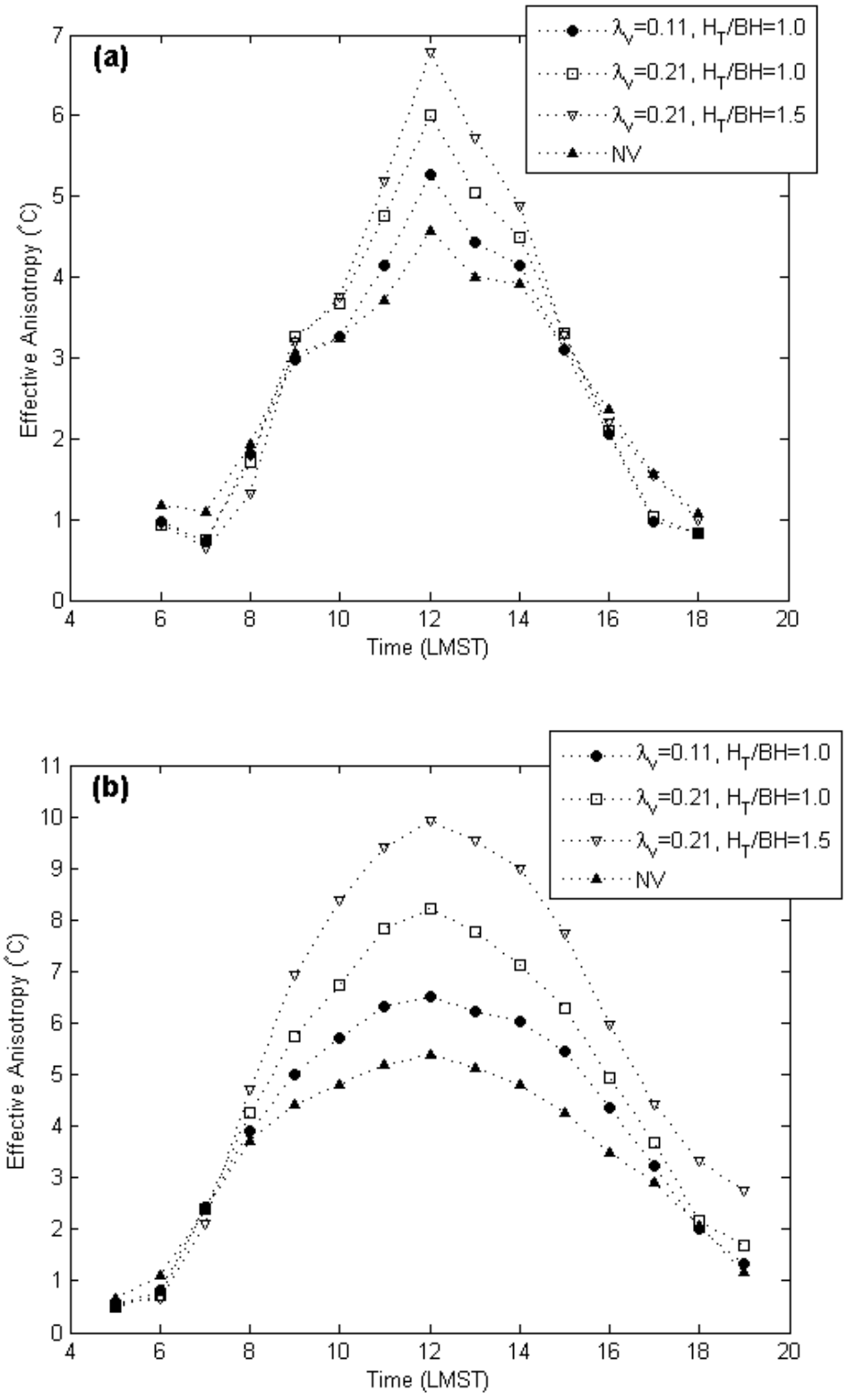


Figure 5.9: Hourly Λ_{MAX} for a high density detached residential land use class ($\lambda_P = 0.17$) at ϕ = 47.6°N on (a) March 28th and (b) June 21st for a number of tree crown configurations. NV indicates the treeless simulation.

5.4 THERMAL ANISOTROPY AS A FUNCTION OF TREE CROWN BIOPHYSICAL PARAMETERS

5.4.1 General Methods

All preceding SUM_{VEG} simulations have focused on neighbourhood-scale changes to vegetation structure by varying λ_V for several regular urban forms, dates, and times. Several biophysical parameters, expected to influence foliage surface temperatures or view factor occupied by foliage within a remote sensor IFOV, and hence the magnitude of Λ_{MAX}, are held constant through all simulations at realistic though otherwise arbitrary values.

Several tests in Chapter 3 examine the influence of a number of tree crown biophysical parameters on the relative proportions of sunlit and shaded leaf elements estimated using the modified 5-Scale model incorporated into SUM_{VEG} (Chen and Leblanc, 1997; 2001). The following section details the results of tests investigating the potential influence of several of these parameters on the magnitude of Λ_{MAX}, including: μ_L, Ω_C, and f_{width}. Simulations are repeated for all three λ_P ratios from Section [5.2] using Basel-Sperrstrasse forcing conditions on June 21st at 1200 LMST, over a range of μ_L, Ω_C, and f_{width}, with $\lambda_V = 0.13$ and $H_T/BH = 1.5$.

Ω_C and μ_L do not influence leaf surface temperature in the leaf temperature model used in SUM_{VEG} since it is a modified single-leaf model treating a single sunlit and single shaded leaf element, albeit integrated over a distribution of leaf inclination angles. However, changing the foliage element width changes the net radiation budget of leaf elements which influences T_{ls} and T_{lh}. All three parameters influence the SUM_{VEG} estimated view factor occupied by foliage within a sensor IFOV; increasing Ω_C, μ_L and f_{width} increases the view factor occupied by tree crown foliage and *vice versa*. These parameters are investigated based upon their influence on Λ_{MAX} by referencing trends in surface view factors[10] and temperatures. The objective here is not to conduct an assessment of the accuracy of SUM_{VEG} but rather to provide a measure of the sensitivity

[10] View factors within SUM_{VEG} are normalized to the total surface view factor in order to estimate the relative contribution of each surface element to T_S.

of the SUM_{VEG} simulations in Section [5.2] to biophysical parameters that were held constant but are nevertheless expected to influence Λ_{MAX} in treed urban domains.

The clumping index implemented into SUM_{VEG} indicates the tendency of foliage to clump along branches and varies from 0 (highly clumped) to 1 (randomly distributed) (Chen and Cihlar, 1995). $\Omega_C > 1$ indicates more uniformly distributed foliage and is not investigated in the following tests. Foliage area density is a measure of total leaf area (m^2) within an individual canopy volume (m^3) where, in SUM_{VEG}, each leaf has the same width (f_{width}). Due to the relationship between the light environment of tree canopies and μ_L, a number of remote sensing techniques, including the use of Light Detection and Ranging (LiDAR), have been developed to describe μ_L distributions (e.g. vertical foliage area density profiles) within individual crowns and forest canopies (e.g. Jupp *et al.,* 2009). μ_L typically varies spatially within tree crowns (Whitehead *et al.,* 1990) and there is a wide variation in values dependent upon tree species and time of year (e.g. leaf fall during cold seasons). In order to simplify gap probability calculations in SUM_{VEG}—and subsequently view factor computation—μ_L does not vary either within or between tree crowns and all leaf elements are equal in size.

5.4.2 Sensitivity of Thermal Anisotropy to Foliage Area Density

Figure [5.10] presents Λ_{MAX} for $\lambda_P = 0.14, 0.28,$ and 0.41, with a 13% tree canopy cover, over a range of realistic Ω_C [5.10a], μ_L [5.10b], and f_{width} [5.10c] values. For the current tests, when varying any one tree crown biophysical parameter, the remaining parameters are held constant at the values used in Section [5.2] (Table [5.2]).

The trend of Λ_{MAX} as a function of μ_L tends to follow a de-accelerating curve whereby initial increases in μ_L result in relatively large increases in Λ_{MAX}. For $\lambda_P = 0.14, 0.28,$ and 0.41, increasing the μ_L from 0.1 m^{-1} to $1m^{-1}$ results in increases in the magnitude of modelled Λ_{MAX} of 6.8°C, 3.5°C, and 2.9°C, respectively. Subsequent increases in μ_L above $1m^{-1}$ result in reduced increases in Λ_{MAX}. For all three urban forms, Λ_{MAX} tends to level out with increasing μ_L; a μ_L of approximately $3m^{-1}$ corresponds to the μ_L past which further increases have minimal to no influence on Λ_{MAX}.

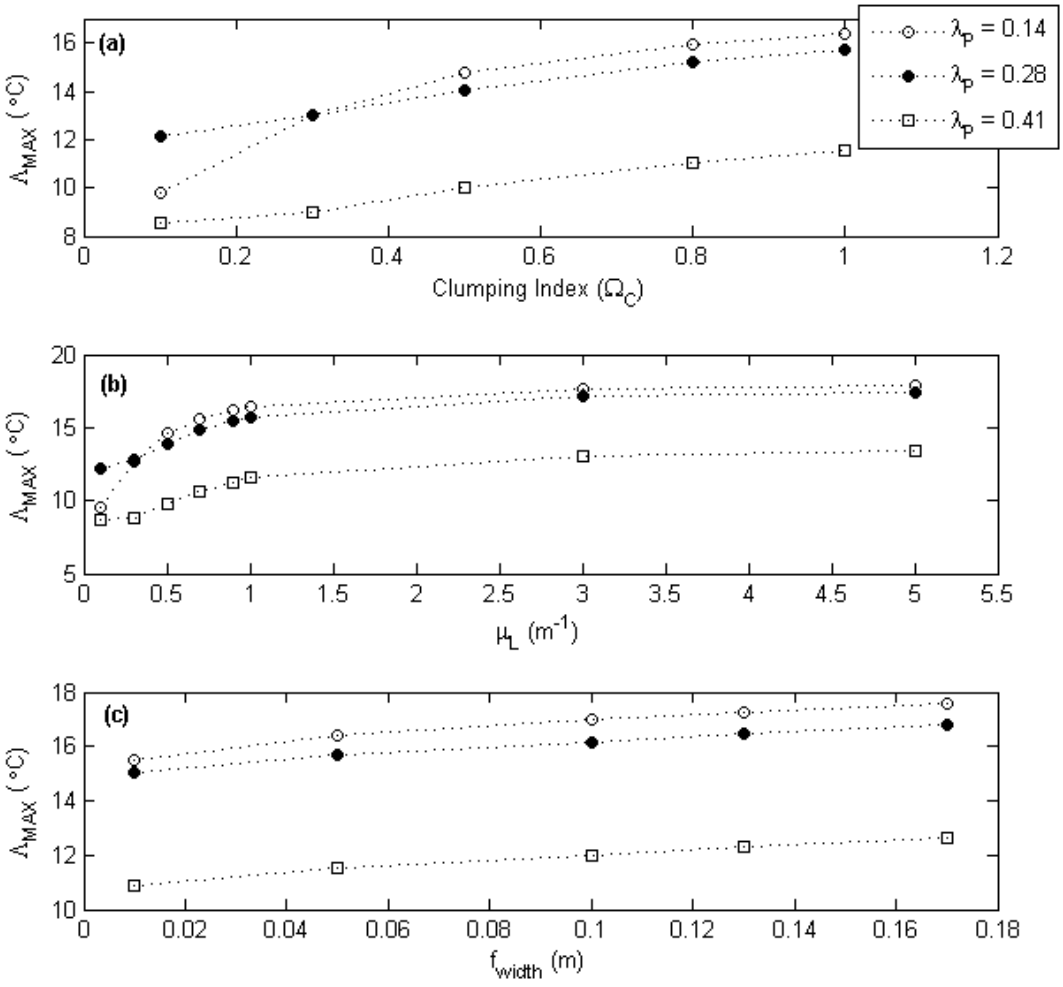


Figure 5.10: Modelled Λ_{MAX} as a function of (a) Ω_C, (b) μ_L, and (c) f_{width} on June 21st at 1200 LMST for ϕ = 47.6°N and $\lambda_V = 0.13$.

Since modifying the μ_L within SUM_{VEG} does not influence sunlit or shaded leaf surface temperature, the change in Λ_{MAX} is due to changing view factors occupied by the various surface components. Figure [5.11] presents the values for the view factor occupied by tree crown foliage (TC), wall, street, and roof surfaces for a south-facing sensor at $\theta_V = 45°$ viewing a treed urban surface with $\lambda_P = 0.28$. The view factor for tree crowns includes both sunlit and shaded foliage while the view factors for wall, street, and roof surfaces include sunlit, shaded, and partially shaded (i.e. shaded by tree crowns) surface components.

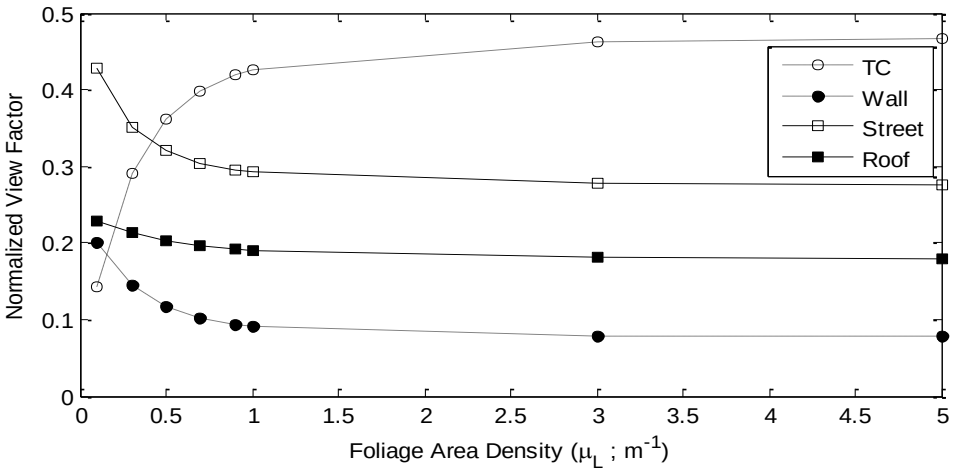


Figure 5.11: Modelled normalized view factors occupied by surface facets as a function of μ_L for a south-facing sensor at $\theta_V = 45°$ viewing a surface with $\lambda_P = 0.28$.

Comparison of the view factors in Figure [5.11] with Λ_{MAX} in Figure [5.10b] explains the trend in thermal anisotropy that occurs with changing μ_L. Increasing μ_L causes an increase in the view factor occupied by tree crown foliage at the expense of the three urban built surface types. The view factor occupied by roof surfaces decreases the least with increasing μ_L due to the fact that trees with a $H_T/BH = 1.5$ occlude a relatively small portion of roof surface from a sensor at 45° off-nadir. Previous tests examining the influence of tree crowns on the magnitude of Λ_{MAX} over the Sunset residential neighbourhood determined that the inclusion of tree crowns increases Λ_{MAX} by decreasing the $T_{S_{MIN}}$ more than $T_{S_{MAX}}$ (Chapter 4). For the current test using Basel-Sperrstrasse forcing conditions on June 21st at 1200 LMST, the inclusion of 13% tree crown coverage increases modelled Λ_{MAX} over the treeless scenario at all λ_P ratios. Increasing μ_L amplifies these increases in Λ_{MAX}. For scenarios where the inclusion of tree crowns decreases the magnitude of Λ_{MAX}—typically compact geometries with tree crowns lower than or equal to building height—increasing μ_L decreases Λ_{MAX} further (i.e. it amplifies the influence of tree crowns at each λ_V) (not shown).

The view factors presented in Figure [5.11] are for a single sensor view angle. The view factor occupied by tree crowns tends to increase with θ_V since, in the current configuration, tree crowns are taller than they are wide. The view factor decrease for the built components, with increasing μ_L, is dependent on θ_V. For example, for a sensor at nadir the view factor occupied by tree crown foliage increases with increasing μ_L mainly

at the expense of street surfaces with relatively minimal change in the view factor occupied by wall and roof surfaces. At a μ_L of around 3m^{-1}, the lack of increase in view factor with further increasing μ_L has two potential and related explanations: 1) closure of all crown foliage gaps such that tree crowns are nearly solid objects within the sensor IFOV, or 2) foliage is so dense that further additions to the crown volume are occluded by other leaf elements and therefore result in a negligible increase in the relative view factor occupied by foliage.

5.4.3 Sensitivity of Thermal Anisotropy to Intra-Crown Foliage Clumping and Leaf Width

Figure [5.12] presents the view factor occupied by the various surface components within SUM_{VEG}, as a function of Ω_C, also for a south-facing sensor at $\theta_V = 45°$ viewing a treed urban surface with $\lambda_P = 0.28$ and $\lambda_V = 0.13$. Decreasing Ω_C simulates increased grouping of leaf elements along branches; $\Omega_C = 1$ indicates foliage randomly distributed within tree crown volumes which is an assumption for all preceding SUM_{VEG} simulations. While the actual density of foliage within individual crowns does not change with Ω_C, increased clumping causes leaf elements to occlude one another which decreases the overall view factor occupied by foliage. Decreasing foliage clumping (increasing Ω_C) decreases the gap size and probability of gap within tree crowns (Chen and Cihlar, 1995).

Similar to the influence of μ_L, Ω_C modifies the magnitude of Λ_{MAX} by amplifying the influence of tree crowns. For simulations where tree crowns increase modelled Λ_{MAX} relative to the treeless surface, decreasing foliage clumping causes further increases in Λ_{MAX} relative to the highly clumped simulations (Figure [5.10a]). While initial increases in Ω_C decrease the frequency of leaf-leaf occlusion, the influence of Ω_C decreases, with reduced foliage clumping, as leaf elements spread out and the removal of leaf-leaf occlusion becomes less frequent.

With low clumping indices (highly clumped foliage) and low foliage density values, Λ_{MAX} magnitude is higher for moderate building plan fractions ($\lambda_P = 0.28$) than low fractions ($\lambda_P = 0.14$). Low values for both of these parameters indicate relatively low tree crown vegetation cover and, with minimal tree crown cover, Λ_{MAX} tends to be maximized at moderate plan area fractions. Simulations in Section [5.2] indicate that tree

crowns tend to have the largest influence on Λ_{MAX} magnitude in low building plan fractions (i.e. relatively open geometries) where shading effects from tree crowns generates temperature contrasts that tend to increase the magnitude of Λ_{MAX}. Decreasing foliage clumping and increasing μ_L, both of which increase the proportion of tree crown foliage visible to a remote sensor, therefore has a more dramatic influence on Λ_{MAX} magnitude in low building plan fraction urban forms.

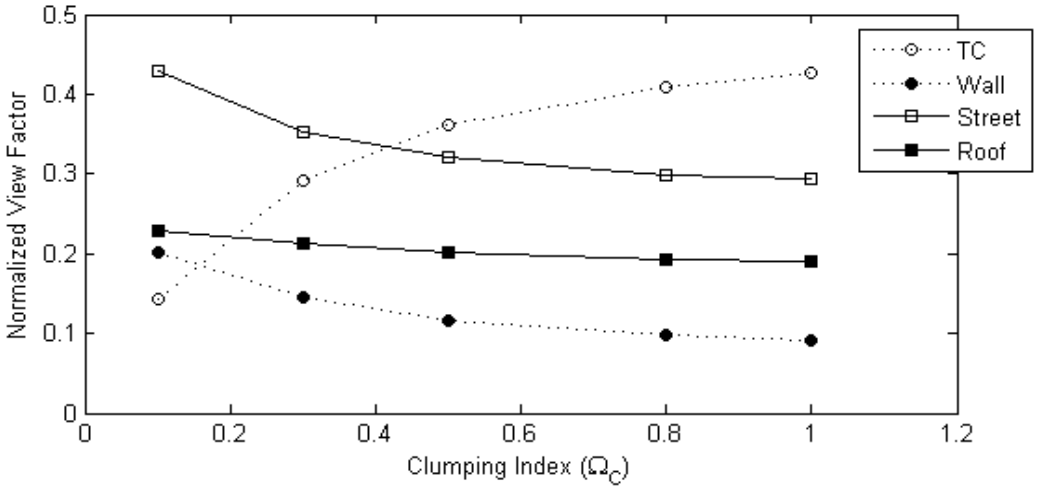


Figure 5.12: Modelled normalized view factors occupied by surface facets as a function of Ω_C for a south-facing sensor at $\theta_V = 45°$ viewing a surface with $\lambda_P = 0.28$.

Figure [5.10c] illustrates the influence of f_{width} on the magnitude of Λ_{MAX}. f_{width} modifies *both* the foliage and built surface view factors and T_{ls} and T_{lh}. In the leaf temperature model incorporated into SUM_{VEG}, T_{ls} values are estimated using a number of parameters that influence the leaf energy budget. T_{lh} calculation uses the same parameters except for the radiation budget term that assumes all shortwave radiation to be in the form of diffuse and forward scattered direct radiation.

Figure [5.13] presents the temperatures for the various surface components in the $\lambda_P = 0.28$ simulation, where the roof and street are the average of sunlit and shaded temperatures and walls are separated into sunlit and shaded temperatures averaged over all four cardinal directions. Depending on the urban form, the inclusion of tree crowns can either increase or decrease Λ_{MAX}. For the current simulation, the inclusion of 13% cover of tree crowns increases modelled Λ_{MAX} for all λ_P ratios. This is due largely to the temperature disparity between foliage and built surfaces. If leaf temperatures were equal

to the temperature of surfaces they occlude from the remote sensor, there would probably be minimal change in the magnitude of Λ_{MAX}. In actuality, leaf surfaces are generally cooler than built facets and lead to a decrease in T_S at all sensor view angles. The relatively linear increase in Λ_{MAX} that results from increasing f_{width} is due mainly to the decrease in T_{lh}. T_{lh} values are lower than all built surface temperatures at every f_{width}. T_{ls} is lower than most surface temperature averages, except for mean shaded wall surface temperatures.

Sunlit foliage is most prevalent at the 'hot spot', which corresponds to $T_{S_{MAX}}$, primarily due to the presence of warm built surfaces seen at this viewing angle. T_{ls} is lower than any other sunlit surface temperature. As a result, increasing T_{ls} typically decreases the 'cooling' effect of leaf surfaces on $T_{S_{MAX}}$ by bringing the temperature of leaf surfaces closer to the temperature of built surfaces, particularly sunlit wall surfaces. Simultaneously, decreasing T_{lh}, at larger f_{width} values, enhances the cooling effect of tree crowns on T_S for view angles at which primarily shaded tree crown foliage is 'seen' (i.e. the cool spot). This generally coincides with $T_{S_{MIN}}$. As a result, increasing f_{width} increases the magnitude of modelled Λ_{MAX} by both increasing $T_{S_{MAX}}$ and decreasing $T_{S_{MIN}}$, compared to those temperatures at smaller f_{width} values. For example, for a surface with $\lambda_P = 0.28$ and $\lambda_V = 0.13$, increasing f_{width} from 0.01m to 0.17m increases $T_{S_{MAX}}$ from 45.6°C to 45.9°C and decreases $T_{S_{MIN}}$ from 30.6°C to 29.1°C which results in an increase in Λ_{MAX} of 1.8°C.

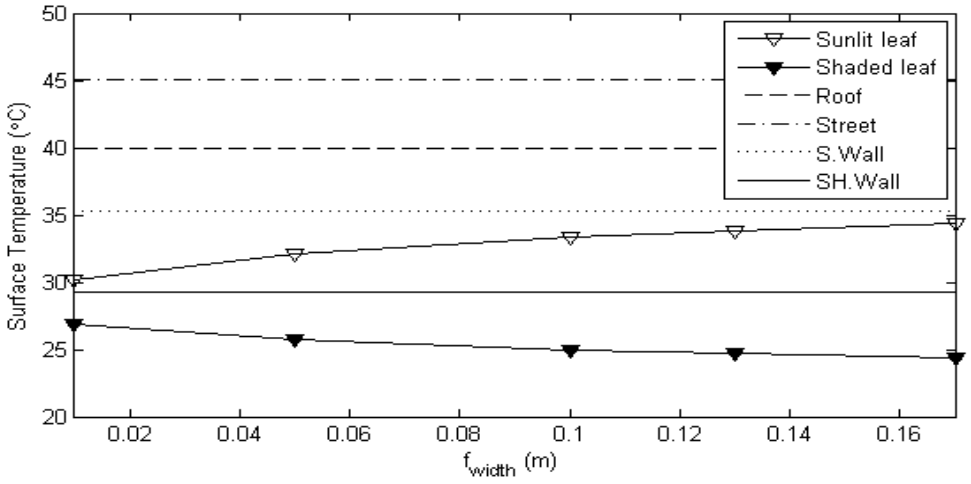


Figure 5.13: Temperatures for surface facets as a function of f_{width} with $\lambda_P = 0.28$.

5.5 SUMMARY

This chapter has presented the results and discussion of Λ_{MAX} estimated using a coupled SUM_{VEG} + TUF-3d model. Simulations are performed for treed residential land use zones for dates near the spring equinox and summer solstice at subtropical and mid-latitude locations. Forcing conditions and solar geometry come from meteorological instruments installed at Basel-Sperrstrasse (ϕ = 47.6°N) and the Miami International Airport (ϕ = 25.8°N). In general, findings support the hypothesis of the dual nature of tree crowns in urban environments; i.e. the ability to both increase and decrease effective thermal anisotropy as a function of urban form.

For simulations with relatively open urban geometries ($\lambda_P = 0.14$), the inclusion of tree crowns initially increases Λ_{MAX} by generating temperature contrasts between opposing sensor view angles which reduces $T_{S_{MIN}}$ more than $T_{S_{MAX}}$. The opposite occurs in more compact geometries ($\lambda_P = 0.41$) where the addition of tree crowns with $H_T/BH \leq 1.0$ 'fills' the relatively narrow urban canyons and reduces the contrast between opposing view directions by decreasing $T_{S_{MAX}}$ more than $T_{S_{MIN}}$. This also occurs because $T_{S_{MIN}}$ typically corresponds to oblique θ_V and the relatively closed nature of the urban canyon (in compact geometries) limits the view factor occupied by tree crown foliage at oblique θ_V; this limits the 'cooling' ability of tree crown vegetation on T_S at these sensor view angles. For moderate to low λ_V values ($\lambda_V \approx 0.0 - 0.15$), the inflection range—above which Λ_{MAX} decreases with increasing λ_V and below which Λ_{MAX} increases with λ_V—typically corresponds to $\lambda_P = 0.25 - 0.30$ and falls with further increases in λ_V.

For the current simulations, characterized by identical building heights, the inclusion of trees with $H_T/BH > 1.0$ simulates roof shading and occlusion of roof surfaces from the sensor by tree crown foliage, depending on the solar and sensor view angle. The resultant temperature contrasts increase the magnitude of Λ_{MAX} for all building plan fractions. Tree crowns with $H_T/BH > 1.0$ also reverse the trend of Λ_{MAX} with increasing λ_V in compact geometries, though, as with open geometries, a critical value exists past which increasing λ_V tends to reduce thermal anisotropy magnitude.

For a high density detached residential land use class ($\lambda_P = 0.17$) on June 21st at ϕ = 47.6°N, the inclusion of tree crowns increases the magnitude of hourly Λ_{MAX} for a majority of the daytime hours with a pronounced effect for several hours on either side of solar noon. Inclusion of just 21% canopy cover—substantially less than the upper limit indicated by Oke (1989) for residential areas—with $H_T/BH > 1.0$ results in a daytime maximum (1200 LMST) of Λ_{MAX} greater than the values modelled by Krayenhoff and Voogt (2007b) for modern high-rise and built-up commercial land use classes (which are characterized by substantially higher modelled Λ_{MAX} magnitudes than the residential surface in the absence of tree crown vegetation).

Λ_{MAX} is sensitive to a number of tree crown biophysical parameters. In particular clumping index (Ω_C), foliage area density (μ_L), and foliage element width (f_{width}) influence the magnitude of Λ_{MAX} by altering the view factors occupied by foliage within a sensor IFOV or, in the case of f_{width}, modifying T_{ls} and T_{lh}. In relatively open geometries—where Λ_{MAX} increases with λ_V—increasing μ_L, f_{width}, and Ω_C increase the magnitude of Λ_{MAX} and *vice versa*. The opposite occurs in compact geometries where increasing the influence of these biophysical parameters magnifies the Λ_{MAX} reduction caused by the inclusion of tree crown cover.

Such results indicate the relative importance of including tree crowns in the characterization of thermal anisotropy over treed urban domains. Based on these results, the following chapter presents conclusions regarding the influence of tree crowns on thermal anisotropy over treed residential domains. Additionally, a number of current model limitations are discussed and potential model applications presented.

Chapter 6

CONCLUSIONS AND FURTHER WORK

6.1 SUMMARY AND CONCLUSIONS

This thesis has detailed the development, evaluation, and testing of the 'Vegetated Surface-Sensor-Sun Urban Model' (SUM_{VEG}). SUM_{VEG} is a version of the Surface-Sensor-Sun Urban Model (SUM—Soux *et al.*, 2004), modified to treat tree crown and simple ground-level vegetation. While a number of sensor view models exist that simulate the thermal anisotropy over vegetation canopies and urban areas separately, none have combined the two with the specific objective of examining the influence of tree crowns on effective thermal anisotropy magnitude in treed urban areas. Additionally, observational campaigns that have examined urban thermal anisotropy have typically concentrated on highly built-up areas with low tree cover. This makes it difficult to infer any generalizations regarding the potential influence of tree crowns. Therefore SUM_{VEG} has been developed with the specific intention of addressing the primary research question: *How do tree crowns influence the magnitude of effective thermal anisotropy in urban areas?*

Chapter 2 details the main modifications required to allow the extension of SUM_{VEG} to treat treed urban geometries. This includes a radiative transfer scheme that is used to weight the relative view factor occupied by tree crown foliage within a sensor IFOV projected onto an urban surface. This scheme uses the 5-Scale model, developed by Chen and Leblanc (1997; 2001), modified to treat individual tree crowns, in order to account for the hot spot effect and complex nature of tree crown foliage. Additionally, the radiative transfer scheme is used to weight the sunlit and shaded surface facet temperatures in order to estimate the temperature for surfaces shaded from direct shortwave radiation by tree crowns. The second main modification is the inclusion of a

leaf temperature model, detailed by Campbell and Norman (1998), to estimate sunlit and shaded leaf surface temperatures assuming a distribution of leaf inclination angles from 0 to $\pi/2$. SUM_{VEG} can use an internal surface representation that simulates an urban surface as a regularly-spaced array of block structure buildings with tree crowns lining the edge of streets along the length of buildings. Alternatively, SUM_{VEG} can use a spatial database of GIS co-ordinates that allows for variable building height, footprint, and spacing as well as individual tree crown placement.

Chapter 3 presents the evaluation and testing of the sub-models incorporated into SUM_{VEG} that allows it to estimate surface temperatures and calculate foliage proportions based on surface-sensor-sun geometry. Combined with the SUM_{VEG} full model evaluation in Chapter 4, these Chapters address the first main research objective:

1) *Validate SUM_{VEG} using directional brightness surface temperature measurements of the Sunset residential neighbourhood of Vancouver, B.C., acquired using a helicopter-mounted TIR camera as part of an observational campaign conducted by Voogt and Oke (1997; 1998).*

Chapters 4 also presents the results from SUM_{VEG} modelled thermal anisotropy for the Sunset residential neighbourhood of Vancouver, B.C. with a realistic surface representation specified using GIS spatial co-ordinates. Chapter 5 presents the results of modelled thermal anisotropy for regularly-spaced, aligned arrays of block structure buildings for several latitudes and dates. Together these chapters address the second and third research objectives:

2) *Use the Sunset residential neighbourhood as a case study to investigate the influence of tree crowns on thermal anisotropy for a realistic GIS-based surface geometry with facet temperatures extracted from TIR images.*
3) *Examine the sensitivity of effective urban thermal anisotropy to tree crown vegetation, as a function of urban form and solar path, for regularly-spaced aligned arrays of block structure buildings representative of typical residential neighbourhood geometries.*

Inclusion of tree crowns into SUM_{VEG} substantially improves its accuracy when estimating remotely-detected brightness surface temperatures acquired from TIR images of a treed residential surface, relative to the non-vegetated SUM. Since the maximum

thermal anisotropy presented here is calculated as the maximum difference in a T_S distribution from a range of sensor viewing angles, by extension inclusion of tree crowns also improves calculation of anisotropy compared to model estimates for surfaces with no tree crown vegetation.

There is a tendency for SUM_{VEG} to both over- and underestimate thermal anisotropy, possibly due to the identical dimensions and biophysical parameters of tree crowns in the current model manifestation. Here, mean sunlit and shaded surface temperatures may also be generating bias in thermal anisotropy estimates; Voogt (2008) indicated the tendency for SUM to underestimate thermal anisotropy when using mean facet surface temperatures. Ideally, future coupling of SUM_{VEG} with a *vegetated* micro-scale energy budget model will enable separation of the potential errors resulting from the identical nature of tree crowns and use of mean surface temperatures.

As hypothesized, tree crowns have the ability to both increase and decrease the magnitude of effective thermal anisotropy as a function of tree crown plan fraction, building plan fraction, and, to a lesser extent, solar path (i.e. date, time, and location). Tree crown foliage, with surface temperatures generally lower than built facets, reduces remotely-detected brightness surface temperatures at every sensor view angle. It is the unequal reduction of T_S across the range of sensor view angles that results in changes to the magnitude of Λ_{MAX}. In relatively compact geometries with tree height less than or equal to building height, Λ_{MAX} tends to decrease with increasing tree crown plan fraction due to a larger decrease in the maximum remotely-detected temperature then the minimum. In open urban geometries, such as the Sunset residential case study, Λ_{MAX} tends to increase with increasing tree crown plan fraction due to a larger decrease in the minimum remotely-detected temperature than the maximum. Typically, the building plan fraction corresponding to the inflection point, above which Λ_{MAX} decreases with the inclusion of tree crowns and below which Λ_{MAX} increases with increasing tree crown plan fraction, generally corresponds to a moderate λ_P range of 0.25–0.30 and $BH/SW \approx 1.0$. However, increasing tree crown plan fraction tends to shift the λ_P inflection point to lower λ_P values.

Results on March 28th and June 21st at latitudes 47.6°N (Basel) and 25.8°N (Miami) for aligned arrays of regularly-spaced block structures indicate the substantial influence

of tree crowns on modelled Λ_{MAX}. For open geometries, there is—within the range of λ_V simulated here—a critical value of λ_V corresponding to the maximum Λ_{MAX} for any given building plan fraction[11]. Further increases in λ_V beyond the point of maximum effect result in a decrease in Λ_{MAX} as tree crown foliage sufficiently 'saturates' the sensor IFOV and decreases the contrast between opposing sensor view angle T_S. The λ_V point of maximum effect is dependent upon building plan fraction; Typically the λ_V point of maximum effect increases with decreasing λ_P (i.e. increasingly open geometries). However, there is also generally a broad area with relatively minimal change in Λ_{MAX} corresponding to low-to-moderate λ_P and a λ_V range that shifts to higher values with decreasing solar zenith angle.

Introducing trees with height greater than building height results in an increase in effective thermal anisotropy for all surface geometries. It also reverses the trend in Λ_{MAX} in compact geometries—that occurs with tree height less than or equal to building height—such that increasing tree crown plan fraction results in an increase in effective thermal anisotropy. However, as with open geometries, there is a point of maximum effect whereby further increases in λ_V past a critical value result in a decrease in Λ_{MAX}.

Several tree crown biophysical parameters also influence effective thermal anisotropy magnitude by changing either the surface temperature or view factor occupied by foliage. Increasing the foliage view factor by reducing leaf clumping, increasing leaf area density, or increasing leaf width tends to magnify the influence of tree crowns on Λ_{MAX}. For example, in simulations with tree height equal to building height, increasing the view factor occupied by foliage by changing leaf biophysical parameters increases Λ_{MAX} in open urban geometries and decreases Λ_{MAX} in compact geometries. Changing leaf surface temperature by increasing leaf width (i.e. increasing sunlit leaf temperature and decreasing shaded leaf temperature) has a similar influence on Λ_{MAX}.

6.1.1 Extension of Thermal Anisotropy Results to Local Climate Zones

From these results, generalizations can be made regarding the influence of tree crowns on thermal anisotropy in a number of urban land use types. Here, the investigation

[11] For compact geometries, this critical value corresponds to $\lambda_V = 0.0$

is limited to a number of urban geometries characteristic of an urban residential domain of varying building density. The three distinct building plan fractions simulated are broadly representative of the urban geometry for three Local Climate Zones (LCZ) identified by Stewart and Oke (2012): sparsely built ($\lambda_P = 0.14$), open lowrise ($\lambda_P = 0.28$), and compact lowrise ($\lambda_P = 0.41$).

$\Lambda_{MAX}$for these three LCZs varies depending on λ_V. In 'sparsely built', the addition of trees creates shadowing effects on the relatively open urban surface that generates temperature contrasts and results in an increase in the magnitude of Λ_{MAX}. For the 'compact lowrise' LCZ, the influence of tree crowns is largely dependent on the height of tree crowns relative to buildings. If tree crown height is lower than buildings, Λ_{MAX} decreases with the addition of tree cover. This results from the relatively narrow street canyons which limit the 'cooling' influence of tree crowns at oblique θ_V. However, with tree crowns taller than buildings, trees added to a compact lowrise LCZ will increase Λ_{MAX} due to the temperature contrasts created by tree crown shading of roof facets. 'Open lowrise' LCZs with λ_P around 0.25-0.33 exhibit the highest thermal anisotropy in the absence of tree crowns (Krayenhoff and Voogt, 2007b). This building plan fraction range typically corresponds to the inflection point of λ_P previously identified, above which Λ_{MAX} decreases with increasing λ_V and below which Λ_{MAX} increases with λ_V.

Given the controlling influence of urban geometry and surface thermal properties on thermal anisotropy, there is potential for the inclusion of thermal anisotropy as a LCZ descriptor. For example, Table [6.1] presents modelled Λ_{MAX} without trees and with tree cover of 32%, resulting from simulations on June 21st at 1200 LMST for ϕ = 47.6°N. 'Critical value' indicates whether the critical value of λ_V has been reached, indicating an initial increase in Λ_{MAX} with the inclusion of tree crowns until a certain value past which further increases in λ_V result in a decrease in Λ_{MAX}; This is only relevant for surface geometries where the initial inclusion of tree crowns results in an increase in modelled Λ_{MAX}. However, further research is required in order to investigate the potential influence of tree crowns on thermal anisotropy in other LCZs. Additionally, the Λ_{MAX} values indicated in Table [6.1] are for a single location, date, and time. Further research is required in order to characterize to more completely the magnitudes and trends of Λ_{MAX}

in these LCZs. Nevertheless, the current results indicate the importance of including tree crowns in the estimation of effective thermal anisotropy for residential urban areas.

Table 6.1: Λ_{MAX} for three Local Climate Zones with ($\lambda_V = 0.32$) and without ($\lambda_V = 0.0$) tree crowns on June 21st at 1200 LMST for simulations at ϕ = 47.6°N. λ_P indicates the range provided by Stewart and Oke (2012) with the actual simulation λ_P in brackets (LCZ diagrams from Stewart and Oke, 2012).

Local Climate Zone (Index)	λ_P	H_T/BH	Λ_{MAX} (°C) ($\lambda_V = 0.0$)	Λ_{MAX} (°C) ($\lambda_V = 0.32$)	**Critical Value**
Sparsely Built (9) 	0.10–0.20 (0.14)	0.50	7.5	9.5	No
		1.00	7.5	12.5	Yes
		1.50	7.5	15.1	Yes
Open Lowrise (6) 	0.20–0.40 (0.28)	0.50	12.3	8.9	–
		1.00	12.3	8.4	–
		1.50	12.3	11.2	Yes
Compact Lowrise (3) 	0.40–0.70 (0.41)	0.50	9.4	5.5	–
		1.00	9.4	4.7	–
		1.50	9.4	9.9	Yes

6.2 Model Limitations and Further Model Development

As with all numerical models, SUM_{VEG} is a simplification of reality and suffers from several limitations and assumptions. Several current limitations and/or assumptions include:

- Accounting for diffuse solar radiation transmittance through tree crowns in the estimation of shaded patch surface temperatures is computationally expensive
- Although the raster model structure allows for the use of sub-facet scale surface temperatures, SUM_{VEG} requires surface temperature measurements or sub-facet scale energy budget model output to take advantage of its sub-facet nature
- All tree crowns are geometrically and biophysically identical
- Tree crowns are located in relation to building and street width. This limits the possible upper limit of λ_V based on λ_P and current restrictions on tree crown location

- Ground-level vegetation has no effective depth—the view factor calculation for ground-level vegetation is treated no differently than built patch view factors.

Future model development and/or careful selection of model parameter input may address these limitations. Coupling of SUM_{VEG} with a vegetated micro-scale urban energy budget model would address the first two model limitations. The first limitation is only of concern when the internal weighting routine within SUM_{VEG} is used to estimate temperatures for surfaces shaded from direct shortwave radiation by the sun. A sub-facet scale energy budget model would, in theory, estimate built and foliage surface temperatures accounting for interaction between the component surfaces. Few sub-facet scale energy budget models exist and even fewer incorporate tree crown vegetation explicitly. However, TUF-3d is currently being modified to include vegetation (Nice *et al*., 2013; Nice *et al*., 2014). Additionally the DART-EB model of Gastellu-Etchegorry (2008) could potentially provide the sub-facet scale surface temperatures required to populate SUM_{VEG}.

Thermal anisotropy over homogeneous grassed surfaces is relatively low compared to those observed over urban surfaces (Voogt and Oke, 1998). The relatively low height of ground-level vegetation in urban areas (e.g. grassed lawns) are expected to have relatively negligible influence on thermal anisotropy compared to the influence of tree crown vegetation. The identical nature of tree crowns is, however, expected to be more problematic, particularly when attempting to replicate real world conditions (e.g. Sunset case study). Including tree crown heterogeneity is relatively simple when using GIS-generated modelled surface domains. However, using homogeneous tree crown shape and biophysical parameters simplifies calculation of foliage proportions and including tree crown heterogeneity will substantially increase computation time. Further research is required to investigate the potential model error associated with the use of identical tree crowns on different scales of measurement.

For regularly-spaced aligned array of block structures, tree crowns are restricted to the edge of streets and are excluded from intersections. In this geometrical configuration, intersections, and to a certain extent streets in open geometries, comprise a substantial portion of the urban surface. Such restrictions currently limit the upper limit of λ_V that can be investigated to about 30%. Oke (1989) indicates that residential neighbourhoods

can have tree canopy cover higher than 40%. One option to address this limitation is to use the GIS-based surface structure that allows for individual placement of tree crowns within the modelled domain. Easing tree crown placement restrictions may also address this limitation, though potentially at the expense of surface realism.

6.3 Future Model Testing

The current evaluation and testing of SUM_{VEG} has been restricted to residential urban geometries, which are expected to exhibit the most evident influence of tree crowns on Λ_{MAX}. Model evaluation is performed for a single day and residential neighbourhood. However, the framework of SUM_{VEG} can represent any number of urban geometries (e.g. industrial, commercial, etc.). Further testing should investigate the capacity of SUM_{VEG} to estimate T_S and Λ_{MAX} for other urban land uses (i.e. LCZs), seasons, and weather conditions. While the foliage proportion routine has been indirectly evaluated via the full model tests here as well as those conducted by Leblanc *et al.* (1999), the foliage view factor routine, which relies upon the foliage proportions estimated using the modified 5-Scale model, would also benefit from direct validation.

The current investigation of the influence of tree crowns is limited to a small subset of dates, times, and locations. While the overall trends in the relationship between λ_V, λ_P, and Λ_{MAX} have been identified, more extensive investigation and sensitivity testing of SUM_{VEG} is necessary, under a wider array of surface and atmospheric conditions. Ideally, such tests will take advantage of the sub-facet scale nature permissible with SUM_{VEG} by using surface temperatures from a vegetated micro-scale energy budget model.

6.4 Potential Model Applications

Given the relatively high fraction of tree canopy cover present in many urban centres, the inability of SUM to represent tree crown vegetation represents a significant model limitation. SUM_{VEG} extends the applicability of SUM to a more diverse range of urban geometries including often heavily vegetated residential neighbourhoods. Soux *et al.* (2004) notes several applications of SUM that also apply to SUM_{VEG}, including:

- Determining optimal height and angle for remote sensing instruments, based on the intended purpose (e.g. determining radiative source area, etc), to derive spatially representative remotely-detected surface temperatures.
- Using information of the directional variation of upwelling longwave emission, in space and time, to derive information about the surfaces viewed (Kimes *et al.*, 1984).

Previous research has used the coupled SUM + TUF-3d model to investigate the influence of thermal surface properties on the magnitude of thermal anisotropy and the lag between the hot spot and the surface directly opposite the sun with the goal of developing parameterizations for surface thermal properties (Dyce and Voogt, 2012). SUM_{VEG} could extend this investigation to also include highly vegetated residential areas. Similarly, it is expected that SUM_{VEG} model output may eventually be used to derive parameterizations for thermal anisotropy based on a number of causal factors. Ultimately, a more thorough understanding of effective urban thermal anisotropy may allow for correction of the directional bias—or a measure of the uncertainty—in surface temperatures derived from TIR remote sensing.

APPENDIX A

NUMERICAL INTEGRATION OF THE HOT SPOT KERNEL

The 5-Scale model of Chen and Leblanc (1997; 2001) and Leblanc *et al*. (1999) is modified and subsequently incorporated into SUM_{VEG} in order to calculate the proportion of sunlit and shaded foliage for an individual tree crown based on a solar (θ_S, φ_S) and sensor (θ_V, φ_V) position. This model accounts for both the hotspot and the complex nature of tree crowns; sunlit foliage visible on the shaded crown side and shaded foliage visible on the sunlit crown side (Chen and Leblanc, 1997). The modified 5-Scale model relies on the angular relationship between the sun and sensor and the gap probability through tree crown elements from both the solar and sensor perspective. Modifications are required in order to include the ability to estimate the sunlit and shaded foliage proportions for individual tree crowns as opposed to forest canopies. For the most part these modifications involve the replacement of gap probabilities that include gaps *between* trees to solely include gaps *within* tree crowns.

The phase angle (ξ) describes the angular difference, including both azimuth and off-nadir angles, between the sun and sensor and is calculated as

$$\xi = acos(cos\,\theta_S \cdot cos\,\theta_V \cdot sin\,\theta_S \cdot sin\,\theta_V \cdot sin\,\Delta\varphi_{s,v}) \qquad \text{(A.1.1)}$$

where $\Delta\varphi_{s,v}$ is the difference between the azimuth of the sun and sensor. The first order scattering phase function of the foliage elements ($\Gamma(\xi)$) is subsequently calculated as $\left(1 - \frac{C \cdot \xi}{\pi}\right)$. In this equation, *C* is a coefficient dependent upon the foliage optical properties. However, assuming tree crowns are solid spheres with a Lambertian surface, *C* is equal to unity and the phase function gives the proportion of sunlit tree crown surface seen by the sensor (Chen and Leblanc, 1997).

The length of path through an individual tree crown is dependent upon the crown dimensions and the angle of incidence. Both the path length through a crown from the sensor (S_V) and from the solar (S_S) position are required and are calculated as

$$S_V = \frac{V_C}{V_{g0} \cdot \cos\theta_V} \quad \text{(A.1.2)}$$

$$S_S = \frac{V_C}{S_{g0} \cdot \cos\theta_S} \quad \text{(A.1.3).}$$

The length of path through a crown is a function of the crown volume (V_C) and the crown shape as described by the projection area on the ground along a line from the sun (S_{g0}) and sensor (V_{g0}). The crown volume is calculated as the volume of an ellipse using Equation [A.1.4] where r_C and H_C are the crown radius and height, respectively:

$$V_C = \frac{2}{3} \cdot \pi \cdot {r_C}^2 \cdot H_C \quad \text{(A.1.4)}$$

V_{g0} and S_{g0} are calculated as:

$$V_{g0} = \frac{\pi \cdot {r_C}^2}{\cos {\theta_V}'} \quad \text{(A.1.5)}$$

$$S_{g0} = \frac{\pi \cdot {r_C}^2}{\cos {\theta_S}'} \quad \text{(A.1.6)}$$

where

$${\theta_S}' = \tan^{-1}\left(\frac{H_C/2}{r_C} \cdot \tan\theta_S\right) \quad \text{(A.1.7)}$$

and

$${\theta_V}' = \tan^{-1}\left(\frac{H_C/2}{r_C} \cdot \tan\theta_V\right) \quad \text{(A.1.8).}$$

For solid spherical tree crowns, two proportions are required: 1) the fraction of sunlit surface visible to the sensor (T_{ib}) and 2) the total crown surface visible to the sensor (T_{ab}). The total crown surface visible to the sensor is calculated as

$$T_{ab} = r_C \cdot \pi \cdot [(H_C/2) \cdot \sin\theta_V + (r_C \cdot \cos\theta_V)] \quad \text{(A.1.9).}$$

If the first order scattering phase function is greater than 0.0 but less than 0.000001, the sunlit crown fraction visible to the sensor is equal to the total visible crown fraction. However, if the function is greater, the sunlit visible fraction is calculated as

$$T_{ib} = \frac{1}{2} \cdot T_{ab} \cdot (1 + \xi') \quad \text{(A.1.10)}$$

where

$$\xi' = cos\,\theta_S{}' \cdot cos\,\theta_V{}' \cdot sin\,\theta_S{}' \cdot sin\,\theta_V{}' \cdot sin\,\Delta\varphi_{s,v} \quad \text{(A.1.11).}$$

The relative proportion of sunlit crown viewed by a sensor (P_{ti}) is calculated as the ratio of viewed sunlit crown and total viewed crown.

The previous crown proportion calculations all assume solid tree crown shapes. Therefore the proportions represent areas of tree crown surfaces typically modelled as spheres or ellipses and do not account for the complex nature of tree crowns. Accounting for this complexity is accomplished by incorporating the gap probability through the tree crown along a line to the sensor (P_V) and calculating the amount of foliage seen on the sunlit (Q_1) and shaded (Q_2) crown side as

$$Q_1 = \{[1 - exp(-(C_S \cdot L_{90} + C_V \cdot L_{90}))] \cdot [(C_V \cdot C_S)/(C_V + C_S)] \cdot P_V\} \cdot \xi \quad \text{(A.1.12)}$$

$$Q_2 = \left\{ \begin{matrix} [(\exp(-C_S \cdot L_{90})) - (\exp(-C_V \cdot L_{90}))] \\ \cdot [(C_V \cdot C_S)/(C_V + C_S)] \cdot P_V \end{matrix} \right\} \cdot \xi \quad \text{(A.1.13)}$$

where L_{90} is the leaf area index accumulated horizontally through the crown calculated as

$$L_{90} = \frac{4}{3} \cdot \mu_L \cdot r_C \quad \text{(A.1.14)}$$

and

$$C_S = \frac{(G_S \cdot S_S \cdot \mu_L)}{L_{90}} \quad \text{(A.1.15)}$$

$$C_V = \frac{(G_V \cdot S_V \cdot \mu_L)}{L_{90}} \quad \text{(A.1.16).}$$

G_S and G_V are the Nilson G-factor values and represent the mean projection of unit foliage area along a line from the sun and sensor, respectively. The G-factor from both the solar and sensor perspective is calculated for a particular leaf angle distribution using Equation [1.5.2]. However, it can be estimated for several hypothetical leaf angle distributions using a simple approximation dependent on the particular leaf angle distribution (Table [1.1]). The probability of viewing sunlit foliage far from the hot spot (P_{Tf}) is subsequently calculated as

$$P_{Tf} = Q_1 \cdot P_{ti} + (1 - P_{ti}) \cdot Q_2 \quad \text{(A.1.17).}$$

However, as the sun and sensor align near the hot spot, Equation [A.1.17] no longer holds true. Instead, a hotspot kernel ($F(\xi)$) is calculated through integration across the range of gap sizes as

$$F(\xi) = \frac{\int_{\lambda_{min}}^{\infty} \left[1 - \frac{\xi}{tan^{-1}(\lambda/H)}\right] \cdot N_S(\lambda) \cdot d\lambda}{\int_{\lambda_{min}}^{\infty} N_S(\lambda) \cdot d\lambda} \quad \text{(A.1.18)}$$

where N_S is the gap number density function of gap sizes (λ) calculated as

$$N_S(\lambda) = \frac{L_t}{W} exp\left[-L_t \cdot \left(1 + \frac{\lambda}{W}\right)\right] \quad \text{(A.1.19).}$$

λ_{min} is the minimum permissible gap size calculated as ($H \cdot \tan \Gamma(\xi)$) where H is the inverse of the foliage area density (μ_L). L_t is the projected tree crown area index calculated as ($G_S/\cos(\theta)$) and W is the mean width of foliage element shadows cast inside tree crowns and is estimated by the foliage element width (f_{width}).

The hotspot kernel is subsequently used to calculate a proportion of seen, sunlit foliage (P_T) based on the solar and sensor position:

$$P_T = P_{Tf} + \left[(1 - P_b) - P_{Tf}\right] \cdot F(\xi) \quad \text{(A.1.20).}$$

In this calculation, P_b is the gap probability in an individual tree crown in the direction of the sun and is assumed to equal the probability of having sunlit ground area (Chen and Leblanc, 1997). Outside of the hotspot, $F(\xi) = 0$ which results in $P_T = P_{Tf}$. At the exact center of the hotspot where $\theta_S = \theta_V$ and $\varphi_S = \varphi_V$, $F(\xi) = 1$ and $P_T = (1 - P_b)$. Since the amount of seen foliage is assumed equal to unity minus the gap probability through a

tree crown from the sensor position ($1 - P_V$), the proportion of seen, shaded foliage (Z_T) is calculated as

$$Z_T = (1 - P_V) - P_T \quad \text{(A.1.21).}$$

APPENDIX B

LEAF SURFACE TEMPERATURE MODEL

The temperature of individual leaf elements within a tree crown or canopy is controlled by the leaf energy and water balance (Fuchs, 1990; Campbell and Norman, 1998) which is a function of a number of leaf biophysical and anatomical parameters (Monteith and Unsworth, 1990). Early studies measured leaf surface temperatures using thermocouples or thermopiles at the leaf surface (e.g. Ansari and Loomis, 1959). These found that shaded leaf elements tend to approximate air temperature though they also noted the tendency for sunlit leaf elements to be several degrees warmer than air temperature. Ansari and Loomis (1959) found that sunlit leafs were 6–10°C warmer than air temperature for thin sunlit leaf elements in still air and 3–5°C warmer with moderate wind speed ($2.2 ms^{-1}$), for example.

Generally, studies now use remote sensors operating in the thermal infrared electromagnetic wavelength to provide accurate and spatially and temporally continuous measurements of leaf or canopy surface temperatures. However, this can be difficult in a tree crown or canopy where the resolution allowed by TIR remote sensors may be too low to distinguish individual leaf elements (Meier and Scherer, 2012). As a consequence, surface temperature estimates may include several leaf elements of varying size, orientation, and degree of surface shading. In a study of the canopy temperature obtained using TIR images acquired over a mixed deciduous forest in Switzerland, Leuzinger and Korner (2007) noted that mean leaf temperature within a vegetation canopy is not sufficiently explained by leaf dimensions or stomatal conductance but instead is also dependent upon canopy architecture. In addition, the environment surrounding tree crowns can influence canopy temperature; Leuzinger *et al.* (2010), in a observational campaign of tree crown canopy temperature using a high resolution TIR camera, found tree crowns surrounded by park area to be significantly cooler than tree crowns surrounded by sealed surfaces.

B.1 SUNLIT AND SHADED LEAF TEMPERATURE

SUM$_{VEG}$ requires measurements of sunlit (T_{ls}) and shaded (T_{lh}) leaf surface temperatures. Alternatively, the leaf temperature sub-model may be used in order to calculate T_{ls} and T_{lh} using

$$T_l = T_a + \left(\frac{\gamma^*}{(\Delta S + \gamma^*)}\right) \cdot \left[\left(\frac{(R_{abs})}{g_{HR} C_P}\right) \cdot \left(\frac{VPD}{P_a \cdot \gamma^*}\right)\right] \quad \text{(B.1.1)}$$

(Campbell and Norman, 1998) and user specified input (Table [B.1]). R_{abs} and *VPD* represent the net absorbed (shortwave and longwave) radiation and vapour pressure deficit, respectively. This method is a single-leaf model that calculates a leaf surface temperature (T_l) for an individual sunlit and shaded leaf rather than a canopy of leaf elements. This is appropriate given the method of leaf proportion calculation that separates the tree crown foliage view factor into sunlit and shaded portions.

In Equation [B.1.1] the heat and radiative conductance $g_{HR} = g_{HA} + g_R$, and the boundary layer conductance for heat (g_{HA}) and radiative conductance (g_R) are calculated as

$$g_{HA} = 1.4 \cdot 0.135 \cdot \sqrt{\frac{U}{d}} \;;\; d=0.72 \cdot f_{width} \quad \text{(B.1.2)}$$

$$g_R = \frac{4\sigma {T_a}^3}{C_P} \quad \text{(B.1.3)}$$

where C_P is the heat capacity of air and d is the characteristic leaf dimension dependent on leaf shape (Campbell and Norman, 1998).

The slope of the saturation vapour pressure curve (ΔS) is calculated, using formulae developed by Tetens (1930) and Murray (1967), as

$$\Delta S = \frac{\left\{\left[4098 \cdot \left(0.6108 \cdot \left(exp([17.27 \cdot T_a/T_a + 237.3])\right)\right)\right]/(T_a + 237.3^2)\right\}}{P_a} \quad \text{(B.1.4)}$$

Table B.1: Input parameters to the modified leaf temperature model incorporated into SUM$_{VEG}$.

Parameter	Description
YD	Day of the year[12]
LMST	Local Mean Solar Time (hr)
ϕ	Latitude (decimal degrees)
α_L	Leaf surface albedo
ε_L	Leaf emissivity
P_a	Air pressure (kPa)
e_a	Vapour pressure (kPa)
g_{vs}	Stomatal vapour conductance ($mmolm^{-2}s^{-1}$)
U	Wind speed (ms^{-1})
T_a	Air temperature (°C)
f_{width}	Maximum leaf element width (m)

The psychometric constant (γ) varies slightly with air pressure (Campbell and Norman, 1998) as

$$\gamma = \left[\frac{C_P \cdot \left(\frac{P_a}{10}\right)}{0.622 \cdot 2.45}\right] \cdot 10 \tag{B.1.5}$$

and the apparent psychometric constant $\gamma^* = \gamma \cdot (g_{HR}/g_V)$. The vapour conductance (g_V) is calculated as

$$g_V = \left(\frac{0.5 g_{VS} g_{VA}}{g_{VS} g_{VA}}\right) + \left(\frac{0.5 g_{VS} g_{VA}}{g_{VS} g_{VA}}\right) \tag{B.1.6}$$

where the vapour conductance in air $g_{VA} = 0.147 \cdot \sqrt{\frac{U}{d}}$. The two terms on the right side of Equation [B.1.6] are used to represent different water vapour conductance values on the adaxial and abaxial surfaces of the leaf (Campbell and Norman, 1998). Unless otherwise stated, all model scenarios assume equal adaxial and abaxial leaf water vapour conductance.

B.2 Radiation Absorbed by Leaf Elements

Solar radiation available to individual leaf elements within a tree crown is controlled by location within the crown volume; light availability decreases according to

[12] *Year, local mean solar time,* and *latitude* are specified in SUM_{VEG} main input file to calculate θ_S and φ_S. If θ_S and φ_S are input, T_{ls} and T_{lh} must also be input.

the Beer- Lambert-Bouguer law along the path through the crown volume (Allen and Richardson, 1968). Additionally, since shortwave radiation is the main energetic input to a sunlit leaf element, leaf angle relative to the solar beam produces considerable variation of sunlit leaf surface temperature proportional to the cosine of the angle between the leaf normal and incident solar beam (Fuch, 1990). Shaded leaf elements receive a relatively small radiative flux density compared to sunlit leaf elements (Fuchs, 1990).

The result of the distribution of leaf angles within a crown is a range of temperatures for both sunlit and shaded leaf categories as a function of individual leaf angle. Net radiation absorbed by at the leaf surface (R_{abs}) is calculated based on leaf albedo and emissivity as well as incoming direct (K_{dir}) and diffuse (K_{diff}) solar radiation and incoming longwave radiation (L_{dn}) components. Incoming shortwave radiation (K_{dn}) is modelled using a subroutine to calculate solar position based on time of year, time of day, and latitude, and a subroutine to estimate incoming radiant flux based on the solar position and atmospheric conditions, originally developed for use in the TUF-3d energy budget model (Krayenhoff and Voogt, 2007a). Calculation of incoming radiative flux requires input of air temperature and calculation of dewpoint temperature (T_d) as

$$T_d = \frac{240.97 \cdot \ln(e_a/0.611)}{17.502 - \ln(e_a/0.611)} \quad \text{(B.2.1)}$$

(Campbell and Norman, 1998). For a more comprehensive presentation of the formulae involved in the treatment of shortwave flux, the reader is referred Krayenhoff (2005). Incoming longwave radiation to the leaf surface is calculated for clear skies using the Prata (1996) formulation:

$$L_{dn} = \left[1 - \left(1 + 46.5 \cdot \frac{e_a}{(T_a + 273.15)}\right) \cdot exp\left(-\left(1.2 + 3 \cdot 46.5 \cdot \frac{e_a}{(T_a + 273.15)}\right)^{0.5}\right)\right] \cdot \sigma \cdot (T_a + 273.15)^4 \quad \text{(B.2.2).}$$

The total solar radiation (direct and diffuse) incident upon a single sunlit leaf element (K_S) is a function of the leaf area at each inclination angular class (θ_L) between leaf inclination angles *a* and *b* (Fuchs, 1990):

$$K_S = K_{dn} \cdot \left[\frac{\cos\left(\theta_{L_a} + \theta_{L_b}\right)}{2}\right] \quad \text{(B.2.3)},$$

Integrating Equation [B.2.3] over leaf inclination angles from 0 to $\pi/2$ provides an incident solar radiation representative of sunlit leaf elements within a canopy (Fuchs, 1990). It is important to note that this formulation assumes incident solar radiation is independent of leaf azimuth angle.

Equation [B.2.3] includes both the direct and diffuse radiation incident upon a leaf surface. However, in order to determine a shaded leaf temperature, solar radiation incident upon a leaf surface is assumed to consist of diffuse radiation and forward scattered direct radiation. The diffuse fraction (d_{frac}) of the total solar radiation is calculated as

$$d_{frac} = \frac{K_{diff}}{K_{dn}} \quad \text{(B.2.4)}.$$

The direct beam fraction (b_{frac}) is therefore equal to ($1 - d_{frac}$). The total solar radiation incident upon a shaded leaf element (K_{SH}) within a crown is calculated using the wavelength dependent leaf absorptivity (α)—equal to 0.8 for photosynthetically active radiation—and is averaged over all leaf angles by using K_S as

$$K_{SH} = \left[(K_S \cdot b_{frac}) \cdot (1 - \alpha)\right] + (K_S \cdot d_{frac}) \quad \text{(B.2.5)}.$$

The term within the square brackets of [B.2.5] estimates the forward scattered direct radiation by assuming all radiation that is not absorbed by a leaf in the top layer (i.e. sunlit leaf element) is intercepted by 'shaded' leaf elements within the crown volume. Equation [B.2.5] does not account for multiple scattering beyond two layers of leaf elements but does provide a more realistic approximation of the total amount of solar radiation incident upon shaded leaf elements within a crown envelope as a function of leaf angle than would be expected using exclusively diffuse radiative flux. The net radiation (shortwave and longwave) absorbed by sunlit ($R_{S_{abs}}$) and shaded ($R_{SH_{abs}}$) leaf elements is calculated as

$$R_{S_{abs}} = ([K_S \cdot (1 - \alpha_L)] + [L_{dn} \cdot \varepsilon_L]) - (\varepsilon_L \cdot \sigma \cdot {T_a}^4) \quad \text{(B.2.6)}$$

and

$$R_{SH_{abs}} = ([K_{SH} \cdot (1 - \alpha_L)] + [L_{dn} \cdot \varepsilon_L]) - (\varepsilon_L \cdot \sigma \cdot {T_a}^4) \qquad \text{(B.2.7)}$$

respectively, where σ is the Stefan-Boltzmann constant equal to $5.67x10^{-8}$ $\mathrm{Wm^{-2}K^{-4}}$, and ε_L and α_L are the leaf emissivity and albedo, respectively. In order to estimate a longwave emittance from leaf elements in the absence of leaf surface temperature, air temperature (T_a) is used as a proxy. Fuchs (1990) makes the same assumption noting that it has minimal impact on the total leaf radiation balance. It is also important to note that this formulation neglects longwave radiation exchange among leaf elements thereby ignoring the effects of canopy temperature (i.e. influence of difference in temperature between leaf elements). $R_{S_{abs}}$ and $R_{SH_{abs}}$ replace R_{abs} in [B.1.1] in order to calculate a sunlit and shaded leaf surface temperature, respectively.

B.3 TEMPERATURES FOR SURFACES SHADED BY TREE FOLIAGE

Temperatures for surface patches shaded from direct solar radiation by tree crown foliage (i.e. termed 'partially shaded') are modelled in $\mathrm{SUM_{VEG}}$ using a weighting algorithm based on crown gap probabilities for direct and diffuse solar radiation. This weighting algorithm is intended as a provisional measure until an appropriate vegetated micro-scale urban energy budget model that explicitly treats tree crown foliage (e.g. vegetated TUF-3d) can be coupled to $\mathrm{SUM_{VEG}}$. However, in order to determine its efficacy for the current investigation, modelled partially shaded patch temperatures are compared to measurements extracted from TIR images for a limited sample of observations. This analysis is not intended as an exhaustive evaluation of the weighting algorithm within $\mathrm{SUM_{VEG}}$.

TIR images used for the evaluation come from Adderley's (2012) investigation of the bias—relative to the 'complete surface temperature'—in surface temperatures measured using thermal infrared remote sensors over Elgin St. in the Sunset residential neighbourhood, Vancouver, B.C. Adderley (2012) used a Thermovision A40M infrared scanner[13] mounted on a mobile tower at approximately 15m vertical height to obtain TIR

[13] Camera Specs.: sensitivity 0.08K at 300K, 2K measurement accuracy, 7.5–15µm wavelength range, 45° FOV with 1.3mrad angular resolution (FLIR Systems, 2004)

images of the Elgin St. surface every 30 minutes on September 14 and 15, 2008. In this procedure, the thermal scanner was rotated in a 360° panorama at tilt angles of approximately 45° and 65° off-nadir (Adderley, 2012).

From the TIR images, a series of radiometric surface temperatures are extracted and averaged to determine mean values of sunlit, shaded, and partially shaded (i.e. by tree crowns) lawn surface temperatures approximately every 30 minutes during the day on September 14th and 15th, 2008. Partially shaded temperatures are extracted from the approximate centre of the shaded area for two trees located on the west side of Elgin St. The analysis is restricted to lawn surfaces due to the fact that the TIR images do not include any significant shading of built surfaces (e.g. wall or road) from direct solar radiation by trees.

The weighting algorithm within SUM_{VEG} is subsequently used to estimate partially shaded surface patch temperatures using tree crown dimensions approximated by scaling with other surface features (e.g. automobiles, house doorways, etc.). Tree crown biophysical parameters are assumed equal to those used for the Sunset full model evaluation (Section [4.1]).

Figure [B.1] details the comparison of modelled and observed partially shaded lawn surface temperatures for September 14 and 15, 2008. Overall, modelled estimates compare well with remotely-detected radiometric surface temperatures. SUM_{VEG} has a tendency to underestimate the temperatures for partially shaded surfaces, particularly lower temperatures corresponding to images acquired in the early morning. This could be due to the relatively low sky view factor for the ground surface beneath tree crowns which would limit the loss of longwave radiant energy during the night and allow the surfaces to maintain higher temperatures into the early morning relative to the pixels chosen to represent ‘sunlit’ and ‘shaded’ lawn. However, as a first approximation, partially shaded surface temperatures estimated using the weighting algorithm provide a valid alternative to temperature observations until SUM_{VEG} can be coupled with a vegetated micro-scale urban energy budget model.

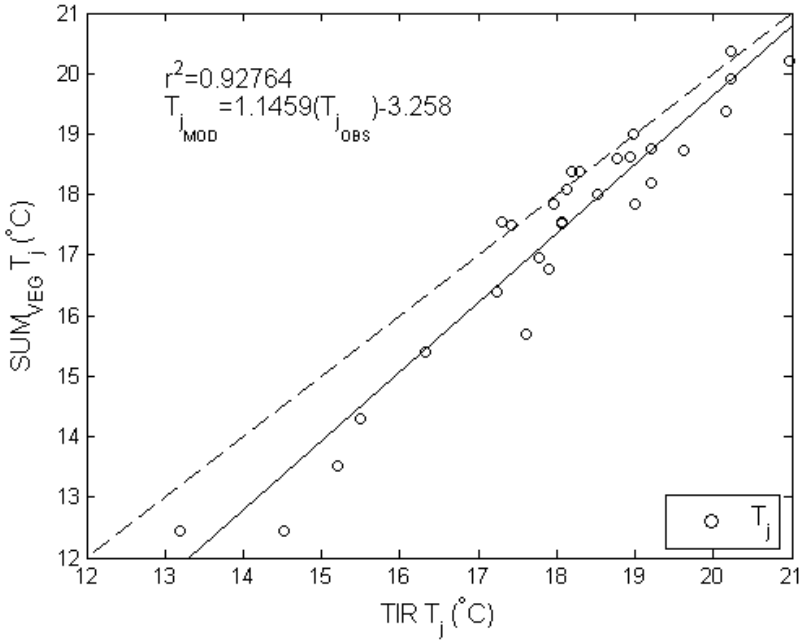


Figure B.1: Linear regression of modelled ($T_{j_{MOD}}$) and observed ($T_{j_{OBS}}$) temperature for lawn surfaces shaded from direct solar radiation by tree crown foliage. Dashed line indicates the 1:1 line.

REFERENCES

Abraha, M.G. and M.J. Savage. 2010. Validation of a three-dimensional solar radiation interception model for tree crops. *Agriculture, Ecosystems, and Environment*. 139: 636–652.

Adderley, C.D. 2012. The effect of preferential view direction on measured urban surface temperature. M.Sc. Thesis. University of British Columbia, Vancouver, British Columbia.

Allen, W.A. and A.J. Richardson. 1968. Interaction of light with a plant canopy. *Journal of the optical society of America*. 58(8): 1023–1028.

Anderson, M.C. 1966. Stand structure and light penetration. 2. A theoretical analysis. *Journal of Applied Ecology*. 3(1): 41–&.

Ansari, A.Q. and W.E. Loomis. 1959. Leaf Temperatures. *American Journal of Botany*. 46(10): 713–717.

Arnfield, A.J. 1982. An approach to the estimation of the surface radiative properties and radiation budgets of cities. *Physical Geography*. 3: 97–122.

Asawa, T., Hoyano, A. and K. Nakaohkubo. 2008. Thermal design tool for outdoor spaces based on heat balance simulation using a 3D-CAD system.

Baldocchi, D. 2012. Lecture 8: solar radiation transfer through vegetation, part 1: theory. ESPM 129 lecture, September 12, 2012. Available from: http://nature.berkeley.edu/biometlab/espm129/notes/Lecture%208%20Solar%20Radiation%20Transfer%20through%20Vegetation%20part%201%20notes.pdf

Campbell, G.S. 1990. Derivation of an angle density function for canopies with ellipsoidal leaf angle distributions. *Agricultural and Forest Meteorology*. 49: 173–176.

Campbell, G.S. and J.M. Norman. 1998. *An Introduction to Environmental Biophysics 2nd Edition*. Springer Verlag, New York. 286pp.

Canham, C.D. 1988. An index for understory light levels in and around canopy gaps. *Ecology*. 69(5): 1634–1638.

Charles-Edwards, D.A. and J.H.M. Thornley. 1973. Light interception by an isolated plant: a simple model. *Annals of Botany*. 37: 919–928.

Chehbouni, A., Nouvellon, Y., Kerr, Y.H., Moran, M.S., Watts, C., Prévot, L., *et al.* 2001. Directional effect on radiative surface temperature measurements over a semiarid grassland site. *Remote Sensing of Environment*. 76: 360–372.

Chen, J.M. and J. Cihlar. 1995. Quantifying the effect of canopy architecture on optical measurements of leaf area index using two gap size analysis methods. *IEEE Transactions on Geoscience and Remote Sensing*. 33(3): 777–787.

Chen, J.M. and S.G. Leblanc. 1997. A four-scale bidirectional reflectance model based on canopy architecture. *IEEE Transactions on Geoscience and Remote Sensing*. 35(5): 1316–1337.

Chen, J.M. and S.G. Leblanc. 2001. Multiple-scattering scheme useful for geometric optical modeling. *IEEE Transactions on Geoscience and Remote Sensing.* 39(5): 1061–1071.

Christen, A., Coops, N.C., Crawford, B.R., Kellett, R., Liss, K.N., Olchovski, I., *et al.* 2011. Validation of modeled carbon-dioxide emissions from an urban neighbourhood with direct eddy-covariance measurements. *Atmospheric Environment*. 45: 6057–6069.

Colaizzi, P.D., O'Shaughnessy, S.A., Gowda, P.H., Evett, S.R., Howell, T.A., Kustas, W.P. and M.C. Anderson. 2010. Radiometer footprint model to estimate sunlit and shaded components for row crops. *Agronomy Journal.* 102(3): 942–955.

Colaizzi, P.D., Evett, S.R., Howell, T.A., Li, F., Kustas, W.P. and M.C. Anderson. 2012. Radiation model for row crops: I. geometric view factors and parameter optimization. *Agronomy Journal*. 104(2): 225–240.

Dawson, T.P., Curran, P.J. and S.E. Plummer. 1998. LIBERTY - modelling the effects of leaf biochemistry on reflectance spectra. *Remote Sensing of Environment*. 65: 50–60.

Dyce, D.R. and J.A. Voogt. 2012. Sensitivity of modelled urban thermal anisotropy to thermal admittance. 8th International Conference on Urban Climate (ICUC8). 6–10 August 2012, University College Dublin, Dublin, Ireland.

FLIR Systems. (2004, October). ThermoVision A40M operator's manual.

FLIR Systems. 2012. User's manual: Flir R&D software 3.3. #T559132; r.5674/5676; en-US.

Francois, C., Ottle, C. and L. Prévot. 1997. Analytical parameterization of canopy directional emissivity and directional radiance in the thermal infrared: application on the retrieval of soil and foliage temperatures using two directional measurements. *International Journal of Remote Sensing*. 18(12): 2587–2621.

Fuchs, M. 1990. Infrared measurement of a canopy temperature and detection of plant water stress. *Theoretical and Applied Climatology*. 42: 253–261.

Gastellu-Etchegorry, J.P., Demarez, V., Pinel, V. and F. Zagolski. 1996. Modeling radiative transfer in heterogeneous 3-d vegetation canopies. *Remote Sensing of Environment*. 58: 131–156.

Gastellu-Etchegorry, J.P., Grau, E. and N. Lauret. 1999. Chapter 2- DART: a 3d model for remote sensing images and radiative budget of earth surfaces. *In*: Alexandru, C. 2012. *Modeling and Simulation in Engineering*. InTech, Chapters, 298pp.

Gastellu-Etchegorry, J.P., Martin, E. and F. Gascon. 2004. DART: a 3d model for simulating satellite images and studying surface radiation budget. *International Journal of Remote Sensing*. 25(1): 73–96.

Gastellu-Etchegorry, J.P. 2008. 3d modeling of satellite spectral images, radiation budget and energy budget of urban landscapes. *Meteorology and Atmospheric Physics*. 102: 187–207.

Gates, D.M. 1980. *Biophysical Ecology*. Springer Verlag, New York. 611pp.

Goel, N.S. 1988. Models of vegetation canopy reflectance and their use in estimation of biophysical parameters from reflectance data. *Remote Sensing Review*. 4: 1–212.

Grimmond, C.S.B. and T.R. Oke. 1999. Heat storage in urban areas. *Journal of Applied Meteorology*. 38: 922–940.

Grimmond, C.S.B., Blackett, M., Best, M.J., Barlow, J., Baik, J.-J., Belcher, S.E., *et al.* 2010 The international urban energy balance models comparison project: first results from phase 1. *Journal of Applied Meteorology and Climatology*. 49(6): 1268–1292.

Grimmond, C.S.B., Blackett, M., Best, M.J., Baik, J.-J., Belcher, S.E., Beringer, J., *et al*. 2011. Initial results from phase 2 of the international urban energy balance model comparison. *International Journal of Climatology*. 31: 244–272.

Guillevic, P., Gastellu-Etchegorry, J.P., Demarty, J. and L. Prévot. 2003. Thermal infrared radiative transfer within three-dimensional vegetation covers. *Journal of Geophysical Research*. 108(D8): ACL 1–13.

Jackson, R.D., Reginato, R.J., Pinter Jr., P.J. and S.B. Idso. 1979. Plant canopy information extraction from composite scene reflectance of row crops. *Applied Optics*. 18: 3775–3782.

Jupp, D.L.B., Culvenor, D.S., Lovell, J.L., Newnham, G.J., Strahler, A.H. and C.E. Woodcock. 2009. Estimating forest LAI profiles and structural parameters using a ground-based laser called Echidna®. *Tree Physiology*. 29(2): 171–181.

Kanda, M. 2006. Progress in the scale modeling of urban climate: review. *Theoretical and Applied Climatology*. 84: 23–33.

Kimes, D.S. 1980. Effects of vegetation canopy structure on remotely sensed canopy temperatures. *Remote Sensing of Environment*. 10: 165–174.

Kimes, D.S., Idso, S.B., Pinter, P.J., Reginato, R.J. and R.D. Jackson. 1980. View angle effects in the radiometric measurement of plant canopy temperatures. *Remote Sensing of Environment*. 10: 273–284.

Kimes, D.S. 1981. Remote sensing of temperature profiles in vegetation canopies using multiple view angles and inversion techniques. *IEEE Transaction on Geoscience and Remote Sensing*. GE-19: 85–90.

Kimes, D.S., Smith, J.A. and L.E. Link. 1981. Thermal IR exitance model of a plant canopy. *Applied Optics*. 20(4): 623–632.

Kimes, D.S. and J.A. Kirchner. 1982. Radiative transfer model for heterogeneous 3-d scenes. *Applied Optics*. 21(22): 4119–4129.

Kimes, D.S., Norman, J.M. and C.L. Walthall. 1985. Modeling the radiant transfers of sparse vegetation canopies. *IEEE Transactions on Geoscience and Remote Sensing*. GE-23(5): 695–704.

Kimes, D.S. 1991. Radiative transfer in homogeneous and heterogeneous vegetation canopies. *In*: Myneni, R.B. and J. Ross. 1991. *Photon-vegetation interactions: applications in optical remote sensing and plant ecology.* Springer-Verlag, Berlin Heidelberg, 565pp.

Kneizys, F.X., Shettle, E.P., Chetwynd, J.H., Abreu, L.W., Anderson, G.P., Gallery, W.O. *et al*. 1988. Users guide to LOWTRAN 7. AFGL-TR-88-0177.

Krayenhoff, E.S. 2005. A micro-scale 3d urban energy balance model for studying surface temperatures. M.Sc. Thesis. Western University, London, Ontario.

Krayenhoff, E.S. and J.A. Voogt. 2007a. A microscale three-dimensional urban energy balance model for studying surface temperatures. *Boundary-Layer Meteorology*. 123: 433–461.

Krayenhoff, E.S. and J.A. Voogt. 2007b. Combining sub-facet scale urban energy balance and sensor view models to investigate the dependence of effective thermal anisotropy on city structure. *Poster Presentation*. Seventh Symposium on the Urban Environment. Poster Session 1. Monday, 10 September 2007. *Available from:* https://ams.confex.com/ams/7Coastal7Urban/techprogram/paper_126542.htm.

Krayenhoff, E.S., Christen, A., Martilli, A. and T.R. Oke. 2014. A multi-layer radiation model for urban neighbourhoods with trees. *Boundary-Layer Meteorology*. 151: 139–178.

Jones, H.G. 1999. Use of infrared thermometry for estimation of stomatal conductance as a possible aid to irrigation scheduling. *Agricultural and Forest Meteorology*. 95: 139–149.

Lagouarde, J.-P., Ballans, H., Moreau, P., Guyon, D. and D. Coraboeuf. 2000. Experimental study of brightness surface temperature angular variations of maritime pine (*Pinus pinaster*) stands. *Remote Sensing of Environment*. 72: 17–34.

Lagouarde, J.-P., Moreau, P., Irvine, M., Bonnefond, J.-M., Voogt, J.A. and F. Solliec. 2004. Airborne experimental measurements of the angular variations in surface temperature over urban areas: case study of Marseille (France). *Remote Sensing of Environment*. 93: 443–462.

Lagouarde, J.-P. and M. Irvine. 2008. Directional anisotropy in thermal infrared measurements over Toulouse city centre during the CAPITOUL measurement campaigns: first results. *Meteorology and Atmospheric Physics*. 102: 173–185.

Lagouarde, J.-P., Hénon, A., Kurz, B., Moreau, P., Irvine, M., Voogt, J. and P. Mestayer. 2010. Modelling daytime thermal infrared directional anisotropy over Toulouse city centre. *Remote Sensing of Environment*. 114: 87–105.

Lagouarde, J.-P., Hénon, A., Irvine, M., Voogt, J., Pigeon, G., Moreau, P., Masson, V. and P. Mestayer. 2012. Experimental characterization and modelling of the nighttime directional anisotropy of thermal infrared measurements over an urban area: case study of Toulouse (France). *Remote Sensing of Environment*. 117: 19–33.

Leblanc, S.G., Bicheron, P., Chen, J.M., Leroy, M. and J. Cihlar. 1999. Investigation of directional reflectance in boreal forests with an improved 4-Scale model and airborne POLDER data. *IEEE Transactions on Geoscience and Remote Sensing*. 37(3): 1396–1414.

Leuzinger, S. and C. Körner. 2007. Tree species diversity affects canopy leaf temperatures in a mature temperate forest. *Agricultural and Forest Meteorology*. 146: 29–37.

Leuzinger, S. Vogt, R. and C. Körner. 2010. Tree surface temperature in an urban environment. *Agricultural and Forest Meteorology*. 150: 56–62.

Li, X. and A.H. Strahler. 1985. Geometric-optical modeling of a conifer forest canopy. *IEEE Transactions on Geoscience and Remote Sensing*. GE-23(5): 705–721.

Li, X. and A.H. Strahler. 1986. Geometric-optical modeling of a conifer forest canopy. *IEEE Transactions on Geoscience and Remote Sensing.* GE-24(6): 906–919.

Li, X. and A.H. Strahler. 1988. Modeling the gap probability of a discontinuous vegetation canopy. *IEEE Transactions on Geoscience and Remote Sensing*. 26(2): 161–170.

Li, X. and A.H. Strahler. 1992. Geometric-optical bidirectional reflectance modeling of the discrete crown vegetation canopy: effect of crown shape and mutual shadowing. *IEEE Transactions on Geoscience and Remote Sensing*. 30(2): 276–292.

Li, X. Strahler A.H. and C.E. Woodcock. 1995. A hybrid geometric optical-radiative transfer approach for modeling albedo and directional reflectance of discontinuous canopies. *IEEE Transaction on Geoscience and Remote Sensing*. 33(2): 466–480.

Liu, B.Y. and R.C. Jordan. 1960. The interrelationship and characteristic distribution of direct, diffuse, and total solar radiation. *Solar Energy*. 4: 1–19.

Mann, J.E., Curry, G.L. and P.J.H. Sharpe. 1979. Light interception by isolated plants. *Agricultural Meteorology*. 20: 205–214.

McGuire, M.J., Balick, L.K., Smith, J.A. and B.A. Hutchison. 1989. Modeling directional thermal radiance from a forest canopy. *Remote Sensing of Environment*. 27: 169–186.

Meier, F. and D. Scherer. 2012. Spatial and temporal variability of urban tree canopy temperature during summer 2010 in Berlin, Germany. *Theoretical and Applied Climatology*. 110: 373–384.

Monteith, J.L. and G. Szeic. 1962. Radiative temperature in the heat balance of natural surfaces. *Quarterly Journal of the Royal Meteorological Society*. 88: 496–507.

Monteith, J.L. and M.H. Unsworth. 1990. *Principles of Environmental Biophysics*. Edward Arnold, London. 291pp.

Murray, F.W. 1967. On the computation of saturation vapour pressure. Journal of Applied Meteorology. 6: 203-204.

Myneni, R.B., Ross, J. and G. Asrar. 1989. A review on the theory of photon transport in leaf canopies. *Agricultural and Forest Meteorology*. 45(1-2): 1–153.

Myneni, R.B. and J. Ross. 1991. *Photon-vegetation interactions: applications in optical remote sensing and plant ecology.* Springer-Verlag, Berlin Heidelberg, 565pp.

Myneni R.B., Marshak, A., Knyazikhin, Y. and G. Asrar. 1991. Discrete ordinates method for photon transport in leaf canopies. *In*: Myneni, R.B. and J. Ross. 1991. *Photon-vegetation interactions: applications in optical remote sensing and plant ecology.* Springer-Verlag, Berlin Heidelberg, 565pp.

Nanni, E. 2010. Source area variations in urban snow cover and its impact on the radiation budget. M.Sc. Thesis. The University of Western Ontario, London, Ontario.

Nice, KA, Coutts, A, Beringer, J, Tapper, N and S. Krahenhoff. 2013. Introducing the TUF-3D/MAESPA urban micro-climate model. 8th International Water Sensitive Urban Design Conference 2013. 25–29 November 2013, Gold Coast, Australia.

Nice, KA, Tapper, N., Beringer, J., Coutts, A. and S. Krayenhoff. 2014. An urban micro-climate model for assessing impacts of Water Sensitive Urban Design. *Poster Presentation*. 11th Symposium on the Urban Environment, 94th AMS Annual Meeting, 2–6 February 2014, Atlanta, GA.

Nilson, T. 1971. A theoretical analysis of the frequency of gaps in plant stands. *Agricultural Meteorology.* 8: 25–38.

Norman, J.M. and J.M. Welles. 1983. Radiative transfer in an array of canopies. *Agronomy Journal*. 75: 481–488.

Oke, T.R. 1979. Advectively-assisted evapotranspiration from irrigated urban vegetation. *Boundary-Layer Meteorology*. 16: 167–174.

Oke, T.R. 1988. The urban energy balance. *Progress in Physical Geography*. 12: 471–508.

Oke, T.R. 1989. The micrometeorology of the urban forest. *Philosophical Transactions of the Royal Society B.* 324: 335–349.

Otterman, J., Brakke, T.W., Fuchs, M., Lakshmi, V. and M. Cadeddu. 1999. Longwave emission from a plant/soil surface as a function of the view direction: dependence on the canopy architecture. *International Journal of Remote Sensing*. 20(11): 2195–2201.

Overby, M., Bailey, B., Stoll, R., Willemsen, P. and E. Pardyjak. 2014. Simulating radiative transport for vegetation in complex urban environments with green infrastructure. 11th Symposium on the Urban Environment, 94th AMS Annual Meeting, 2–6 February 2014, Atlanta, GA.

Paw U, K.T., Ustin, S.L. and C. Zhang. 1989. Anisotropy of thermal infrared exitance in sunflower canopies. *Agricultural and Forest Meteorology.* 48: 45–58.

Paw U, K.T. 1992. Development of models for thermal infrared radiation above and within plant canopies. *ISPRS Journal of Photogrammetry and Remote Sensing*. 47: 189–203.

Pinty, B., Gobron, N., Widlowski, J.-L., Gerstl, S.A.W., Verstraete, M.M., Antunes, M., *et al*. 2001. Radiation transfer model intercomparison (RAMI) exercise. *Journal of Geophysical Research*. 106(D11): 11937–11956.

Pinty, B., Widlowski, J.-L., Taberner, M., Gobron, N., Verstraete, M.M., Disney, M., *et al.* 2004. Radiation transfer model intercomparison (RAMI) exercise: results from the second phase. *Journal of Geophysical Research*. 109(D06210). 19pp.

Prata, A.J. 1996. A new long-wave formula for estimating downward clear-sky radiation at the surface. *Quarterly Journal of the Royal Meteorological Society*. 122: 1127–1151.

Roberts, S.M., Voogt, J.A. and T.R. Oke. 2009. Outdoor scale model experiment to evaluate the complete urban surface temperature. Eighth Symposium on the Urban Environment. Joint Session 3- Measurements in the Urban Environment- II. Tuesday, 13 January 2009. *Available from:* https://ams.confex.com/ams/89annual/techprogram/paper_144424.htm

Ross, J. 1975. The radiation regime and architecture of plant stands. Leningrad, Gidrometeoizdat, 342pp (in Russian).

Roth, M., Oke, T.R. and W.J. Emery. 1989. Satellite-derived urban heat islands from three coastal cities and the utilization of such data in urban climatology. *International Journal of Remote Sensing*. 10(11): 1699–1720.

Schmid, H.P., Cleugh, H.A., Grimmond, C.S.B. and T.R. Oke. 1991. Spatial variability of energy fluxes in suburban terrain. *Boundary-Layer Meteorology*. 54: 249–276.

Smith, J.A., Ranson, K.J., Nguyen, D., Balick, L., Link, L.E., Fritschen, L. and B. Hutchison. 1981. Thermal vegetation canopy model studies. *Remote Sensing of Environment*. 11: 311–326.

Smith, J.A., Ballard Jr., J.R. and J.A. Pedelty. 1997. Effect of three-dimensional canopy architecture on thermal infrared exitance. *Optical Engineering*. 36(11): 3093–3100.

Soux, A. Voogt, J.A. and T.R. Oke. 2004. A model to calculate what a remote sensor 'sees' of an urban surface. *Boundary-Layer Meteorology*. 111: 109–132.

Stewart, I.D. and T.R. Oke. 2012. Local climate zones for urban temperature studies. *Bulletin of the American Meteorological Society*. 93: 1879–1900.

Strahler, A.H. and D.L.B. Jupp. 1991. Modeling bidirectional reflectance of forests and woodlands using boolean models and geometric optics. *Remote Sensing of Environment.* 34: 153–166.

Tetens, O. 1930. Uber einige meteorologische Begriffe. Z. Geophys. 6: 297–309.

Verhoef, A., De Bruin, H.A.R. and B.J.J.M. Van Den Hurk. 1997. Some practical notes on the parameter kB^{-1} for sparse vegetation. *Journal of Applied Meteorology*. 36: 560–572.

Verhoef, W., Jia, L., Xiao, Q. and Z. Su. 2007. Unified optical-thermal four-stream radiative transfer theory for homogeneous vegetation canopies. *IEEE Transactions on Geoscience and Remote Sensing.* 45(6): 1808–1822.

Voogt, J.A. and T.R. Oke. 1997. Complete urban surface temperatures. *Journal of Applied Meteorology*. 36: 1117–1132.

Voogt, J.A. and T.R. Oke. 1998. Effects of urban surface geometry on remotely-sensed surface temperature. *International Journal of Remote Sensing*. 19(5): 895–920.

Voogt, J.A. and T.R. Oke. 2003. Thermal remote sensing of urban climates. *Remote Sensing of Environment*. 86: 370–384.

Voogt, J.A. and E.S. Krayenhoff. 2005. Modelling urban thermal anisotropy. 5th International Symposium on Remote Sensing of Urban Areas. March 14–16, 2005, Phoenix, AZ.

Voogt, J.A. 2008. Assessment of an urban sensor view model for thermal anisotropy. *Remote Sensing of the Environment.* 112: 482–495.

Wang, W.-M., Li, Z.-L. and H.-B. Su. 2007. Comparison of leaf angle distribution functions: effects on extinction coefficient and fraction of sunlit foliage. *Agricultural and Forest Meteorology*. 143: 106–122.

Welles J.M. and J.M. Norman. 1991. Photon transport in discontinuous canopies: a weighted random approach. *In*: Myneni, R.B. and J. Ross. 1991. *Photon-vegetation interactions: applications in optical remote sensing and plant ecology*. Springer-Verlag, Berlin Heidelberg, 565pp.

White, H.P., Miller, J.R. and J.M. Chen. 2002. Four-scale linear model for anisotropic reflectance (FLAIR) for plant canopies- part II: validation and inversion with CASI, POLDER, and PARABOLA data at BOREAS. *IEEE Transactions on Geoscience and Remote Sensing*. 40(5): 1038–1046.

Whitehead, D., Grace, J.C. and M.J.S. Godfrey. 1990. Architectural distribution of foliage in individual *Pinus radiate* D. Don crowns and the effects of clumping on radiation interception. *Tree Physiology*. 7: 135–155.

Widlowski, J.-L., Taberner, M., Pinty, B., Bruniquel-Pinel, V., Disney, M., Fernandes, R. *et al*. 2007. Third radiation transfer model intercomparison (RAMI) exercise: documenting progress in canopy reflectance models. *Journal of Geophysical Research*. 112. 28pp.

Willmott, C.J., Ackleson, S.G., Davis, R.E., Feddema, J.J., Klink, K.M., Legates, D.R., *et al*. 1985. Statistics for the evaluation and comparison of models. *Journal of Geophysical Research*. 90(C5): 8995–9005.

Zhan, W., Chen, Y., Voogt, J.A., Zhou, J., Wang, J., Ma, W. and L. Wenyu. 2012. Assessment of thermal anisotropy on remote estimation of urban thermal inertia. *Remote Sensing of Environment*. 123: 12–24.

CURRICULUM VITAE

Name:	Daniel Roy Dyce
Post-secondary Education and Degrees:	Western University London, Ontario, Canada 2011–2014 M.Sc. (Physical Geography) University of Guelph Guelph, Ontario, Canada 2007–2011 BSES EAAS (Earth and Atmospheric Science)
Honours and Awards:	**University of Guelph** Entrance Scholarship (2007) OAC Dean's honours list (2010) **Western University** Queen Elizabeth II Graduate Scholarship in Science and Technology (2011–2012 and 2012–2013 (declined)) Natural Sciences and Engineering Research Council PGS-M (2012–2013) Edward G. Pleva Teaching Award (2011–2012 and 2012–2013)
Related Work Experience:	Researcher Western University and Middlesex London Health Unit Geography Department January 2014–June 2014 Teaching Assistant and Research Assistant Western University Geography Department 2011–2013 Research Assistant University of Guelph School of Environmental Sciences April 2011–August 2011

Conference Proceedings and Presentations:

Dyce, D.R. and J.A. Voogt*. 2014. Characterizing the urban heat island effect in Middlesex-London. Climate Change and Health Vulnerability in Middlesex-London, Workshop hosted by Middlesex-London Health Unit, March 27, 2014, London, Ontario. (Invited presentation; *presenting author).

Dyce, D.R. and J.A. Voogt. 2014. Effects of vegetation on urban thermal anisotropy. AMS 94th Annual Meeting, 11th Symposium on the Urban Environment. Atlanta, Georgia, February 2–6, 2014. (Oral Presentation)

Dyce, D.R. and J.A. Voogt. 2012. Sensitivity of modeled urban thermal anisotropy to thermal admittance. 8th International Conference on Urban Climate (ICUC8). University College Dublin, Dublin, Ireland, August 6–10, 2012. (Oral Presentation and Proceedings)